A Study of the Process of the Typhoon Formation and Development Using the Satellites Data(Dissertation_全文)

AUTHOR(S):

Heta, Yurie

(2)

An Analysis of Tropical Wind Fields in Relation to Typhoon Formation over the Western Pacific

By Yurie Heta
Disaster Prevention Research Institute, Kyoto University, Uji, Kyoto 611, Japan

(Manuscript received 29 May 1989, in revised form 24 November 1989)

Journal of the Meteorological Society of Japan
Vol. 68, No. 1
Meteorological Society of Japan

An Analysis of Tropical Wind Fields in Relation to Typhoon Formation over the Western Pacific

By Yurie Heta

Disaster Prevention Research Institute, Kyoto University, Uji, Kyoto 611, Japan
(Manuscript received 29 May 1989, in revised form 24 November 1989)

Abstract

The characteristics of the upper (200 mb) and the lower (850 mb) tropospheric wind fields for the period between July and October 1980 over the tropical western Pacific are analyzed, focusing on typhoon formation. GMS satellite wind data and rawinsonde data are used to produce the grid point wind fields. The MASCON model (Dickerson, 1978) was used to adjust the interpolated lower wind fields.

Most of the typhoons and tropical storms that occurred during 1980 originated from easterly wave disturbances in the ITCZ. The easterly wave disturbances move in a westward direction before recurving and propagating north and northeastward along the region of large high cloud amounts in which they develop into storm intensity. The origin of the wave disturbances is traced back to as far as near or east of the international date line. The intensity of a given wave disturbance in its early stage is not related to the intensity at its most developed stage. Whether the disturbance develops to tropical storm intensity or not is related to the large scale wind fields surrounding the disturbance. Development of easterly wave disturbances into tropical depressions and storms occurs around the area where the easterlies from the east are confluent with both the westerlies from the west and the southerly winds form the southern hemisphere. This confluence area moves eastward and westward over a period of 10 to 30 days and most of the typhoons and tropical storms appear when the westerly wind region expands eastward.

1. Introduction

The formation of typhoons, in spite of enormous efforts of past researchers, has not been clearly understood due to the deficiency of observational station data over the tropical region. Recent developments in wind vector analysis from geostationary meteorological satellite (GMS) images have increased the amount of wind information in this region.

According to early studies by Yanai (1961, 1968) and other research works, typhoon formation is considered to be correlated with easterly wave disturbances, while Fett (1968) examined the relationship with the intertropical convergence zone (ITCZ). In a more recent study the role of cloud clusters was investigated by Muramatsu (1985), and upper-level phenomena such as wave disturbances (Kuroda, 1981), the cold vortex (Shimamura, 1981) and the tropical upper tropospheric trough (TUTT; Sadler, 1976, 1978) were also examined. Love (1985) examined the cross equatorial flow in relation to typhoon developments while Nakazawa (1986) studied intraseasonal variations of cloud activities. Typhoon development related to the amplitude modulation phenomena of short-term tropical disturbances was investigated by Yamazaki and Murakami (1989). All of the above factors relating to typhoon development may not be independent of each other. However, from present knowledge, it is difficult to say which one or ones are the most important for typhoon formation.

In the present paper, typhoon formation in the equatorial western Pacific area was analyzed to clarify what factor is most closely correlated with typhoon formation, using the more reliable wind fields as the composite of the GMS wind vectors analyzed by the Japan Meteorological Satellite Center (JMSC) and land station data for 1980. This year was not an El Niño year and was classified into cold SST summer by Nitta (1987). Most of tropical storms, including typhoons, are generated in low latitudes of 8N~16N and this can be regarded as normal conditions. The development of 11 typhoons (maximum wind speed $\geq$64 knots) and 5 tropical storms (34–63 knots) occurred from July to October of 1980. Besides these, during this period, thirteen tropical depressions ($\leq$33 knots) appeared over the western North Pacific area but did not develop into

tropical storms.

2. Data and method of analysis

GMS cloud wind vector data were acquired at the cirrus and the cumulus levels which correspond to the 200 mb and 850 mb level wind, respectively (Hamada, 1982). The station rawinsonde data at the 200 mb and 850 mb levels were incorporated into the upper and lower level satellite wind data. The wind fields at 00Z were mainly used for analysis during the period from July to October of 1980. When the number of observations at 00Z was sparse, the data at 12Z were additionally analyzed and substituted. On the average there were 250 wind data at the upper level and 290 data at the lower level for every map time in the equatorial area (20S–30N and 90E–170W). Approximately a half of them were land station wind data. Since the spatial distribution of the data was not uniform, they were interpolated to grid point data of $1^\circ \times 1^\circ$ in latitude and longitude using the interpolation method shown by Dickerson (1978). The interpolation formula for the wind field is as follows,

$$V_i = \sum_{j=1}^{N} V_{ij} exp(-\beta r_j{}^2) / \sum_{j=1}^{N} exp(-\beta r_j{}^2), \quad (1)$$

Where V_i is the calculated i-th (east-west or north-south) component of the wind velocity estimated at the grid point, V_{ij} is the i-th component of wind velocity at j-th station and r_j the distance from the grid point of j-th data of N closest observations. The constant β is the weighting parameter. After several numerical trials, values of 10^{-12} for β and 5 for N were chosen for the present study.

The interpolated fields of upper wind vectors were directly used for analysis. However, the lower level wind field obtained by the above mentioned manner is irregular owing to the low level wind complexity caused by the surface topography of large islands or continental peninsulas. Therefore, the lower level wind fields were readjusted or smoothed independent of the upper wind fields using the Mass Consistent Atmospheric Flux (MASCON) model developed by Dickerson (1978), based on the variational technique of Sasaki (see the lecture note, 1979).

This model basically adjusts the initial field to satisfy the mass continuity equation by a variational method. The variational function is expressed as

$$\begin{aligned} I &= \iint [\alpha_1{}^2(u-u_0)^2 + \alpha_1{}^2(v-v_0)^2 \\ &+ \alpha_2{}^2(w-w_0)^2 + \lambda\{\partial(hu)/\partial x \\ &+ \partial(hv)/\partial y + w\}]\, dxdy \end{aligned}$$

where λ is the Lagrangian multiplier, which is a function of the observational errors and deviations from the constraint. The Gaussian precision moduli $\alpha_1{}^2$ and $\alpha_2{}^2$ are related to the effects of horizontal and vertical velocities, respectively. The initial zonal, meridional and vertical velocity are given by u_0, v_0, w_0, respectively, and u, v, w, are the adjusted velocities. The depth of inversion layer is given as $h=H_{inv}-H_s$, where H_{inv} is the height of the inversion layer and H_s, the height of surface topography.

In this formulation, w represents outflow through the base of the inversion. The initial vertical velocity w_0 is assumed to be zero over the entire domain and values of u_0, v_0 are interpolated using Eq. (1). The height of the inversion layer is not measured and is assumed to be a constant value of 3100 m, slightly higher than the highest mountain in the domain. The lateral boundary condition is such that the adjusted velocities are equal to the observed values, which is satisfied by making λ to vanish at the boundary. The Gaussian precision moduli whose ratio is used to simulate the atmospheric stability, must be decided in advance. Although the results are very sensitive to the value of the ratio, $(\alpha_1/\alpha_2)^2$, there is no clearly formulated method to decide this value. After the following consideration, the value of 0.01 was adopted for the ratio $(\alpha_1/\alpha_2)^2$ in this study.

Statistically, $\alpha_1{}^2$ and $\alpha_2{}^2$ correspond to the reciprocal of the sum of the error variance of the observed and analytical values. Therefore, $\alpha_2{}^2$ is estimated from the integral of the square of the difference between the adjusted and observed vertical velocity, where the adjusted value is calculated with the proper initial value of α_2. Further, $\alpha_1{}^2$ is estimated from the sum of the meridional and zonal components of the wind velocity in the same manner as the vertical component. The process was iterated several times, and the final values of $\alpha_1{}^2$ and $\alpha_2{}^2$ were obtained.

On the other hand, the values of $\alpha_1{}^2$ and $\alpha_2{}^2$ can also be determined by minimizing the error variance, by changing the ratio of $(\alpha_1/\alpha_2)^2$. This method of determining the ratio is considered to be similar to that of Barnard and Weglay (1987). They found values of these parameters through an optimization procedure, In their results, the optimum values had an obscure relationship to the actual atmospheric stability, and the parameters varied with different cases. In the present study, however, the values of α_1 and α_2 are chosen to be constant as shown above, for every case, since the scale of the grid in this study is larger than theirs.

3. Typhoon tracks and flow patterns during July-October 1980

The distribution of four-month averaged amount of high cloud during the period from July to October, 1980 is shown in Fig. 1. This is obtained from the 5-day mean high cloud amounts derived from a histogram of infrared equivalent Black Body

Temperature (T_{BB}) data by GMS within a 1° latitude/longitude area. Cloud amount is given as the ratio (multiplied by ten) of the number of cloud pixels to the total number of pixels in the area. The amount of high cloud is estimated from the cloud pixels whose T_{BB} are lower than the air temperature at the 400 mb level. The amount of high cloud defined in this way is shown to be a good indicator of convective activity and the rate of precipitation over the tropical oceans (Nitta, 1987). The high convective activity area (≥ 2) extends zonally between 5N~10N, corresponding to the ITCZ. A branch of high clouds extends south-eastward crossing the equator to the east of New Guinea (around 5S, 155E). This branch is a part of the so called South Pacific Convergence Zone (SPCZ). Another high cloud is located in the Bay of Bengal.

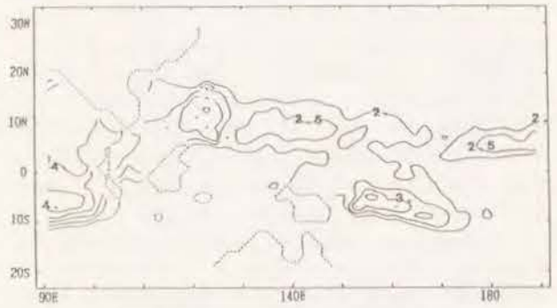

Fig. 1. Four-month mean high cloud amount over July, August, September and October 1980. Contour interval is 0.5 and the contours greater than 2.0 are drawn.

During the period of the present analysis, 29 tropical depressions were formed with 16 developing to above tropical storm intensity (TS), 11 of which reached typhoon intensity (T). The tropical storms (including typhoons) are numbered by the JMA for each calendar year. The 13 tropical depressions (TD) which did not develop to tropical storm intensity were labeled separately from A to M for the purposes of this paper. They are hereafter termed "non-developing cyclones", while both typhoons and tropical storms are termed "developing cyclones". Developing and non-developing cyclones are together termed "tropical cyclones" in this paper. The paths and the positions of all of the tropical cyclones at 09JST are shown in Fig. 2.

Most of the tropical cyclones first appeared in the area around 140E–160E, 5N–20N and moved west-northwestward and then recurved to the east around 20N~30N. Some non-developing cyclones appeared in the far west area of 140E compared with other cyclones and move west-northwestward, and tracked over land and weakened. It required about 1 to 3 days for tropical depressions to develop into tropical storm intensity and about 2 days for tropical storms to reach typhoon intensity. The tropical depressions traveled less than 10° of longitude along the northwestward path before they developed to tropical storm intensity.

In order to study the relationship between the wind field and tropical cyclone formation, 10-day mean wind fields were compiled from the daily wind fields described above. The 10-day mean was chosen to be long enough to eliminate the effect of small scale tropical disturbances on the mean flow. They

Fig. 2. Tracks of tropical cyclones between July and October in 1980. Large open circles, closed circles and circles with a dot show the position where the wave disturbance develops into a tropical depressions, tropical storm and typhoon intensity, respectively. Small open circles show the positions at 00Z.

are shown in Fig. 3 for both the 850 mb and 200 mb levels. In this figure the area of 10-day mean high cloud of amount greater than 4 is also shown by contour lines with the wind flow pattern.

The upper level wind fields reveal conspicious anticyclonic outflow from regions of large high cloud amounts. In general, the center of the outflow is located near the equatorial region east of the 140E line, except for the cases when the cloud regions shifted northward (Fig. 3g, 3i). At the end of July (Fig. 3c), the cloud area around 10N is broken and a new cloudy area is seen around 22N, 153E. There appear two centers of outflow in this case. One is around 28N, 150E and one is around 10N, 170E. In August(Fig. 3d, 3e, 3f) and early October (Fig. 3j) the upper tropospheric trough can be distinguished around the north-east region of the analyzed area. This trough was located north or northwest of the center of the outflows.

On the other hand, the lower wind fields are characterized, as seen in the beginning of the analyzed period in July (Fig. 3a, 3b), by westerlies from the western part of the analysis area, easterlies from the eastern boundary and southerly winds from the southern hemisphere. These flows converge in the area 0~20N and 120E~140E, and then propagate northward, forming the cloudy region that extends from the southeast to the northwest in the equatorial region. In early September (Fig. 3g), the westerly wind region together with south-westerly region is located to the north and as far east as the 140E line, while the cloudy region moves slightly north. During mid October (Fig. 3j) the westerly wind region is no longer observed, and the area is dominated by easterly wind at the end of October. In this period, southerly winds increased and the convergence area shifted to 0~10N and 120E~160E. In October it appears that the position of the cloudy region and the centers of outflow in the upper layer shift slightly south, however, the seasonal changes are not very pronounced.

4. Variations in the wind fields and formation of tropical cyclones

4.1 Zonal wind in the zone around 10N

In the previous section it was found, in most cases, that low level westerlies and easterlies in the zone 5N~15N along with the flow from the southern hemisphere converge at a certain point and flow into the higher latitudes. This convergence area mostly coincides with the center of high clouds. From this high clouds region anticyclonic outflows are seen in the upper level wind field. The time-longitudinal sections of the averaged zonal wind between 5.5N and 12.5N for lower and upper wind fields are shown in Fig. 4. The thick lines in these figures indicate the longitudinal positions of tropical cyclones within the zone from 5N to 30N. The small closed circle is the point of first appearance of a tropical depression. This occurs at the time of the intensification of the lower westerly wind, near the eastern boundary of the westerly region. The large closed circle is the point where a tropical depression developed into a tropical storm, which is seen near the boundary in lower westerly region. On the other hand, in the upper wind fields, it is in the easterly wind region. Slightly east of the convergence zone in the lower wind field, a divergence point in the upper wind field can be found.

4.2 Divergence and vorticity fields

In the preceeding subsection, it was shown that the majority of tropical depressions develop into tropical storms at the eastern boundary of the westerly wind region in the lower wind fields. The boundary of westerlies and easterlies in lower wind fields may be considered as the boundary of tropical zonal circulation cells. Most of the tropical cyclones propagate westward, even in the region with westerly winds at the lower level. The majority of the developing cyclones can be traced upstream in the zone of easterly wind. Therefore, the origin of the tropical cyclones should be located in the easterlies, even though their development is affected by large scale tropical zonal circulations.

Divergence and vorticity fields are compared for the lower and upper wind fields in time-longitude sections in Figs. 5 and 6. From these figures, westward propagation of divergence and convergence zones can be seen crossing the boundary of the lower westerly and easterly winds. Around a tropical cyclone, convergence at lower level and divergence at upper level are seen. Most of tropical cyclones can be traced far to the east, and some of them to the eastern boundary of analysis region at 170E. The westward propagation is more clearly seen in the relative vorticity fields. Lower positive and upper negative vorticity regions are moving westward with tropical cyclones, and these regions are seen before their appearance as tropical depressions such as the cases for TS8007, T8008, T8009. These regions appear at the same longitudinal position with an interval of 3 to 6 days and move westward with a speed of about 5~10° longitude per a day. These disturbances appear to have similar characteristics of horizontal divergence, relative vorticity and meridional wind distributions (not shown) that may correspond to those of the so-called easterly wave disturbance shown in Reed and Recker (1971).

4.3 Day to day changes in the westward moving disturbances

The horizontal structure of the wave disturbance is seen in the daily position of its vorticity and divergence fields shown in Fig. 7 for the case of Typhoon 8009. An example of divergence and vorticity fields at 200 mb is shown in 7a and 7b, respectively. The

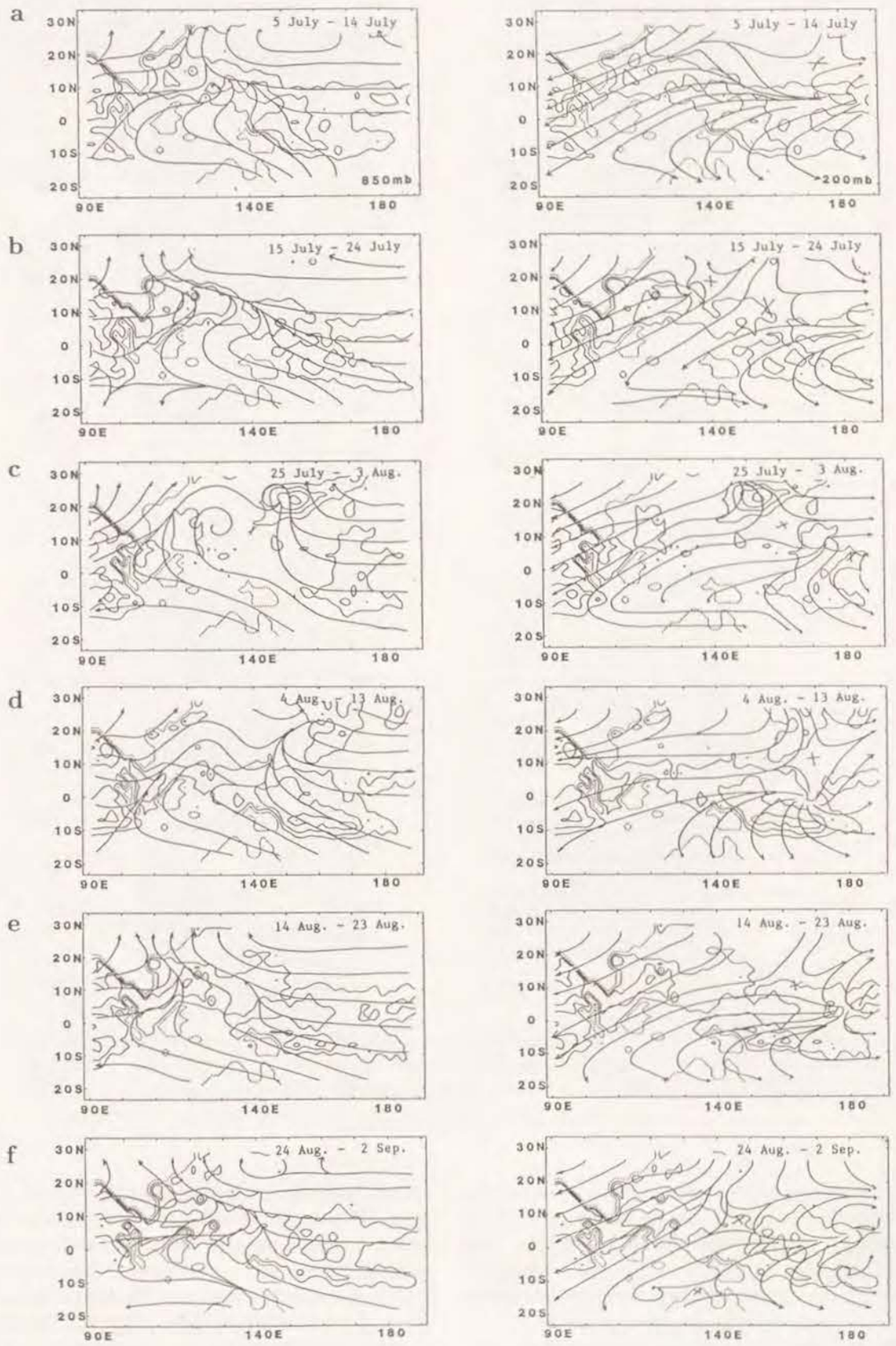

Fig. 3. 10-day mean 850 mb (left) and 200 mb (right) level streamlines and distributions of high cloud amount (≥4). Contour interval is 2.

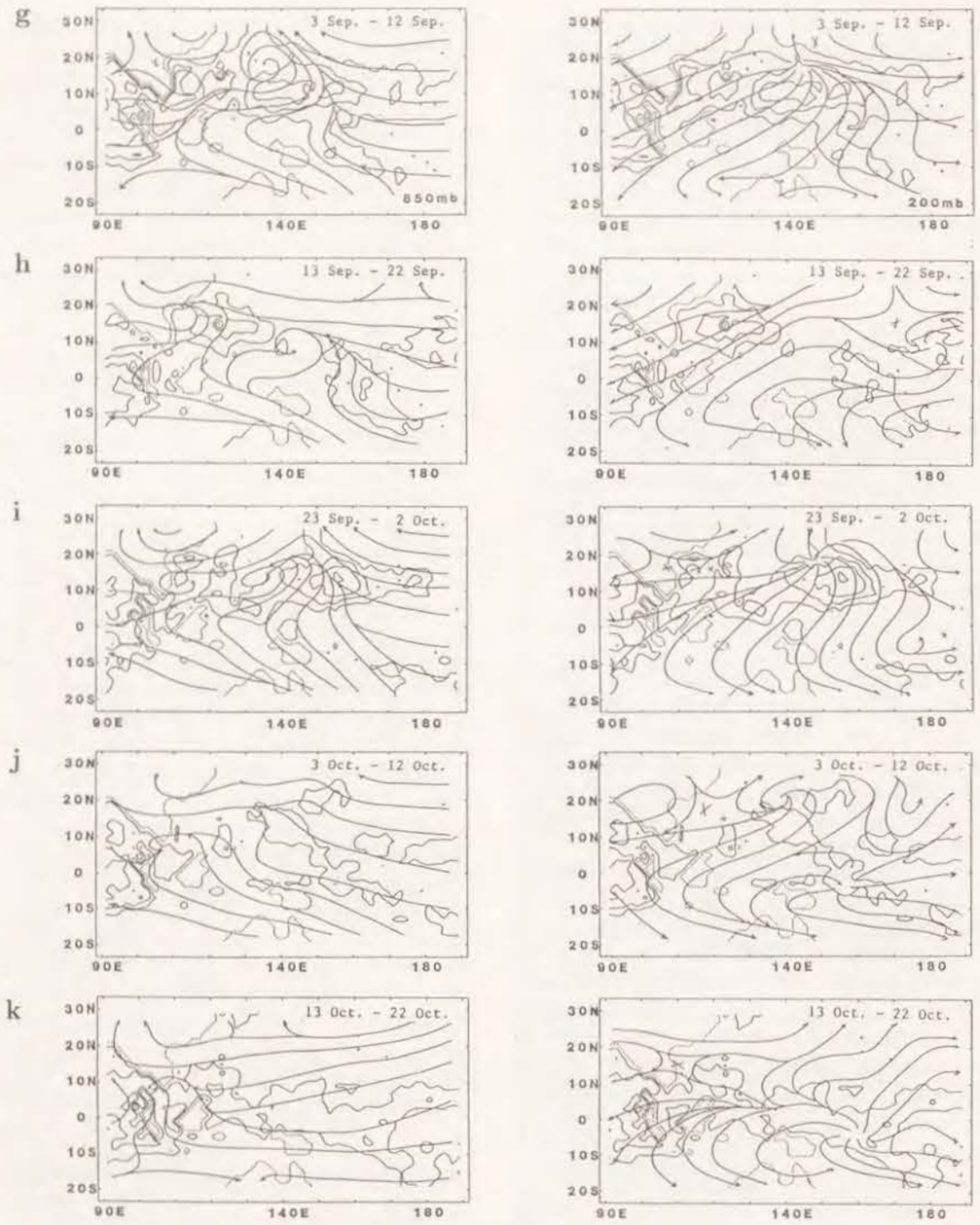

Fig. 3. (Continued)

daily positions of regions of divergence greater than a threshold value at 200 mb is shown in Fig. 7c, while Fig. 7d and 7e show relative vorticity at 200 mb and 850 mb, respectively. The daily positions of the tropical cyclone are superimposed on these figures. As suggested by the cross sectional analysis, the disturbance can be traced back to the region around 170E, 5N on September 17th, about 3 days before the reported formation of the tropical depression shown in Fig. 2. A small westward moving region of upper divergent and lower positive vorticity is seen corresponding to a large cloud cluster found in cloud images. The upper negative relative vorticity region is found several degrees east of the location of the tropical depression on September 20th and moved to 5° ~10° north of the tropical cyclone's positions on the 21th. At 200 mb, positive vorticity regions are located northwest of negative vorticity regions.

The positions of the disturbance shown in the upper and lower divergence and vorticity fields (Fig. 7) do not strictly coincide with the position of the cyclone, but are seen to move westward together with

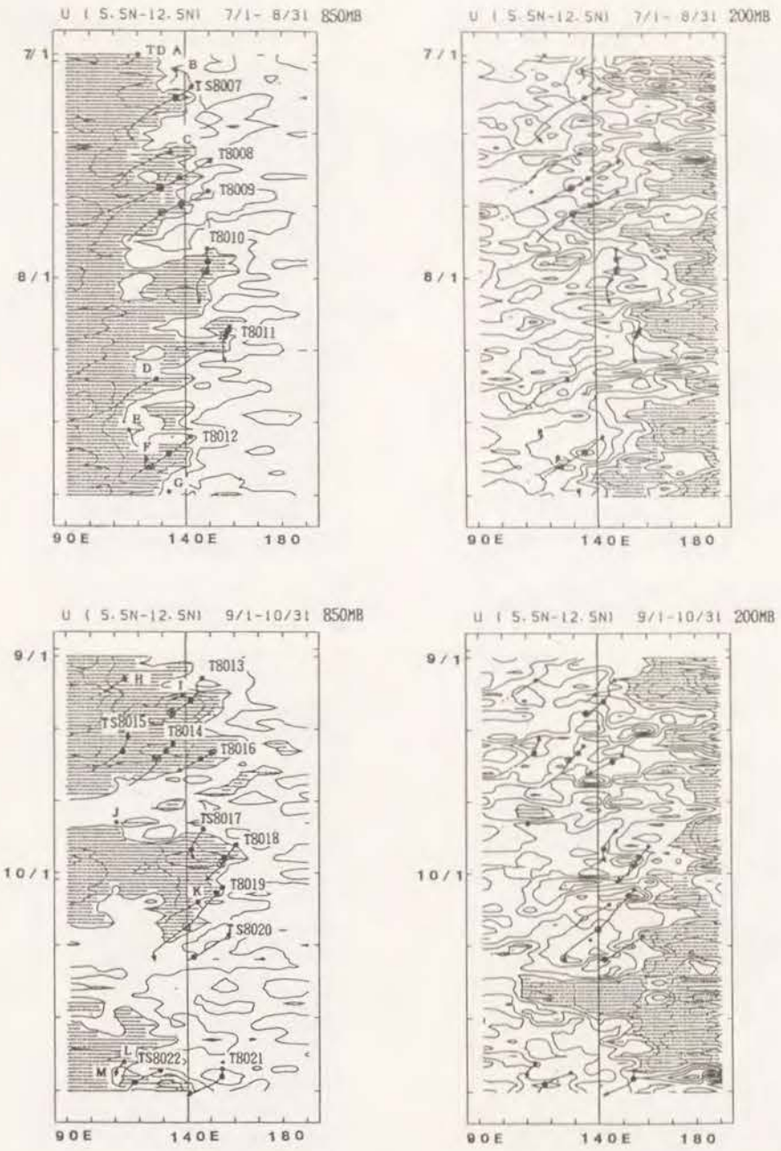

Fig. 4. Time-longitude sections of the zonal wind component averaged between 5.5N and 12.5N at 850 mb (left) and at 200 mb (right). The contour interval is 5 meters. Regions of positive values are shaded. Thick lines denote the longitudinal positions of tropical cyclones during the period. Symbols are the same as in Fig. 3, but large open circles are replaced by small closed circles.

the tropical cyclone. Accordingly, the rough trace of the initial disturbance before developing to a tropical depression is defined from the movement of these regions for most developing cyclones and two non-developing cyclones, These trace give rough paths of the initial wave disturbances which later develop to tropical depressions. They were plotted in Fig. 8, distinguishing typhoons from other tropical cyclones that did not develop to typhoon intensity. Most of the initial disturbances of tropical cyclones are seen first near the date line along 5N~15N zone, and move westward. Some initial disturbances such as T8010, T8011 are seen first near 30N and move southwestward. The tracks and the intensity of the initial disturbances of non-developing cyclones, tropical storms and typhoons, shown in Fig. 8, are not distinct enough to predict whether or not they later develop into typhoons.

5. Discussion

In the previous section it is shown that most of the initial wave disturbances of tropical cyclones are

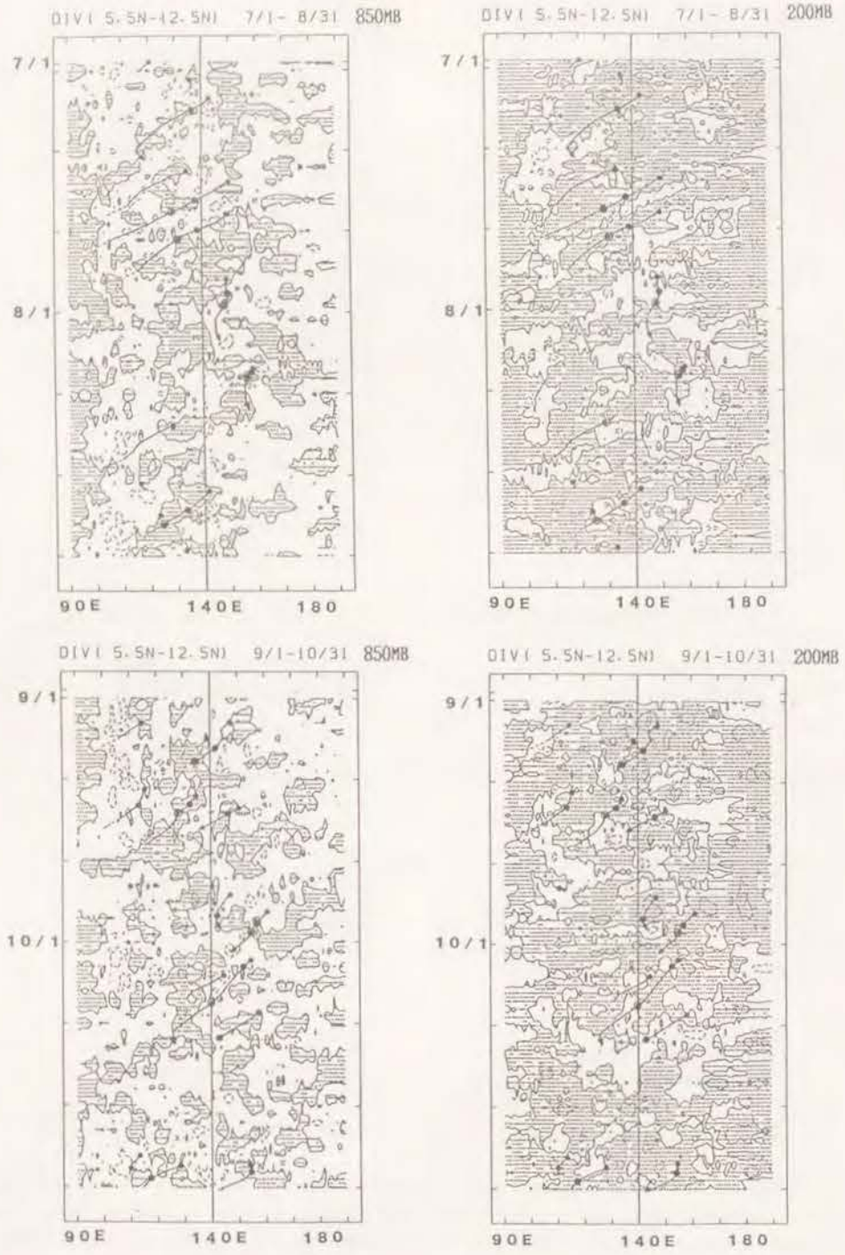

Fig. 5. Time-longitude sections of horizontal divergence between 5.5N~12.5N. The contour interval is $10 \times 10^{-6}(\mathrm{sec}^{-1})$ at 850 mb and 20×10^{-6} at 200 mb. Shaded regions denote positive values. Broken lines denote contours of negative values. Thick lines and symbols are same as in Fig. 4.

first seen around the international date line and, moving westward along the ITCZ, develop into tropical depressions near the convergence region of the zonal circulation at lower level. This zonal circulation is similar to one shown by Madden and Julian (1971, 1972), although they studied deviation fields. The axis of the ascending current, suggested by convergence and divergence of the lower and upper zonal wind fields (Fig. 4), tilts to the east with height.

The trajectories of the initial wave disturbances which later develop to tropical depressions are seen in Fig. 8. In relation to the path of the most intense tropical cyclone, Nitta and Takayabu (1985) analyzed wave disturbances in the tropics, using the 1979 FGGE IIIb data, and suggested the existence

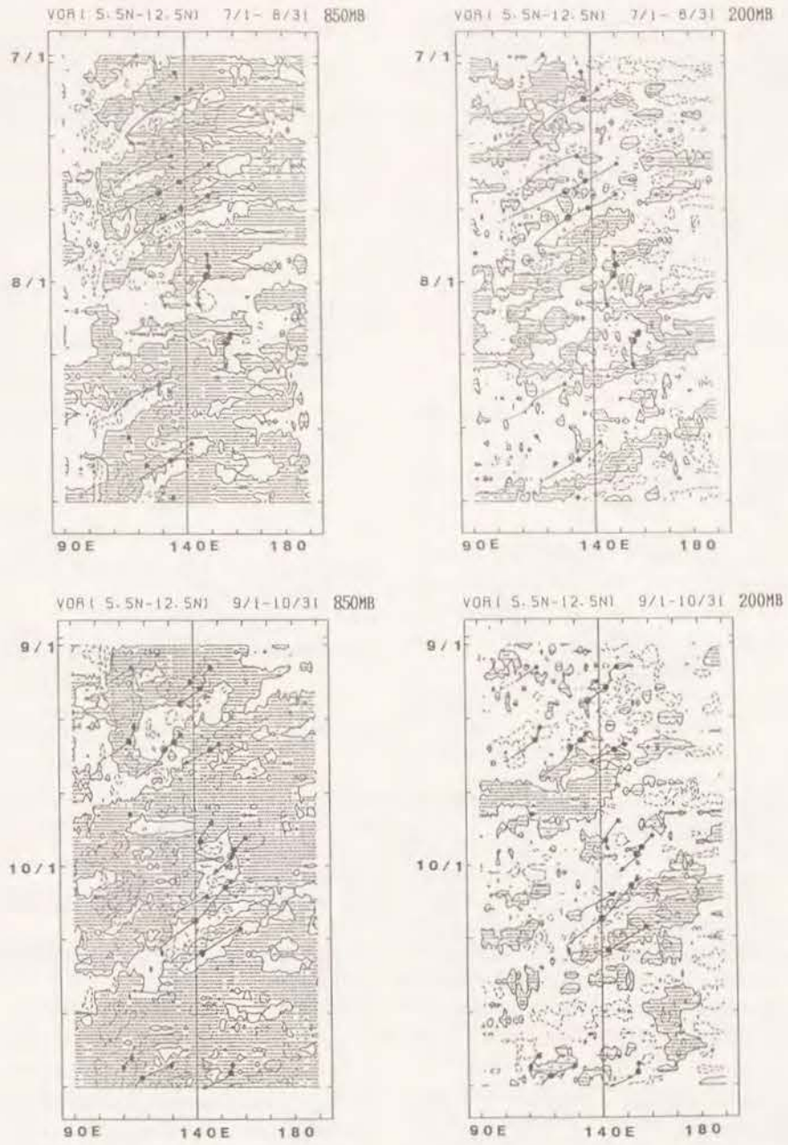

Fig. 6. Time-longitude sections of relative vorticity between 5.5N~12.5N. The contour interval is $10 \times 10^{-6}\mathrm{sec}^{-1}$ at 850 mb and $20 \times 10^{-6}\mathrm{sec}^{-1}$ at 200 mb. Shaded regions denote positive vorticity. Thick lines and symbols are same as in Fig. 4.

of two generating regions for tropical cyclones in the western Pacific. One is located in the area centered around 5N and 170E and the other is in the central Pacific east of the date line. They indicated that tropical disturbances generated in the former region eventually develop to tropical storm intensity, while those in the latter region did not. They also stated that the disturbances accompanying cyclones that develop into tropical storms are not connected with the easterly waves propagating along the ITCZ in the central Pacific. The trajectories of initial wave disturbances in the present analysis are shown in Fig. 8, distinguishing typhoons from other tropical cyclones that did not develop to typhoon intensity. However, it is not clear from this figure that the trajectories of the two types of wave disturbances can be separated. Judging from the streamlines and cloud distribution, there is no reason to suppose that tropical storm generation is not connected with the ITCZ for the cases in 1980. The track and the intensity of initial disturbances before they develop to the level of tropical depressions are not distinct enough to predict whether or not they later develop into typhoons. Foster and Lyones (1988) stressed,

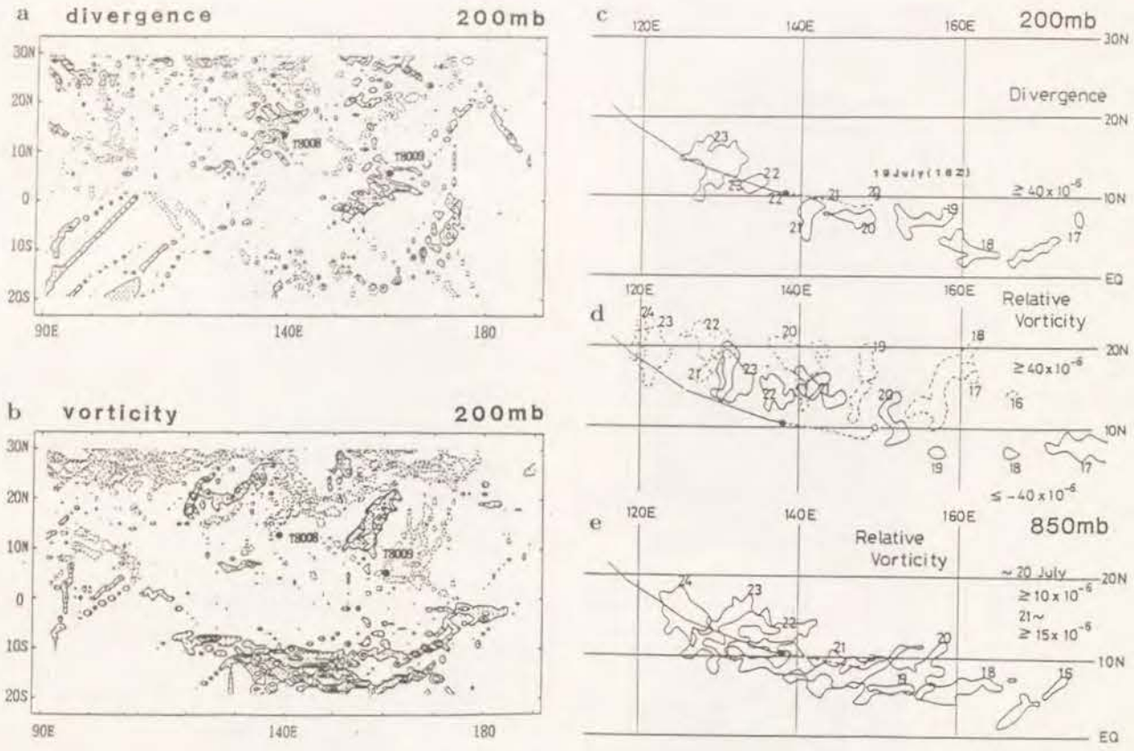

Fig. 7. (a) 200 mb horizontal divergence field at 00Z on 18 July 1980. The contour interval is 20×10^{-6}sec^{-1} and the area greater than 20×10^{-6}sec^{-1} are shaded. Closed circles denote the positions of tropical depression and initial wave disturbance which later developed into typhoons.
(b) 200 mb relative vorticity field. Contours and circles are the same as in (a).
(c) Position of 200 mb divergent region (greater than 40×10^{-6}sec^{-1}) at 00Z, which relates to Typhoon KIM (8009). The solid line indicates the trajectory of the typhoon.
(d) Position of 200 mb positive relative vorticity region (broken lines) and negative regions (solid lines). Regions less than -40×10^{-6}sec^{-1} or greater than 40×10^{-6}sec^{-1} are drawn.
(e) Position of 850 mb positive relative vorticity. Before 20 July, greater than 10×10^{-6}sec^{-1} regions are drawn while after 21 July, greater than 15×10^{-6}sec^{-1}.

through case studies of tropical cyclones which appeared during the austral summers of 1979/1980 and 1980/1981, that disturbances having a stronger low-level cyclonic circulation often did not develop afterwards. Their results are consistent with the present findings that the values of relative vorticity of the disturbances are not related to later development.

In the present study the origin of the trajectories of the wave disturbances is near the eastern edge of the present analysis region, and some of them may originate further east. Studies over a larger region are required to clarify the origin of these wave disturbances.These easterly wave disturbances are closely related to the tropical cyclones as shown above by the time longitude sections of meridional wind, divergence and relative vorticity fields.

In the formation of a tropical cyclone, it is suggested that the features of the wind fields surrounding the area where the wave disturbance grows into a tropical depression play an important role in its development, even though the very origin of the disturbance may be related to an easterly wave disturbance. From the analysis of the daily 850 mb wind field, the positions at which tropical disturbances develop into tropical cyclones are classified into three cases. (a) The most typical case is the location where the easterlies, westerlies and south-westerly winds converge. These conditions are often found together with wave disturbances propagating from an eastern area. (b) The region west of 120E and north of the lower westerly region. Many of the disturbances appeared in this area were non-developing cyclones. (c) The area north of the easterlies near 20N. Fig. 9 displays a schematic view of these positions along with the average wind field pattern.

These areas locally correspond to those shown by Muramatsu (1985) for tropical storms during 1978 and 1979. In his study, the cases corresponding to

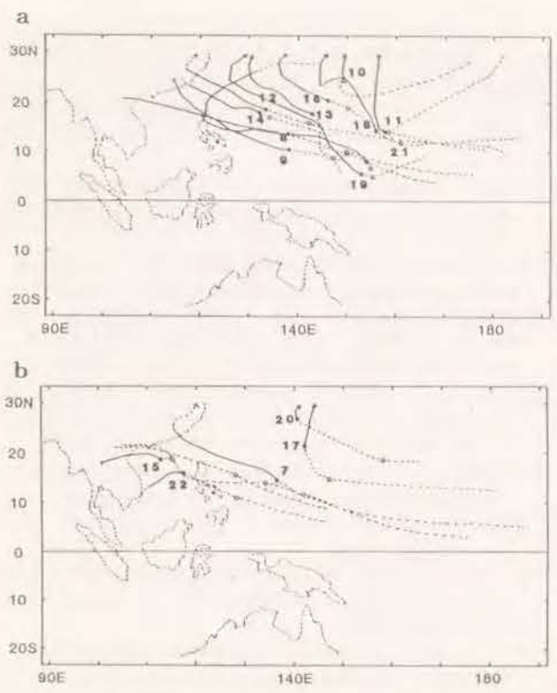

Fig. 8. (a) Trajectories of wave disturbances which later developed into typhoons during the period from July to October 1980. Open circles denote the location where they became tropical depressions and closed circles denote the position where they became tropical storms. Numerals denote the number of the tropical storms.
(b) As in (a), except for those which did not develop into typhoons.

(c) are explained in relation to the upper cold vortex while the cases related to (a) are explained as a coupling of the upper level easterly waves along 20N and a cloud cluster within the ITCZ. Pertaining to the upper level easterly wave development, Kuroda (1981) suggested that when an upper level cold vortex moves south, intensifying the ridge, the wave is strengthened. In the present study, the structure of temperature fields is not analyzed, leaving a more detailed study to the future.

In relation to type (a), the tropical cyclones appear when the region occupied by lower westerlies extends eastward. The point of lower convergence or upper divergence changes its position with a period of 10 to 30 days. This fact is thought to coincide with the results by Nakazawa (1986) that the tropical cyclones form during the active phase of the intraseasonal variations of outgoing long wave radiation (OLR). Tropical depressions develop into tropical storms (shown by large closed circles in Fig. 4) when they encounter the lower westerly wind region or the region of ascending air. Most of the tropical cyclones move westward in the lower westerly region with the same velocity of the convergence region. Although an individual tropical cyclone moves towards the west, the points of first appearance of tropical depressions translate eastward with a constant interval, such as the series TD C - T8008-T8009, and TS8015-T8014-T8016. The lower southwesterly maintained and enlarged eastward by the tropical cyclone at the western position might be favour to the development of another tropical cyclone in the east.

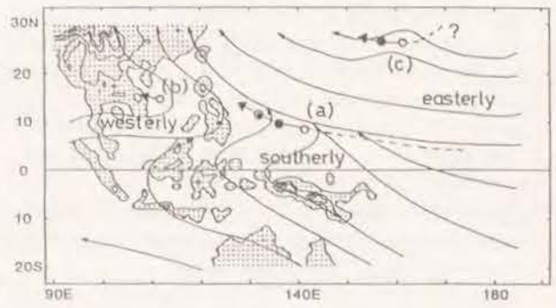

Fig. 9. Schematic depiction of 850 mb streamlines and the position of the formation and development of tropical cyclones. Broken lines show the trajectories of disturbances before becoming tropical depressions. Symbols are the same as in Fig. 3.

Low level south-westerly winds flow from the southern hemisphere, turning from a south-easterly direction around the equator. As pointed by Love (1985), these southerly winds are thought to be important in typhoon development. The position where these southerly winds change their direction is west of 140E and tropical cyclones develop over the regions where these southerly winds and zonal winds converge. There may be some local effects caused by the mountain range of New Guinea on southerly wind flow. Analysis of a larger area that includes the southern hemisphere as well as the eastern Pacific is expected to support the above results.

6. Conclusions and remarks

The results of the present analysis of typhoon formation in the western North Pacific can be summarized as follows. The origin of most tropical cyclones are easterly wave disturbances in the ITCZ which can be seen as the areas of large amounts of high cloud. Their origin can be traced back to near the date line. Their paths change north or south, following the region of large high cloud amounts.

The intensity of the initial wave disturbance of a tropical cyclone is not related to its most developed level of intensity, but the large scale wind field surrounding the wave disturbance is related to its de-

velopment to tropical storm intensity. The point at which a disturbance develops is where the easterlies from the east are confluent with both the westerlies from the west and southerlies from the southern hemisphere. This convergence point moves eastward or westward with a period of 10 to 30 days and tropical cyclones often develop when the region of westerlies expands eastward. South-westerly winds are observed, especially west of 140E where many tropical storms develop into typhoons.

Relating the results with the points of tropical cyclone formation mentioned in the introduction, it reveals that easterly wave disturbances along the ITCZ are important as the origin of the tropical cyclones. Cross equatorial flow in the form of a southerly wind is often found in the region where the disturbances develop into tropical depression or storm intensity and appears to be quite important for typhoon development. The area where the easterlies, westerlies and southwesterly winds converge moves to the east and west. Many of the easterly wave disturbances develop into tropical depressions when the region of westerlies expands eastward. These facts may be related to intraseasonal variations and the amplitude modulation of short-term tropical disturbances.

Further analysis over a larger area, including the southern hemisphere, central Pacific and mid latitudes is required to confirm the present results and to clarify the mechanism of typhoon formation.

Acknowledgements

The author would like to thank Professor Y. Mitsuta for his continuous guidance and encouragement. The author is also grateful to Professor Y.K. Sasaki, University of Oklahoma, for his valuable suggestions concerning the parameters of the MASCON model. Thanks are due to Dr. N.K. Sanga and Mr. N. Nishi for their help in compiling the satellite wind data and rawin sonde data. The author is indebted to the Japan Information Service Co. for their support in the MASCON programing.

References

Barnard, J.C. and H.L. Wegley, 1987: Improving the performance of Mass-Consistent Numerical Models using optimization techniques. *J. Clim. Appl. Met.*, **26**, 675–686.

Dickerson, M.H., 1978: MASCON-Mass Consistent Atmospheric Flux Model for regions with complex terrain. *J. Appl. Meteor.*, **17**, 241–253.

Fett, R.W., 1968: Typhoon formation within the zone of the intertropical convergence. *Mon. Wea. Rev.*, **96**, 106–117.

Foster, I.J. and T.J. Lyones, 1988: The development of tropical cyclones in the northwest of Australia. *Quart. J. Roy. Meteor. Soc.*, **114**, 1187–1199.

Hamada, T., 1982: Representative heights of GMS satellite winds. *Meteor. Satellite Center Technical Note*, **6**, 35–47.

Kuroda, Y, 1981: Convective cloud band associated with easterly wave, *Meteor. Satellite Center Technical Note*, **4**, 21–42 (in Japanese).

Love, G., 1985: Cross-equatorial interactions during tropical cyclogenesis. *Mon. Wea. Rev.*, **113**, 1499–1509.

Madden, R.A. and P.R. Julian, 1971: Detection of a 40–50 day oscillation in the zonal wind in the tropical Pacific. *J. Atmos. Sci.*, **28**, 702–708.

Madden, R.A. and P.R. Julian, 1972: Description of global-scale circulation cells in the tropics with a 40–50 day period. *J. Atmos. Sci.*, **29**, 1109–1123.

Muramatsu, T., 1985: *A study on the changes of the three dimensional structure and the movement speed of the typhoon through its life time.*, Tech. Rep. Meteor. Res. Inst. No.14, 117pp.

Nakazawa, T., 1986: Intraseasonal variations of OLR in the tropics during the FGGE year. *J. Meteor. Soc. Japan*, **64**, 17–34.

Nitta, T., 1987: Convective activities in the tropical western Pacific and their impact on the Northern Hemisphere summer circulation. *J. Meteor. Soc. Japan*, **65**, 373–390.

Nitta, T. and Y, Takayabu, 1985: Global analysis of the lower tropospheric disturbances in the tropics during the northern summer of the FGGE year part II : Regional characteristics of the disturbances, *PAGEOPH*, **123**, 272–292.

Reed, R.J., and E.E. Recker, 1971: Structure and properties of synoptic-scale wave disturbances in the equatorial western Pacific. *J. Atmos. Sci.*, **28**, 1117–1133.

Sadler, J.S., 1976: A role of the tropical upper tropospheric trough in early season typhoon development. *Mon. Wea. Rev.*, **104**, 1266–1278.

Sadler, J.S., 1978: Mid-Season typhoon development and intensity changes and the tropical upper tropospheric trough. *Mon. Wea. Rev.*, **106**, 1137–1152.

Sasaki, Y.K., 1979: *Lecture notes on variational methods for environmental analysis and prediction problems.* Severe Storm Research Notes, **1**, Disaster Prevention Research Institute, Kyoto University, 174pp.

Shimamura, M., 1981: The upper-tropospheric cold lows in the northwestern Pacific as revealed in the GMS satellite data. *Geophys. Mag.*, **39**, 119–156.

Yamazaki, N. and M. Murakami, 1989: An intraseasonal amplitude modulation of the short-term tropical disturbances over the western Pacific. *J. Meteor. Soc. Japan.*, **67**, 791–807.

Yanai, M., 1961: A detailed analysis of typhoon formation. *J. Meteor. Soc. Japan*, **39**, 187–214.

Yanai, M., 1968: Evolution of a tropical disturbance in the Caribbean Sea region. *J. Meteor. Soc. Japan*, **46**, 85–109.

台風発生に関係する熱帯域の流れの場の解析

邊田有理江

（京都大学防災研究所）

熱帯太平洋上の上部および下部対流圏の流れの場の解析を台風発生と関連して行った。期間は1980年7月から10月である。GMSの衛星風データとゾンデのデータをもとに緯度経度1度の格子点でのデータを内挿し、下層については2次元MASCONモデルによる補正を加えて求め、それを基に解析した。

その結果、1980年の多くの台風はITCZ上を西進する偏東風波動擾乱にその起源を求められ、擾乱は日付変更線付近まで相対渦度場等でさかのぼれた。発達する以前の擾乱の強さはその後の擾乱の発達には関係せず、台風に発達していくかどうかにはその擾乱をとりまく大規模な場が重要であることが示唆された。多くの擾乱が熱帯低気圧、台風へと発達していくのは、下層の西側の西風域、東側の東風域が接する付近で、その付近へは南半球から南西風が吹き込んでいた。西風東風域の境界は10日から30日の周期で東西に移動しており、西風域が東へひろがったとき台風が発生発達する傾向がみられた。

The Origin of Tropical Disturbances in the Equatorial Pacific

By Yurie Heta
Disaster Prevention Research Instutute, Kyoto University,
Uji, Kyoto 611, Japan

(Manuscript received 30 July 1990, in revised form 29 March 1991)

Journal of the Meteorological Society of Japan
Vol. 69, No. 3
Meteorological Society of Japan

The Origin of Tropical Disturbances in the Equatorial Pacific

By Yurie Heta

Disaster Prevention Research Institute, Kyoto University, Uji, Kyoto 611, Japan
(Manuscript received 30 July 1990, in revised form 29 March 1991)

Abstract

Tropical wave disturbances, which later developed into tropical storms over the equatorial Pacific (110E~90W, 30S~30N), are analyzed using the satellite and rawinsonde wind data in July and September, 1980. Daily wind fields at upper (200 mb) and lower (850 mb) levels on grid of $1^\circ \times 1^\circ$ are composed and analyzed in relation to tropical storm development. There were 10 tropical storms during these two months in the western Pacific, and 5 of them are analyzed, their initial wave disturbances coming from a far-eastern area in the western hemisphere, except one which appears in higher latitudes. The four tropical storms developed from the easterly wave disturbances, which travel with easterly wave of about 5 day in period along 10N line from the eastern Pacific, around 150W. With the westward movement of easterly wave disturbances, the upper cold lows are cut off from the Mid Pacific Trough in the middle latitudes at about 150W and move westward along 20N. The upper cold low is located north to north–east of the easterly wave disturbances in the early stage, but it is seen in the north–west portion of the easterly wave disturbance in the western Pacific.

These tropical disturbances in the western Pacific, as well as those in the eastern Pacific around 110W, develop into tropical storms when they encounter the ascending motion of the zonal circulation cells, which are seen around 140E and 110W. The position and the strength of the zonal circulation cell changes with some periodicity in relation to intraseasonal variation. The subsidence motion is suggested around 140W for the western cell, and the initial wave disturbances of typhoons are first recognized to the west of this subsidence.

1. Introduction

It has been recognized and widely accepted, since the early studies of Riehl (1948, 1954), that not a small number of tropical cyclones develop from pre-existing disturbances such as easterly wave disturbances. Yanai (1961, 1963, 1968) made case studies of the development of tropical storms from easterly waves. Many kinds of studies have been done to explain the wave-like disturbances using a variety of analytic methods. Reed and Recher (1971) showed the vertical structure of the wave disturbances in the equatorial western Pacific using the composite method. In their results, convergence predominates at low levels, upward vertical motions and strong divergence centered at the upper level were reported near the trough axis. As for vorticity fields, positive vorticity in the trough in the lower troposphere (900~700 mb), and negative vorticity above the surface northerly wind area west of the trough axis were shown.

The rapidly increasing quantity and quality of wind data from satellites provides invaluable information for understanding the tropical phenomena over the stationless ocean area. Nitta and Takayabu (1985) analyzed the characteristics of the wave disturbances in the tropical lower troposphere using the First GARP Global Experiment (FGGE) analyses for 1979. From the 850 mb analyses, clear northwestward propagation of disturbances are shown from about 5N, 165E toward the East and South China seas. They also studied the trajectories of cyclonic vortices at 850 mb and recognized two kinds of paths of disturbances, one is located along the Intertropical Convergence Zone (ITCZ) and the other located from near equator around 165E extending northwest. Their developments into typhoons are more often recognized for the northwestward propagating disturbances. Lau and Lau (1990) described the tropical wave disturbances during the northern summer with twice-daily ECMWF global gridded analyses for the 1980–1987 period using various techniques, such as lag-correlation and regression statics and Extended Empirical Orthogonal Function (EEOF) techniques. In their results, clear northwestward propagation of disturbances are revealed west of 160E in the 850 mb level analyses.

Muramatsu (1985) showed as the result of detailed case studies of the characteristics of cloud clusters of many tropical storms, that there are close relations between cloud clusters along 10N and wave distur-

bances in the upper troposphere along 20N. These upper tropospheric wave disturbances are accompanied with the westward-moving upper cold lows (Sadler, 1976, 1978, Shimamura, 1981, 1982) with periods of 4~5 day and wavelengths of 3000~4000 km. These cold lows were cut from the westerly trough (Shimizu, 1983) or the Mid Pacific Trough (MPT). Muramatsu (1985) showed that cloud clusters in the (ITCZ) had organized in the southern extension of the ridge area of a westward-traveling easterly wave along 20°~25° latitude.

In the previous paper, Heta (1990) analyzed tropical cyclones, which appeared during the summer of 1980 over the western Pacific, based mainly on the Geostationary Meteorological Satellite (GMS) wind data. The disturbances were detected from the mean position of the positive vorticity and convergence regions at the 850 mb level and negative vorticity and divergence regions at the 200 mb level. It was shown that westward-moving easterly wave disturbances along the ITCZ from the region near the date line, the eastern end of GMS visual field, are the initial disturbances of most of those tropical cyclones. However, there remained some uncertainties about the origins of these initial disturbances. The easterly wave disturbances originate in a far eastern equatorial area. Analysis including the data over the central Pacific east of 170W in both the upper and lower troposphere was performed.

The main purpose of the present study is to clarify the trajectory and the origin of easterly wave disturbances in the eastern part of the Pacific, which later develop into tropical storm intensity or above, and to determine the horizontal structure of the disturbances for both divergence and vorticity fields at upper and lower tropospheric levels.

The second purpose is to study the relations between wave disturbances usually analyzed at 850 mb level and the wave-like disturbance in the upper troposphere along 20N north of the ITCZ in the upper troposphere shown by Muramatsu (1985), and determine whether the wave disturbances along 20N make any contribution to the development of typhoons or not. On this point, Shimamura (1981) showed as the results of case studies that one of the cold lows eventually became a warm core disturbance, and pointed out that the upper cold low and the low-level disturbances were interacting with each other. The analysis for the whole Pacific area at the 200 mb level may reveal interactions between initial disturbances and disturbances located about 10° north.

The third purpose of the present study is to reanalyze the large-scale wind fields surrounding the development of tropical storms over the whole Pacific. In the previous analysis (Heta, 1990), it was shown that the development of the tropical storms into typhoon intensity occured near the area of as-

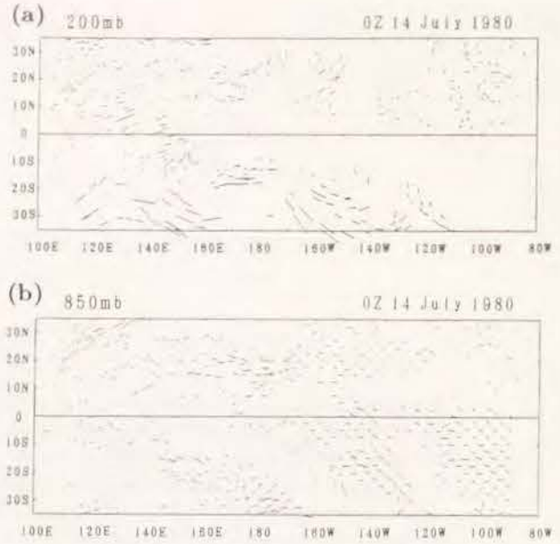

Fig. 1. Distributions of observational wind data at (a) the 200 mb level and (b) the 850 mb level at 00Z on 14 July, 1980.

cending motion of a large-scale zonal wind cell.

These points are analyzed using the Geostationary Observational Environment Satellite (GOES) at 135W and GMS at 140E wind data for the whole equatorial Pacific area (110E~90W, 30S~30N) and others in July and September, 1980 as shown in the next section.

2. Data and analysis

The data and the method of analysis are similar to those in Heta (1990), except for enlarging the area of analysis toward the east by adding the GOES satellite wind data. The upper (200 mb) and lower (850 mb) tropospheric wind fields at 00 GMT were mainly prepared based on GMS and GOES cloud wind vectors and the station rawinsonde data at the 200 mb and the 850 mb levels, respectively. GOES wind data at 21 or 22 GMT of the previous days were mingled with other data without correction. The analyzed area of the present study has expanded to the whole equatorial Pacific, 30S~30N and 110E~90W.

Figure 1 shows an example of the distribution of the original wind data in the area 35N~35S, 105E~85W used to interpolate the wind fields on the grid of 1°×1° in longitude and latitude. On average, there were original 550 wind data points at the lower level and 370 data points at the upper level. The interpolation formula was based on Dickerson (1978). The interpolated fields of upper wind vectors were directly used for the analysis. However the lower level wind fields were readjusted using the MASCON model (Dickerson, 1978). This model produces an adjusted wind field in such a way that the mass is conserved and the observational data

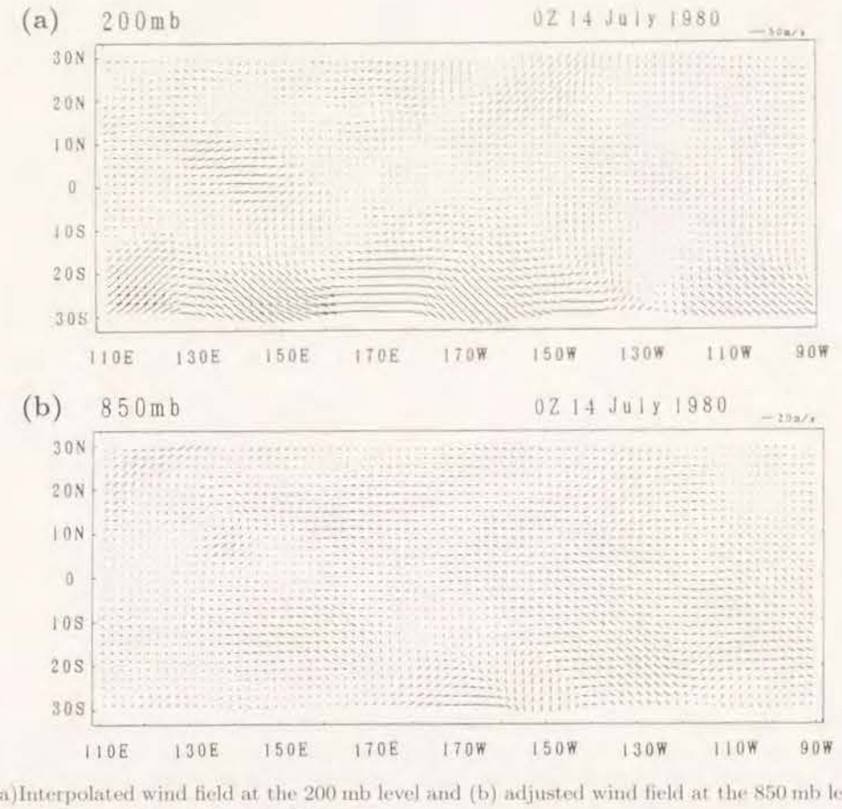

Fig. 2. (a)Interpolated wind field at the 200 mb level and (b) adjusted wind field at the 850 mb level using the MASCON model at 00Z on 14 July, 1980.

are changed in a minimal way, using spatially sparse wind data interpolated and/or extrapolated to the grid point. The accuracy of the wind fields are based on the number and distribution of observed wind data, which changes from day to day. The wind fields thus obtained are as shown in Fig. 2.

The averaged fields of sea surface temperature (SST), and water vapour transport over the same area and the same period are analyzed in another paper (Heta, 1991). The distribution of Outgoing Longwave Radiation (OLR) data obtained from NOAA polar orbiting satellites, that indicates high cloud activity, is used as the information on the convective activity. In 1980, equator crossings of the NOAA satellite were at about 7:30 a.m. and p.m. local sun time (Gruber and Krueger, 1984). Daily OLR data are calculated from these twice-daily data by averaging.

In Fig. 3, the distributions of monthly averaged OLR are shown with trajectories of tropical cyclones in July and September, 1980. The ITCZ is recognized as the low OLR region ($\leq 240\,W/m^2$) along the 10N zone. From 160E, another branch of low OLR regions extends southeastward, which indicates the South Pacific Convergence Zone (SPCZ). On July (Fig. 3a), cloud activity on the ITCZ is weak at 140W compared with western and eastern regions. Trajectories of tropical cyclones are located at the northern edge of the highest cloud activity regions.

Figure 4 and Fig. 5 show the monthly-averaged wind divergence field at the upper and the lower tropospheric level, respectively. At the 200 mb level, the divergence zone along 10N is prominent especially in September. The distribution of the divergence area is coincident with high cloud activity areas in Fig. 3. A southeastward-stretching branch of divergence area is notable centered at 160E. Convergence areas are located around 140W, 20N and from 150W to 90W along 10S in July and from 170W to 100W in September. On the other hand, at the lower level (Fig. 5), many convergence areas are scattered along the 10N zone. In the western region of 160E, the centers of convergence areas are located more equatorward compared with the eastern Pacific region. Roughly speaking, 850 mb and 200 mb levels have opposite values, which suggests the existence of Hadley Cells with upward motion along 10N and subsidence motion along 10S and 30N.

Figure 6 shows the monthly-averaged relative vorticity at the 200 mb level. A negative vorticity zone (shown by dashed lines) is extending on the western side of 180E along 10N. Positive vorticity areas are seen in the southern hemisphere and northern part

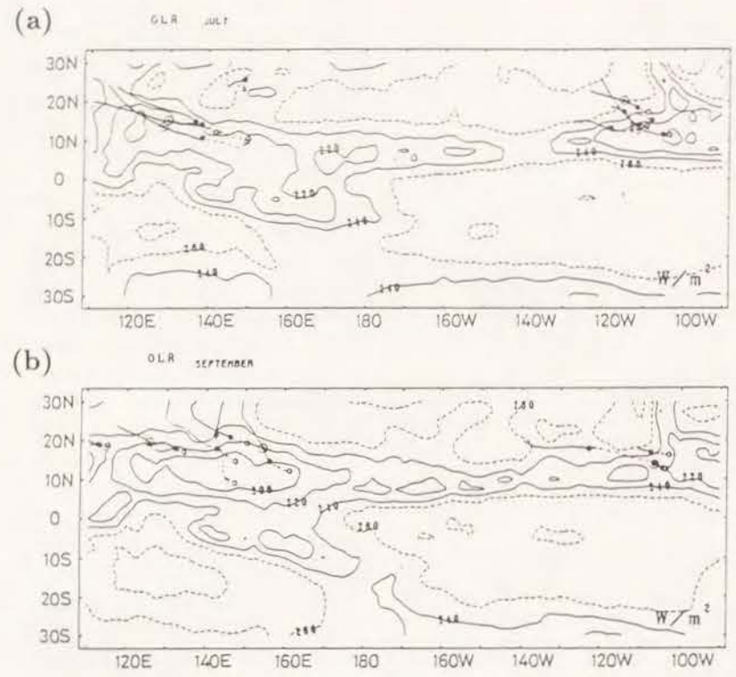

Fig. 3. Distribution of Outgoing Longwave Radiation (OLR) and trajectories of tropical storms on (a) July and (b) September, 1980. The contour interval is 20 W/m^2. Open circles, closed circles and circles with a dot indicate the positions where the disturbance reached the tropical depression (TD), tropical storm (TS) and Typhoon (T) or Hurricane (Hu) intensity, respectively.

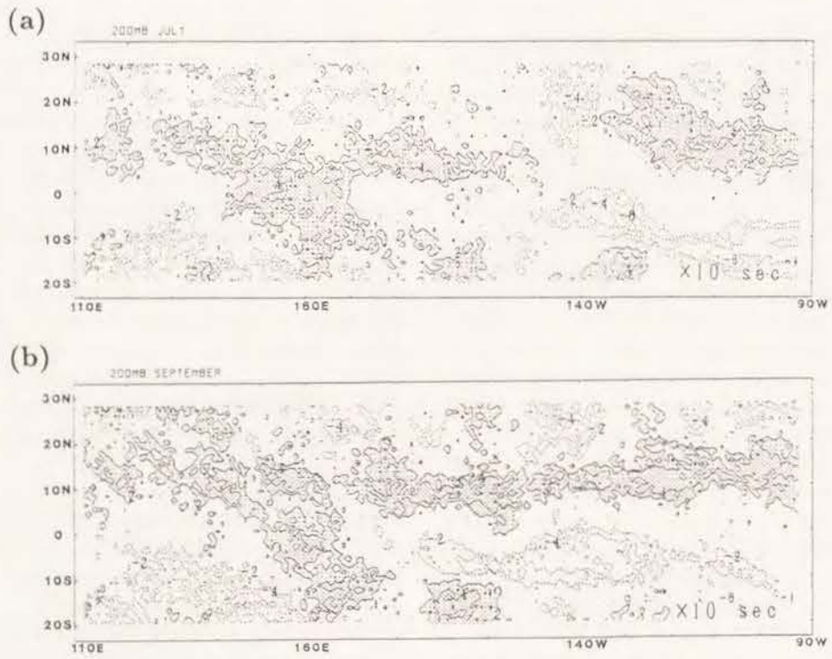

Fig. 4. (a) Upper-level monthly-averaged divergence fields for July, 1980. The contour interval is 2×10^{-6}sec^{-1}. The shaded area indicates a divergence area ($\geq2\times10^{-6}$sec^{-1}).
(b) As in (a), except for September, 1980.

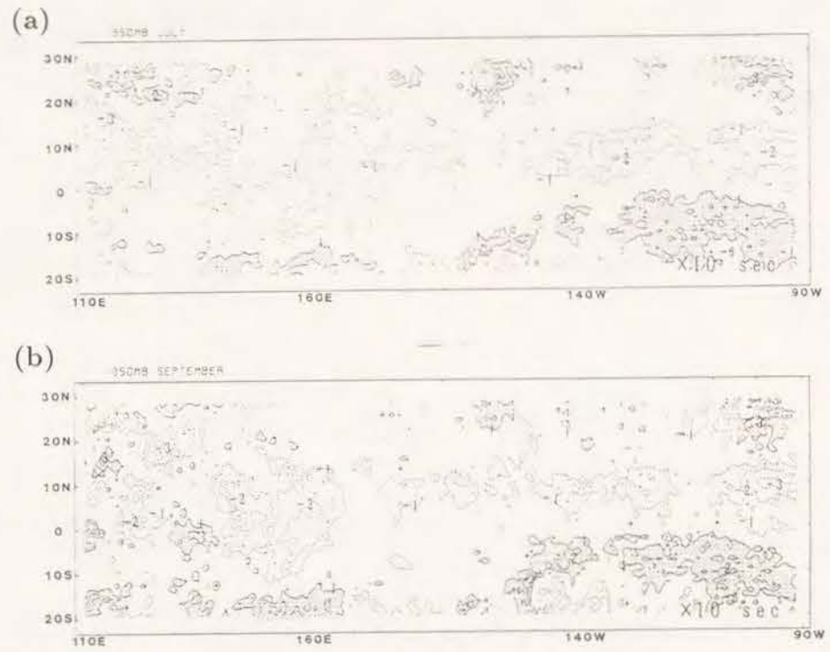

Fig. 5. (a) Lower-level monthly-averaged divergence fields for July,1980. The contour interval is 1×10^{-6}sec^{-1}. The shaded area indicates a divergence area ($\geq1\times10^{-6}$sec^{-1}).
(b) As in (a), except for September, 1980.

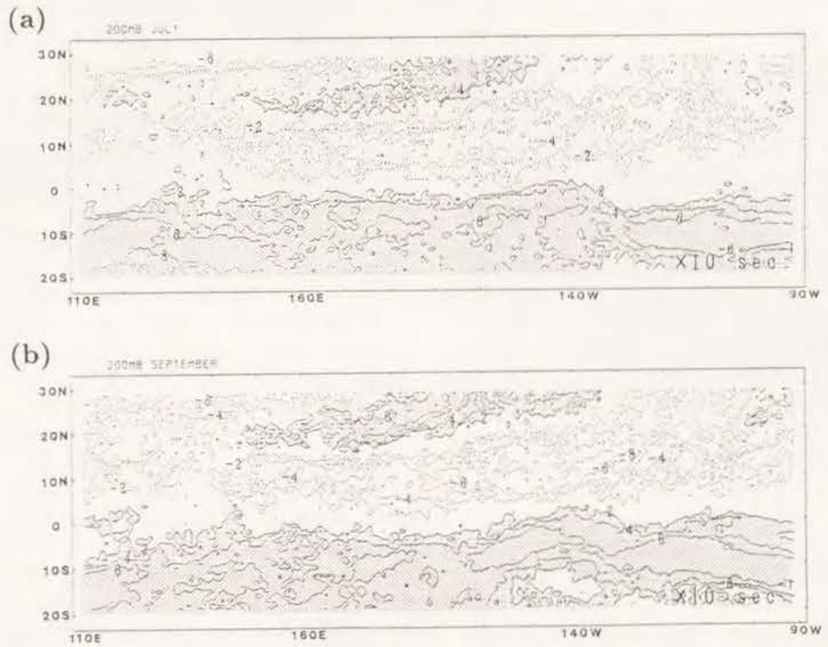

Fig. 6. (a) Upper-level monthly-averaged relative vorticity fields for July, 1980. The contour interval is 2×10^{-6}sec^{-1}. The shaded area indicates a positive vorticity area ($\geq2\times10^{-6}$sec^{-1}).
(b) As in (a), except for September, 1980.

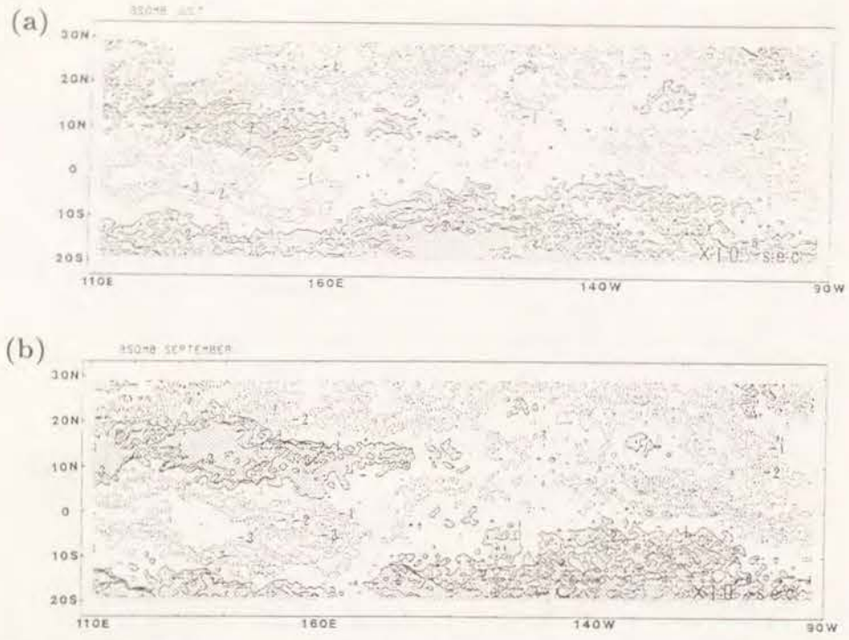

Fig. 7. (a) Lower-level monthly-averaged relative vorticity fields for July, 1980. The contour interval is 1×10^{-6}sec^{-1}. The shaded area indicates a positive vorticity area ($\geq1\times10^{-6}$sec^{-1}).
(b) As in (a), except for September, 1980.

from 150W, 30N to 150E, 20N in July and from 140W, 30N to 150E, 20N in September. The positive vorticity areas are thought to show the MPT and/or the trajectories of upper cold lows. The negative vorticity zone ($\leq-4\times10^{-6}$ sec^{-1}) is extending from 140W, 15N to 160E, 10N in July and from 120W, 30N to 150E, 10N in September at a distance of 10° or 15° in latitude southward of the northern positive vorticity zone. The monthly-averaged relative vorticity at the 850 mb level is shown in Fig. 7, in which a strong positive vorticity zone is seen from 160E, 10N to 120E, 15N in July and 180E, 10N to 110E, 15N in September. This zone has a width of 10° especially in September, and the location of this positive vorticity region agrees with the result by Lau and Lau (1990). It is interesting that the positive vorticity zone at the 850 mb level is clearly seen from the region where upper negative vorticity zone along 10N and positive vorticity zone along 20N are poorly defined.

3. The origin of easterly wave disturbances

There appeared 4 tropical storms (TS) in July, 1980, and 6 appeared in September in the western Pacific in 1980. Six of them developed into typhoons (T), and 4 of them were traced far back to the origin of the initial easterly wave disturbances near the south of Hawaii; the other 3 are of the same nature but originated in the earlier month. The easterly wave disturbances could be recognized on the daily map of divergence and relative vorticity field as the negative vorticity ($\leq-2\times10^{-5}$ sec^{-1}) and divergence ($\geq2\times10^{-5}$ sec^{-1}) area at the 200 mb level and the positive vorticity ($\geq1\times10^{-5}$ sec^{-1}) and convergence ($\leq-1\times10^{-5}$ sec^{-1}) area at the 850 mb level. These areas were successfully traced back to the east.

As an example, the positions of the early disturbance at 00Z for Typhoon 8009 (Kim) are shown in Fig. 8, which is the same case as shown in the previous study (Heta, 1990, Fig. 7). Figure 8a shows positions of the 200 mb negative relative vorticity regions on alternate days (thin solid lines), and axes and centers of positive regions (thick solid line and closed circle). Contours of -2×10^{-5} sec^{-1} are shown. Figure 8b shows the positions of the 200 mb divergent regions ($\geq2\times10^{-5}$ sec^{-1}) on the same days. Figure 8c and 8d show the positions of the 850 mb positive relative vorticity and 850 mb convergence regions.

Comparing these figures Fig. 8a~8d, the positions of negative vorticity regions at 200 mb, the divergence region at 200 mb, positive vorticity region at 850 mb and convergence region at 850 mb are close to each other, with some exceptions. The position of the disturbance may be determined as the averaged position of these four kinds of regions shown by thin closed curves in Fig. 8a~8d; the positions are shown by a small open circle for each day. These open circles are linked together by a broken line, which shows the trajectory of the disturbance. The regions are not found on the fields for some cases, such as the negative vorticity region on 12 July (Fig. 8a). For some other cases one kind of region is far from the other three kinds of regions. On 14 July, only the negative vorticity region is located near equator, far from the other regions. For these cases, the distributions of the observed data are so poor that we can not find any data near the disturbance.

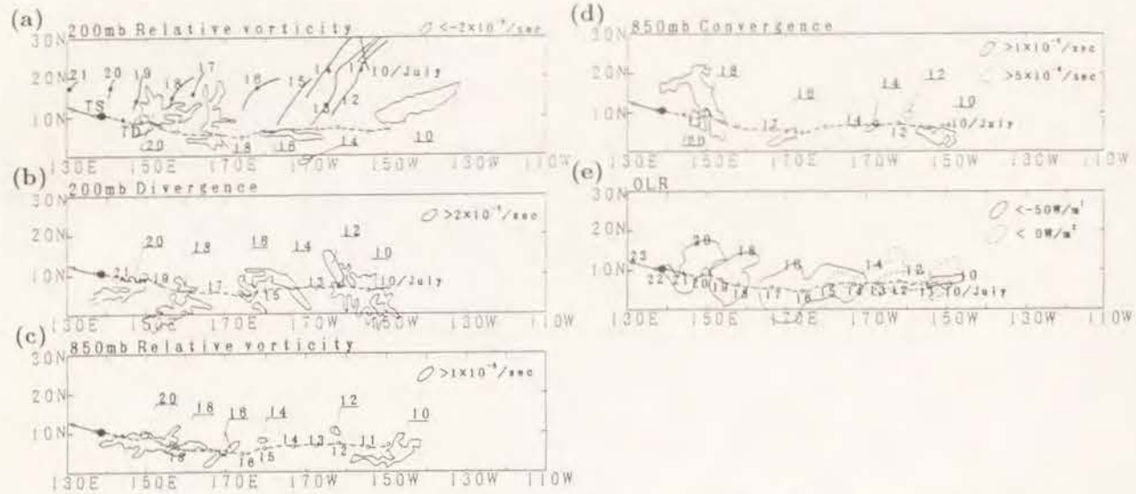

Fig. 8. (a) Position of 200 mb negative relative vorticity regions (thin solid lines) on alternate days, and the axis and center of positive vorticity regions (thick solid lines with closed circles) at 00Z, which relates to Typhoon Kim (8009). Regions less than -2×10^{-5}sec^{-1} and greater than 2×10^{-5}sec^{-1} are noted. Small open circles with smaller numerals show the daily positions of tropical disturbances at 00Z. Numerals mean day of each month. Large open circles and large closed circles indicate the positions where the disturbance had a TD and TS intensity, respectively. (○-18Z, 19 July, ●-18Z, 21 July).
(b) Position of 200 mb divergent regions (greater than 2×10^{-5}sec^{-1}) at 00Z on alternate days.
(c) Position of 850 mb positive relative vorticity regions on alternate days. Regions greater than 1×10^{-5}sec^{-1} are drawn using solid lines.
(d) Position of 850 mb convergent regions on alternate days. Regions greater than 1×10^{-5}sec^{-1} are drawn using solid lines and regions greater than 5×10^{-6}sec^{-1} are drawn using broken lines.
(e) Position of negative anomaly regions of OLR from monthly average on alternate days. The daily OLR data is obtained by averaging twice-daily data.

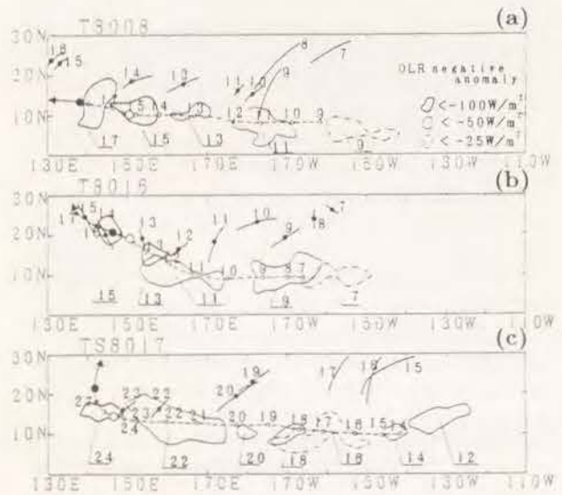

Fig. 9. Position of negative OLR anomaly regions on altenate days, which relate to (a) Typhoon 8008, (b) Typhoon 8016 and (c) Tropical Storm 8017. Thick solid lines and closed circles indicate the axes and centers of negative vorticity regions at the 200 mb level as in Fig. 8(a). Symbols are the same as in Fig. 8.

Figure 8e shows positions of the OLR negative anomaly from the monthly mean value on the same days. This figure shows that the disturbances detected by divergence and vorticity fields are thought to coincide with the region of high cloud activity. The magnitude of the OLR anomaly is smaller around 160W compared with regions in the western area, indicating that the disturbance has a less developed cloud system in early stage. This disturbance traveled about 7000 km in 10 days before it developed into a tropical storm. The disturbance was first recognized on July 10 and it developed into a tropical storm intensity on July 22, and into a typhoon intensity on July 23. Development from July 22 to 24 was very fast, the central pressure decreasing from 1000 mb to 950 mb within two days.

Figure 9 shows the positions of the OLR anomaly for other typhoons, T8008, T8016 and T8017. They are traced back to around 150W along 5~10N, though the absolute value of the OLR anomaly is

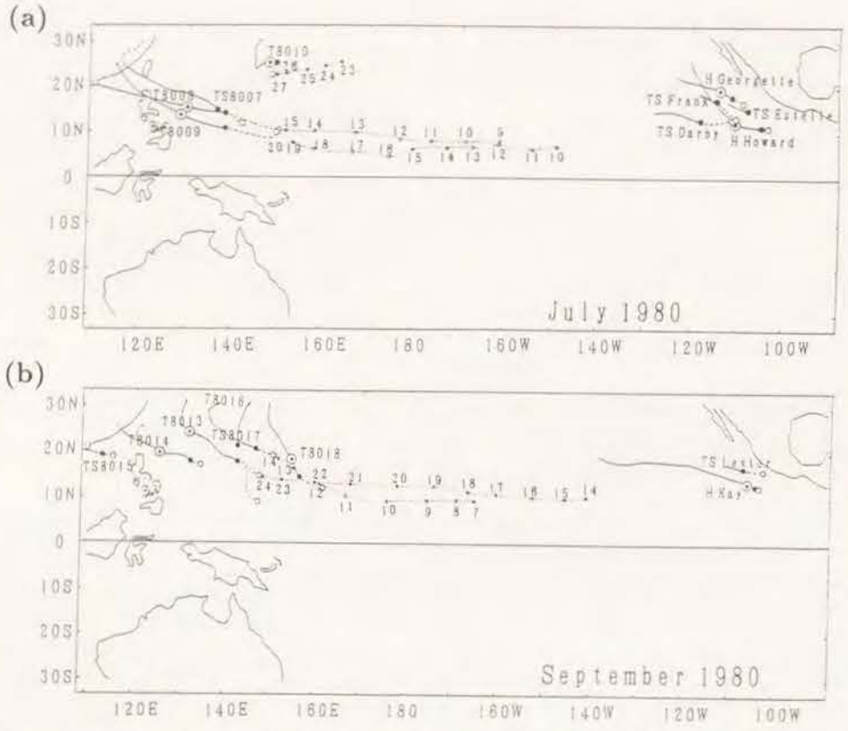

Fig. 10. Dotted lines show the trajectories of wave disturbances which later developed into tropical storms during (a) July and (b) September, 1980. Symbols are the same as in Fig. 8.

smaller in the region 170W~150W. For these typhoons, the positions of the easterly wave disturbances were decided to be the averaged point of the upper and lower divergent and vorticity regions for each day, just the same as for T8009 (Fig. 8). The summarized results of trajectories of all of the easterly wave disturbances, which later developed into tropical storms, are shown in Fig. 10. For typhoons T8008, T8009, T8016 and T8017, the initial easterly wave disturbances were traced back to around 150W.

T8010 was formed a little north compared with other typhoons. Its initial disturbance was traced back to around 170E, 30N, near the northern end of the analyzed area. During the period when T8010 was formed and developed the cloud band of the ITCZ along 10N was not clear, and the cloud band extended west-southwestward from north of 30N (Heta, 1990, Fig. 3c). The upper cold low could not be analyzed in relation to T8010, and might be located beyond the analyzed area.

Other tropical storms, which appeared in the same months in 1980, were all included on Fig. 10. Several tropical storms were formed in the eastern Pacific around 110W, 15N, moving westward or northwestward, and disappeared over the cold SST area in the north-eastern Pacific (Heta, 1991).

For many tropical storms in the eastern Pacific, the westward propagation of divergence and negative vorticity regions at the 200 mb level, and convergence and positive vorticity regions at the 850 mb level were also analyzed from 90W. For the hurricanes in the eastern Pacific, the existence of the initial wave disturbances similar to the wave disturbances in the western Pacific are also inferred, but their origins are outside and to the east of the boundary of the present analysis.

Westward propagation of the easterly wave disturbances was seen over a wide area, 90W~120W and 150W~110E, but they developed into tropical storms only in the area around 140E and 110W. In the next section, the characteristics of the positions where the tropical storms developed into hurricanes, and the points of origin of the easterly wave disturbances, were discussed for the whole Pacific region.

4. The origin and development of a tropical storm in relation to the large-scale wind field

In the previous section it was shown that the initial wave disturbances of tropical storms in the western Pacific were first seen around 150W, 10N and, moving westward along the ITCZ, developed into tropical storms around 140E. On the other hand, for the tropical storms in the eastern Pacific, westward moving initial wave disturbances were recognized from the eastern boundary of the analyzed area and developed into storms around 110W. In

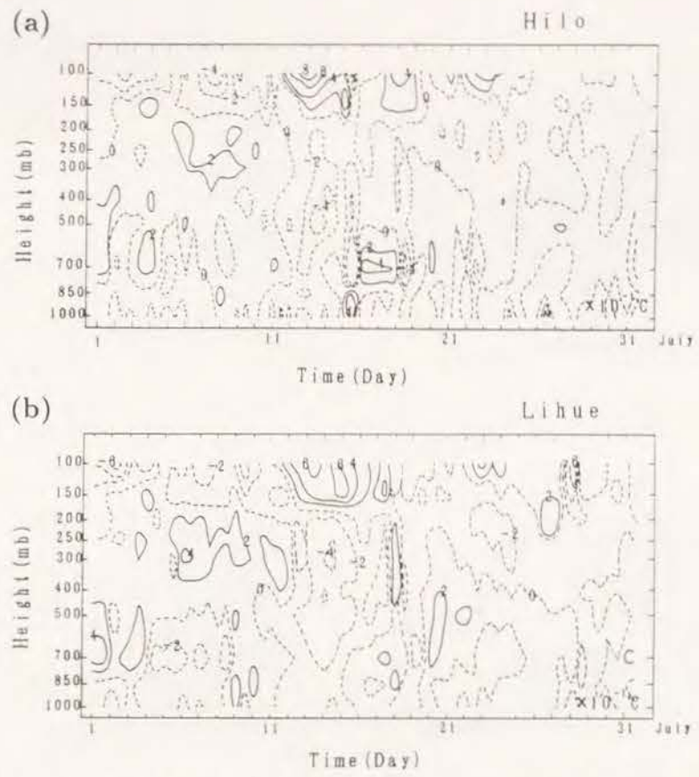

Fig. 11. The time cross section of temperature anomaly at (a) Hilo, and (b) Lihue. Solid and dashed lines show temperature positive and negative anomaly from the monthly mean for each island in July, 1980. The contour interval is 0.2°C.

this section the relation between the easterly wave disturbances along the ITCZ and disturbances along 20N at 200 mb level are first analyzed, and then the large-scale wind fields surrounding the easterly wave disturbances and tropical storms are studied.

As shown by the thick lines in Fig. 8a, the positive relative vorticity regions are recognized over the northern part of disturbances at the upper level. They were considered to denote the positions of the MPT or the upper-level cyclonic cell cut off from the extended trough. For the case of T8009, the easterly wave disturbance was located at the southern end of the upper trough in the period July 10 to 16. After July 17, the upper-level cyclonic cell was located to the northwest of the easterly wave disturbance and moved westward along 15~20N with almost the same speed as the easterly wave disturbance along 5~10N.

Figure 11a shows the time cross section of the temperature anomaly from the monthly mean value of July 1980 at Hilo (19.43N, 155.04W), which indicates the existence of a cold core of −0.4°C at 500 mb at12Z, July 13 and 400 mb at 00Z, July 14, and an intense warm core of +0.8°C at 100 mb at 00Z July 14. At Lihue station (21.59N, 159.21W) shown in Fig. 5b, the cold core of −0.4°C at 300 mb was seen on July 14, and an intense warm core of +0.6°C at 100 mb on July 13 and 15. The axis of the positive relative vorticity area extended far southwestward from the mid latitude as shown in Fig. 8a by the thick solid line. This temperature structure may correspond to the upper cold low discussed by Shimamura (1982). The vertical structure of the temperature anomaly shown in Fig. 11 was thought to be the structure of a part of the MPT. On the 500 mb map, we could identify a cut off of the trough on 13 July.

Westward motion of upper cold lows can also be recognized for three other tropical cyclones, as shown in Fig. 9. The axis of the positive vorticity regions are first detected around 150W, 25N, moving southwestward and then west or northwestward. The trajectories of these upper cold lows are also recognized as the positive vorticity region on the monthly averaged relative vorticity fields shown in Fig. 6. The upper cold lows are located in the northwestern portion of wave disturbances in the western Pacific by, at the latest, two days before the development into a tropical depression. This pattern of location is quite common for the development of tropical cyclones (Sadler, 1976, 1978, Shimamura, 1981, 1982). Positive vorticity regions become smaller and

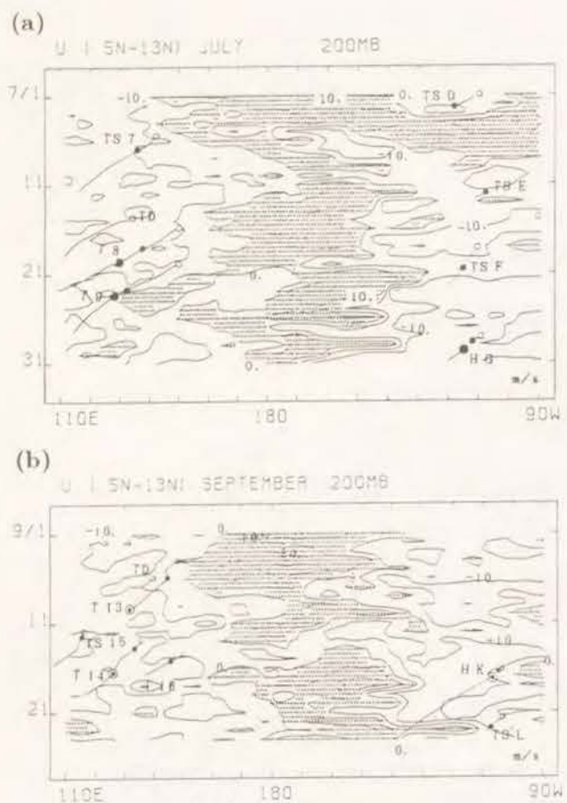

Fig. 12. Time-longitude sections of the zonal wind component averaged between 5N and 13N at 200 mb. The contour interval is 10 m/s. Regions of westerly wind are shaded. Thick lines and symbols are the same as in Fig. 3.

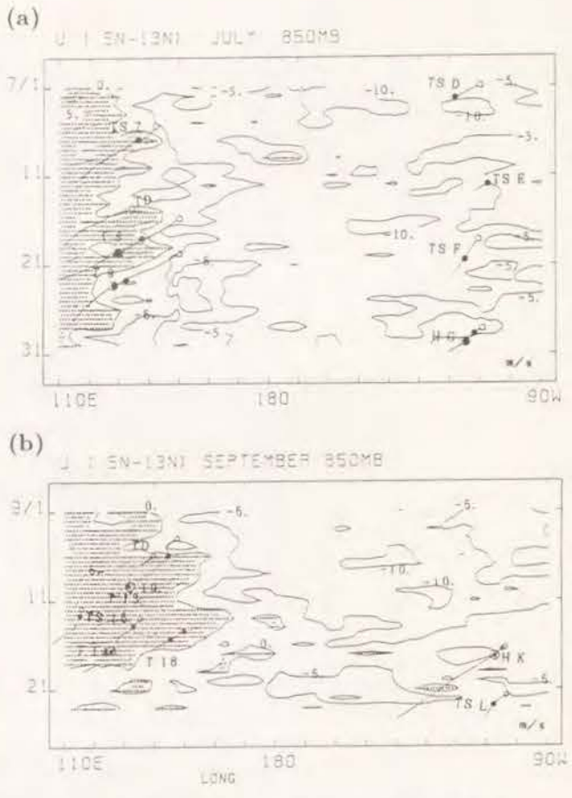

Fig. 13. As in Fig. 12 except at the 850 mb level.

rounder with the westward motion of the regions, and their value increases beyond 6×10^{-5} sec^{-1}.

In the large-scale wind fields, as discussed in Heta (1990) for the western Pacific, the strength of initial wave disturbances was not related with their later development into typhoons. The development of tropical storms was generally recognized around the triple confluent point of the easterlies from the east, the westerlies from the west and southerlies from the southern hemisphere at the 850 mb level.

Figure 12 shows the time-longitude sections of zonal wind at the upper level. At this level, the contour of 0 m/s between westerlies in the east and easterlies in the west is seen around 150E in the western Pacific, and 100W in the eastern Pacific. The points where the tropical depressions (TD) were formed and developed into storms (TS), are located in the easterly wind region a little west of the westerly wind region in both the eastern and the western Pacific. On the other hand, at the 850 mb level (Fig. 13), these positions of storm development in the western Pacific are near the contour of 0 m/s between westerlies in the west and easterlies in the east. However, in the eastern Pacific, only weak easterly winds are recognized.

Figure 14 shows the monthly mean zonal vertical wind shear between 200 mb and 850 mb for July and September, 1980. The points, where the initial disturbances develop into the tropical storms, locate in the areas of small zonal vertical wind shear in both the eastern and western Pacific. Along the zone of 10N, there are three points where the shear is zero, around 150E, 140W and 100W. But no tropical storm developments are seen around 140W, where convergence at the upper level is expected (Fig. 12). The existence of east–west circulations is suggested along 10N zone from Fig. 12, Fig. 13 and Fig. 14. Two zonal cells are seen over the Pacific, as suggested by Krishnamurti (1971) and Krishnamurti *et al.* (1973). The eastern cell is small and weak compared with the western cell. The development of the tropical storms is detected around the ascending motion of these zonal circulations.

The zero vertical shear around 140W is located roughly on the southeastward extension of the MPT. There are convergence areas around this point at the 200 mb level in July as shown in Fig. 4a, and

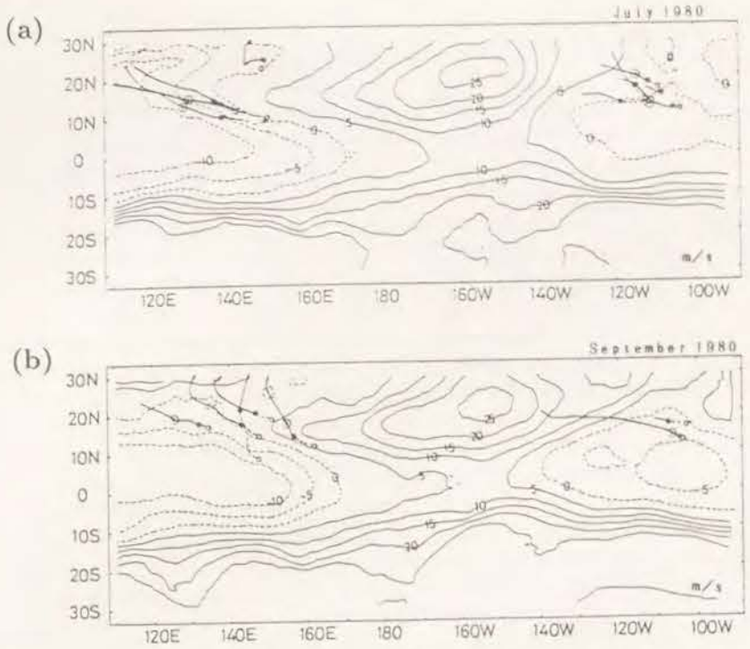

Fig. 14. Monthly mean values of the vertical zonal wind shear between 200 mb and 850 mb. Positive values indicate that the zonal wind at 200 mb is stronger from the west or weaker from the east than the zonal wind at 850 mb. Units are 5 m/s. Thick lines and symbols are the same as in Fig. 3.

the subsidence of air is suggested around this point.

5. Discussion

For September, however, there is the divergence region around 140W at 200 mb (Fig. 4b). At the 850 mb level (Fig. 5), a divergence area can not be seen because of strong convergence caused by the meridional wind confluence. Distinguishing the zonal divergence (du/dx) and meridional divergence (dv/dy) separately, in the same way as Sanga (1990), the region around 140W, 10N is the region of the convergence at the lower level and divergence at the upper level for the meridional component, but is the region of the divergence at the lower level and the convergence at the upper level for zonal circulation. Tropical storms or wave disturbances are not clearly identified around this area, where the ITCZ spreads over a relatively warm SST region. On the other hand, the regions centered 140E, 10N and 110W, 10N are the regions of the convergence at the lower level and the divergence at the upper level for both zonal and meridional components. Development of the tropical storms is seen around the large-scale ascending area of the zonal circulation along 10N over both the western and eastern Pacific.

This fact indicates that the wave disturbances initiating to the west of decending zonal circulation and moving westward along the ITCZ begin to develop into tropical cyclones when they move into the area of ascent of the zonal circulation.

Summarizing the present results, the lower and upper wind fields over the equatorial Pacific are schematically shown in Fig. 15. The middle figure shows the zonal and meridional circulation around the 10N zone, based on Figs. 4, 5, 12, 13 and 14. The origin of the initial wave disturbance in the western Pacific is found around 150W, 10N, near and west of the subsidence point of the zonal circulation cell and also to the south–east of the MPT. The subsidence region of the zonal cells around 140W, 10N is related with the boundary between the cyclonic cell in the Mid Pacific (Mid Pacific Trough) and the anticyclonic cell around 120W, 20N at the 200 mb level. We found both southwestward-moving positive vorticity regions from around 150W, 30N at 200 mb and westward-moving disturbances along 10N from 150W, 10N moving in time with each other. The starting point of rapid development into a tropical storm and typhoon is located around the lower converging and upper diverging point of the zonal circulation cell along the ITCZ, which is also on the lower converging zone of the meridional circulation cell. The same situation is also seen for the tropical storms in the eastern Pacific. The disturbances from the east of 90W develop into tropical storms at the ascending point of zonal circulation at 110W. When the initial wave disturbances move into the regions of ascending motion, they might gain the condition for fast development into tropical storms.

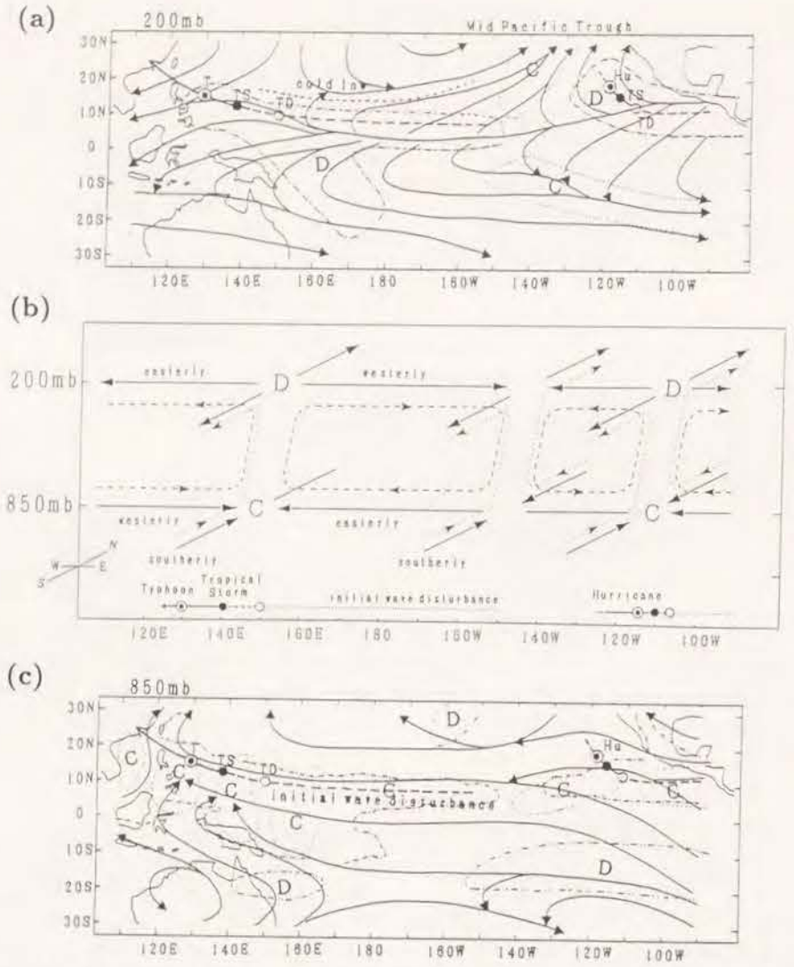

Fig. 15. Schematic view of streamlines at the 200 mb and 850 mb levels. The middle figure shows the zonal and meridional circulation cells along the 10N zone. C and D indicate convergence and divergence, respectively. Dotted lines, dash and double dotted lines and dash-dotted lines indicate convergence, divergence and low values of OLR ($<240\,W/m^2$), respectively. Symbols are the same as in Fig. 3.

The regions of the ascending air, which were recognized as the 0 m/s contour of the zonal wind around 140E in the time-longitude sections, moved west and east with some periodicity as shown in Figs. 12 and 13. Madden and Julian (1971, 1972) have shown that the global scale zonal circulation cells in the tropics change with 40–50-day period. Their result suggests that the intensity and the positions of zonal circulation cells or the positions of ascending motion are changing with an intraseasonal time-scale. The change in the positions of tropical cyclone development are thought to be strongly related to the intraseasonal variation of the large-scale wind field. Yamazaki and Murakami (1989) analyzed the intraseasonal change of the activities of tropical disturbances by the aid of the idea of amplitude-modulation of the easterly wave. They described from the composite analysis how the lower tropospheric westerly and the upper-level easterly are enhanced at the time of the enhanced activity of the tropical disturbances. This idea can be re-expressed in terms of the composition of the zonal circulation and meridional circulation in the present analysis. The forecasting of tropical cyclone development might be done by watching the daily change of the large-scale tropical wind field.

Love (1985) pointed that the southerly wind from the winter hemisphere influences the genesis of tropical cyclones in the summer hemisphere. He suggested in his scenario that a cold surge in the winter hemisphere, caused by mid-latitude cyclogenesis, propagates equatorward enhancing equatorial westerlies, and converges at a lower level. The southerly wind in the southern hemisphere might reinforce the east-west circulation. In the present analysis, a stronger southerly wind at the lower-level is recognized three to five days before the appearance of a tropical depression on daily wind fields (figures are not shown). Before the appearance of tropical depressions, a strong southwesterly is recognized to the southwest. Because of this strong southwesterly, convergence regions at 850 mb are extended not only along 10N but also southeastward to the south of the equator (Fig. 5). The convergence regions and positive vorticity regions at the 850 mb level are sometimes noticed to spread equatorward near about 160E (Fig. 8) about two or three days before the rapid development into tropical storms. This fact suggests the influence of the winter hemisphere on the development of tropical storms across the equator around 160E. These results are not inconsistent with Love's scenario. However, more analyses are expected to improve the understanding of the relations and the mechanisms of tropical cyclone development including the winter hemisphere.

In the present study, in the case of Typhoon 8009, it is clear that the upper cold low is cut off from the Mid Pacific Trough around 160W and moves westward along the 20N parallel with a nearly constant intensity, accompanying the easterly wave disturbances moving along the 10N parallel. For other cases, upper cold lows are also analyzed and shown as the positive vorticity region in Fig. 9.

The existence of the upper tropospheric cold low has been analyzed since as early as Palmen (1949) and Palmer (1951). From some case studies Sadler (1976, 1978) stressed the role of the upper tropospheric cold low in the development of the tropical storms. His analyses indicated that westward-moving upper cyclonic cells in the extension of the MPT furnish the developing low-level cyclones with an outflow channel to the north. He also suggested that north to northwest of the tropical cyclones is the optimum position of the upper cold cell for efficient mass and heat evacuation. In the present study, it is seen that upper cold lows are located almost north or northeast of the lower initial easterly wave disturbances in the early stage, and later they move northwestward of the wave disturbances, keeping almost the same distance from them. The position of the upper cold low, being to the northwest of the wave disturbance along the 10N parallel, is also said by Muramatsu (1985) to be favorable for development of the wave disturbances. In the present analysis, large values of the OLR anomaly are found when the disturbance moves to the west of 170W line. At that time the upper cold lows are located at the north-western portion of the disturbances. This fact suggests that the south–east of the upper cold lows are favorite positions for the maintenance and the development of the disturbances.

When the upper cold low is cut off from the MPT around 160W, 25N, easterly wave disturbances are first recognized southeast of the upper cold lows around 150W, 10N. Though they move westward together, the regions of positive vorticity at the 200 mb level, which indicate the MPT or upper cold low, change meridionally. They extend southwestward and then move westward or northwestward. On the other hand, easterly wave disturbances move westward along the ITCZ. At first, in the central Pacific, the position of the upper positive vorticity region is about north or northeast of wave disturbances along 10N. However, later in the western Pacific, they are located in the northwestern portion of the easterly wave disturbance.

From the analysis, mainly for the 850 mb level, Tai and Ogura (1987) suggested that wave disturbances in different tropical regions have different origins, rather than globally similar ones. The present analysis shows that the origin of the wave disturbances in the western Pacific is located around 150W, 10N, which is west of the zonally subsiding region south of the MPT. For many studies of the lower troposphere (Nitta and Takayabu, 1985, Lau and Lau, 1990), wave disturbances are clearly recognized especially to the west of the date line. On the other hand, the result of the present analysis which includes the upper troposphere strongly indicates that the trajectory of westward-moving disturbances is along 10N from a more easterly region. In the eastern Pacific area, the wave disturbances originate from the area east of the present analysis region of 90W. The three-dimensional analysis of the wave disturbance can demonstrate a clear relation between upper level disturbances and easterly wave disturbances along 10N.

Futher analyses are necessary to clarify the mechanism of the formation of the easterly wave disturbances and the relation between the easterly wave disturbances and the upper cold lows, including the cut off of the MPT.

6. Conclusions

The initial wave disturbances, which later developed into tropical storms in the equatorial Pacific, were analyzed using the GMS and GOES satellites wind data in July and September, 1980. The locations of the wave disturbances were determined from convergence and positive relative vorticity at lower level, and divergence and negative vorticity at the upper level. Easterly wave disturbances originating around 150W traveled with an easterly wave of about 5 days in period along the 10N parallel and rapidly developed into a tropical storm or typhoon around 150E. The westward-moving initial wave disturbances were also analyzed for the hurricanes in the eastern Pacific and came from the eastern edge of the analyzed area or central America.

The intensity of the initial wave disturbances was not related to the intensity of their later development. These wave disturbances developed into trop-

ical storms when they encountered the region of ascending motion in the large-scale zonal circulation along the ITCZ. In the time-longitude sections of the zonal wind fields, the double cells of the zonal circulations were analyzed over the Pacific, though the subsidence motion area and the eastern cell were not clearly defined by comparison with the western cell. The ascending motion was seen around 140E and 110W. The subsiding motion was inferred around 140W, where no disturbances were seen. The easterly wave disturbances originated to the west of the subsiding area, traveled along the lower branch of the zonal circulation cells toward the ascending motion area, and they developed rapidly soon after they encountered an ascending-motion area with small zonal vertical shear.

The positions of this ascending motion and the intensity of the zonal circulation changed their positions with a periodicity related to intraseasonal variations.

In the mid latitude of about 160W, there usually exists the MPT and the upper cold lows are cut off and move westward along the 20N parallel accompanied by easterly wave disturbances along 10N. The easterly wave disturbances are located around south to southwest of the south-westward-extending MPT or the upper cold lows in the central Pacific, but they change their locations to southeast of the upper cold lows in the western Pacific. An interaction between these extratropical phenomena and easterly wave disturbances is suggested.

Acknowledgement

The author expresses her thanks to Professor Y. Mitsuta for his continuous guidance and encouragement. The author is also grateful to Dr. N.K. Sanga and Mr. N. Nishi for their help in compiling the GMS satellite wind and rawinsonde data. The author is indebted to the Japan Information Service Co. for their support in the MASCON programing.

References

Dickerson, M.H., 1978: MASCON-Mass Consistent Atmospheric Flux Model for regions with complex terrain. *J. Appl. Meteor.*, **17**, 241–253.

Gruber, A. and A.F. Krueger, 1984: The statues of the NOAA outgoing longwave radiation data set. *Bull. Amer. Meteor. Soc.*, **65**, 958–962.

Heta, Y., 1990: An analysis of tropical wind fields in relation to typhoon formation over the western Pacific. *J. Meteor. Soc. Japan*, **68**, 65–77.

Heta, Y., 1991: Water vapour transport over the equatorial Pacific as observed from satellites. (submitted to *J. Meteor. Soc. Japan*)

Krishnamurti, T.N., 1971: Tropical east-west circulations during the northern summer. *J. Atmos. Sci.* **28**, 1342–1347.

Krishnamurti, T.N., M. Kanamitsu, W.J. Koss and J.D. Lee, 1973: Tropical east-west circulations during the northern winter. *J. Atmos. Sci.*, **30**, 780–787.

Lau, K.H. and N.C. Lau, 1990: Observed structure and propagation characteristics of tropical summertime synoptic scale disturbances. *Mon. Wea. Rev.*, **118**, 1888–1913.

Love, G., 1985: Cross-equatorial interactions during tropical cyclogenesis. *Mon. Wea. Rev.*, **113**, 1499–1509.

Madden, R.A. and P.R. Julian, 1971: Detection of a 40–50 day oscillation in the zonal wind in the tropical Pacific. *J. Atmos. Sci.*, **28**, 702–708.

Madden, R.A. and P.R. Julian, 1972: Description of global-scale circulation cells in the tropics with a 40–50 day period. *J. Atmos. Sci.*, **29**, 1109–1123.

Muramatsu, T., 1985: A study on the changes of the three dimensional structure and the movement speed of the typhoon through its life time., *Tech. Rep. Meteor. Res. Inst.*, **No. 14**, 117pp.

Nitta, T. and Y. Takayabu, 1985: Global analysis of the lower tropospheric disturbances in the tropics during the northern summer of the FGGE year part II: Regional characteristics of the disturbances. *PAGEOPH*, **123**, 272–292.

Palmen, E., 1949: Origin and structure of high-level cyclones south of the maximum westerlies. *Tellus*, **1**, 22–31.

Palmer, C.E., 1951: On high-level cyclones originating in the tropics. *Trans. Amer. Geo. Uni.*, **33**, 683–696.

Reed, R.J. and E.E. Recker, 1971: Structure and properties of synopticscale wave disturbances in the equatorial western Pacific. *J. Atmos. Sci.*, **28**, 1117–1133.

Riehl, H., 1948: On the formation of typhoons. *J. Meteor.*, **5**, 247-264.

Riehl, H., 1954: *Tropical meteorology.* McGraw Hill Book Co.

Sadler, J.S., 1976: A role of the tropical upper tropospheric trough in early season typhoon development. *Mon. Wea. Rev.*, **104**, 1266–1278.

Sadler, J.S., 1978: Mid-Season typhoon development and intensity changes and the tropical upper tropospheric trough. *Mon. Wea. Rev.*, **106**, 1137–1152.

Sanga, N.K., 1990: An observational study of tropical large-scale fields: Part III: On the annual cycle and the interannual variability of the wind field. (submitted to *J. Meteor. Soc. Japan.*)

Shimamura, M., 1981: The upper-tropospheric cold lows in the Northwestern Pacific as revealed in the GMS satellite data. *Geophys. Mag.*, **39**, 119–156.

Shimamura, M., 1982: An Application of GMS satellite data in the analysis of the upper cold low in the Western North Pacific. *Geophys. Mag.*, **40**, 113–151.

Shimizu, N., 1983: Westward propagation of upper tropospheric wind disturbances during the mid-season typhoon development of 1979. *Geophys. Mag.*, **40**, 297–311.

Tai, K.S. and Y. Ogura, 1987: An observational study of easterly waves over the eastern Pacific in the northern summer using FGGE data. *J. Atmos. Sci.*, **44**, 339–361.

Yamazaki, N. and M. Murakami, 1989: An intraseasonal amplitude modulation of the short-term tropical disturbances over the western Pacific. *J. Meteor. Soc. Japan*, **67**, 791–807.

Yanai, M., 1961: A detailed analysis of typhoon formation. *J. Meteor. Soc. Japan*, **39**, 187–214.

Yanai, M., 1963: A comment on the warm core in incipient tropical cyclone. *J. Meteor. Soc. Japan*, **41**, 183–187.

Yanai, M., 1968: Evolution of a tropical disturbance in the Caribbean Sea region. *J. Meteor. Soc. Japan*, **46**, 85–109.

赤道太平洋の熱帯擾乱の起源

邊田有理江

（京都大学防災研究所）

1980年の多くの台風はITCZを西進する偏東風波動擾乱にその起源を求められたが、その擾乱の初期について東半球を含めた熱帯太平洋の上部下部対流圏の流れの場の解析を行った。以前と同様にGMSの衛星風データとゾンデのデータ、さらに東太平洋についてGOESの衛星風データをもとに格子点データを内挿補正により求めた。1980年7月9月の2カ月間にみられた、10個の擾乱のうち、擾乱を初期までさかのぼれた5個について解析した。そのうちの4個について日々の発散場、渦度場から10 N帯にそって、周期約5日の偏東風波動擾乱を、150 W付近までさかのぼれた。そうした擾乱の西進に対応して、150 W, 30 N付近のMid Pacific Troughからupper cold lowが切離され、20 Nにそって西進するのが、解析された。Mid Pacific Troughが南西に延びてきたあたりでは、擾乱はupper cold lowの南か南西に位置するが、西太平洋では、南東に位置していた。

西太平洋の熱帯擾乱は東太平洋の擾乱と同様にそれらが、東西循環セルの大規模上昇流域にさしかかった付近、すなわち、140 E及び110 W付近で台風強度へと発達していた。この東西循環の位置や強さは季節内変動と関係した周期性をもって変化していた。東西循環の下降流域は140 W付近に示唆されたが、台風の初期擾乱が解析されたのは、この下降流域の西側であった。

Three dimensional assimilation of tropical wind field by MASCON model

(Submitted to J.Meteor.Soc.Japan)

By

Yurie Heta

Disaster Prevention Research Institute

Kyoto University, Uji, Kyoto 611, Japan

Abstract

Assimilation of tropical wind fields was developed using the three-dimensional MASCON model based on Sasaki's variational method(1970). Variational calculus techniques are used to adjust the spatially sparse wind data set of satellite cloud and rawinsonde to satisfy the continuity equation. Three-dimensional wind fields (u, v, ω) are provided over the whole troposphere using p^* coordinate, which is a hybrid of p and σ- coordinate. This model can give us the fine-mesh three-dimensional wind field in the tropical region.

Reanalysis of the tropical wind field surrounding tropical disturbances indicate the similar characteristics with the previous two-dimensional MASCON model(Heta, 1990, 1991). Moreover vertical velocity is calculated directly in the three-dimensional model. Upward motion area is recognized around the pre-typhoon disturbance and upward motion increases with the development of the disturbance.

1. Introduction

In the area with sparcee observational data such as over tropical Pacific Ocean, the data should be assimilated before applying advanced analysis technics or progonostic computation. The global scale assimilation systems have been developed by the European Centre for Medium Range Weather Forecasts(ECMWF) and the Geophysical Fluid Dynamics Laboratory(GFDL) and others using governing equations of motion(Bengtsson et al,1982, Lorenc,1981, Daley et al,1985, Trenberth et al,1988). And many researchers have analyzed the tropical wave disturbance using gridded wind fields assimilated by these methods(Nitta and Takayabu,1985, Lau and Lau,1990 and Liebmann and Hendon,1990). However, these assimilation methods are laborious to complete and implicates difficulties in applying the governing equation in the equatorial area(Hollingsworth et al,1986) .

The purpose of this paper is to describe the new simple three dimensional assimilation method using simple governing equation of continuity for equatorial wind field, which is an extension of two dimensional method developed by the present author(Heta,1990) following MASCON method to obtain $1^{\circ} \times 1^{\circ}$ mesh wind field from station and satellite cloud wind informations.

2. Model description

Based on Sasaki's variational method(1970), Dickerson(1978) developed two dimensional Mass Consistent Atmospheric Flux Model(MASCON) model using the equation of continuity as the constraint condition, which the first model of the present author(Heta,1990) has followed to. In extending the model into three -dimensions, there may be various kind of vertical coordinates for numerical calculation, as shown by Kasahara(1974). The simplest one is the z-coordinate used by Sherman(1978) who developed the mass-adjusted three-dimensional wind field (MATHEW) model for lower tropospheric wind fields over the complex terrain. The present system adopted pressure coordinate p^* to include the whole troposphere of equatorial area difined by

$$p^* = \begin{cases} (p_o - p_m) * (p_m - p) / (p_m - p_s) + p_m & (p \geq p_m) \quad (1) \\ p & (p < p_m) \end{cases}$$

where p_s is the surface pressure at $z = z_s$ and p_o being a constant presure corresponding to the bottom of the model. As shown in Fig.1, only the layers below p_m is affected by the orography, which is relatively low in the tropics. This coordinate is a hybrid of p - coordinate and σ - coordinate, and was chosen to incooperate the topography of tropical Pacific in the model, where the highest point is about 700mb in New Guinea.

In this coordinate, we define the time change of p^* as

$$\omega^* = dp^*/dt = (p_o - p_m) \times (\omega - v \cdot \nabla_{p^*} p) / (p_s - p_m) \quad (2)$$

where $\omega = dp/dt$.

Then the continuity equation of (x, y, p^*) becomes,

$$\partial(\varepsilon u)/\partial x + \partial(\varepsilon v)/\partial y + \partial(\varepsilon \dot{\omega}^*)/\partial p^* = 0 \qquad (3)$$

where,

$$\varepsilon = \begin{cases} (ps - pm)/(po - pm) & (p \geq pm) \\ 1 & (p < pm) \end{cases} \qquad (4)$$

As p^* is basically pressure coordinate, the whole troposphere can be handled without assumptions about air density, and the p^* coordinate also has an advantage for wind analysis because the usual wind observation are reported at standard pressure levels.

Even though the pressure of the ground surface, ps is strictly a function of time, fixed values are used in this study following climatological relations with heights in the tropical atmosphere given by

$$ps = 1016.17\,(\exp(-0.11746 * Zs) - 1) + po \quad (mb) \qquad (6)$$

The specific functional of three-dimensional variational analysis(Sasaki,1979) used in the present study is

$$E(u,v,\dot{\omega}^*,\lambda) = \int \{ \{\alpha_1^2(u-\tilde{u})^2 + \alpha_1^2(v-\tilde{v})^2 + \alpha_2^2(\dot{\omega}^* - \tilde{\dot{\omega}}^*)^2\} + \lambda(\partial u/\partial x + \partial v/\partial y + \partial \dot{\omega}^*/\partial p^*)\}\, dxdydp^* \qquad (7)$$

where x,y are horizontal coordinates, $u,v,\dot{\omega}^*$ adjusted velocity components in the x,y,p^* directions respectively, $\tilde{u},\tilde{v},\tilde{\dot{\omega}}^*$ the observed variables, $\lambda(x,y,p^*)$ the Lagrange multiplier and α_k being Gaussian precision moduli for horizontal(k=1) and vertical(k=2) directions.

The associated Euler-Lagrange equations whose solution minimizes Eq. (7) are,

$$u = \tilde{u} + 1 / (2 \alpha_1^2 \gamma) \cdot \partial \lambda / \partial x \quad (8)$$

$$v = \tilde{v} + 1 / (2 \alpha_1^2 \gamma) \cdot \partial \lambda / \partial y \quad (9)$$

$$\omega^* = \tilde{\omega}^* + 1 / (2 \alpha_2^2 \gamma) \cdot \partial \lambda / \partial p^* \quad (10)$$

$$\partial u / \partial x + \partial v / \partial y + \partial \omega^* / \partial p^* = 0 \quad (11)$$

The bottom and upper boundary condition is $\partial \lambda / \partial n = 0$, which means "no-flow-through" boundaries, while the lateral, on the x -direction and y-direction, boundary conditions are open boundary or $\lambda = 0$.

In this formulation, from the initial wind field$(\tilde{u}, \tilde{v}, \tilde{\omega}^*)$ at each grid point, we can obtain adjusted wind field(u, v, ω^*), which satisfies continuity equation and also fits the observation in a least squares manner, using MASCON model. In this process, it is important to interpolate the proper initial wind field $(\tilde{u}, \tilde{v}, \tilde{\omega}^*)$ from the observation. In the next section, the interpolation method is described in detail.

3. Interpolation method

Randomly distributed observation must be spatially interpolated to the grid points as the initial condition to apply the MASCON model. Since measurement of the vertical velocity ω is not available, they are initially set to zero, similar as the MATHEW model. Initial values of u and v at the grid point(x,y,p^*) above p m (500mb) level were prepared in two dimensional interpolation scheme without respect to adjustment layer similar to that of Dickerson(1978), shown as follows,

$$Vi = \sum_{j=1}^{N} S\, Vij \quad \exp\ (-\beta\, rj^{2}) / \sum_{j=1}^{N} S \exp\ (-\beta\, rj^{2}) \qquad (12)$$

where Vi is the interpolated east-west(i=1) or north-south(i=2) velocity compornent at the grid point, Vij and rj are the i-velocity component and distance to the grid point of the j-th closest observation, and N is the number of the closest observations to the grid point that are used for interporation. β is the weight depending on horizontal distance being 10^{-12} same as the previous two- dimensional MASCON model(Heta,1990,1991). For this study we have chosen a value of 5 for N in usual. In addition,we have added the weight,S , which varies with the kind of observation. After several trials changing S, we decided S=1 for sonde and S=0.9 for satellite wind data. In Fig. 2 ,there is an typical distribution of wind observations. The satellite wind is included only in the 850mb and 200mb layers following the results of comparison with the rawin sonde data(Hamada,1982).

Below the layer of p m, we adopted the three-dimensional interpolation. Then the distance of the grid point of the j-th closest observation, rj in eq(12) is given by

$$rj^{2} = (x - \tilde{x}_{oj})^{2} + (y - \tilde{y}_{oj})^{2} + (p^{*} - \tilde{p}_{oj})^{2} \times Wz^{2} \qquad (13)$$

where $\tilde{x}_{oj}$, $\tilde{y}_{oj}$, $\tilde{p}_{oj}$ is the position of j-th nearest observational point. W z is the vertical weight to represent the heterogeneousness of vertical coordinate. The vertical weight Wz has much effect on the resultant wind fields especially for layers of sparse data, such as 1000mb or 700mb. If the value of Wz is larger, the interpolation is horizontal, but if it is smaller, the resulted wind fields show more similar pattern for all layers . After several trials, the value of Wz was desided to be 50 for all layers below p m, that minimizes the root mean square difference between obseravational wind and interpolated wind at the nearest grid point. The values of root mean square differences are about 2 ~5m/s.

The interpolated method stated above is quite dependent of wind data on the adjacent observations. We examined the possibility to improve the interpolated wind field by using the data at the previous time especially in the area of sparse data, such as the case that only m($<$N) observation existed within a certain radius of r m. In this test case the adjusted wind data at the previous time, Vpi at the same grid point was used for the interpolation;

$$Vri=\frac{m+N-1}{2N}\frac{\sum_{j=1}^{\tilde{N}} Vij\,S\exp(-\beta r_j{}^2)}{\sum_{j=1}^{\tilde{N}} S\exp(-\beta r_j{}^2)}-\frac{N+1-m}{2N}\,Vpi \qquad (15)$$

As the results, this treatment has not so significant effect on the results, because data was also sparse at the previous time for many cases of 24 hours interval calculation. But for the case that the data density is high at the previous time, this treatment is useful, however in the present paper this process is not used except for the case the observation is quite poor compared with the previous day.

Fig.3 shows an example of the distribution of the number of observational

points within the radius of $r_m = 10^\circ$ from the grid point for 18 July,1980. The regions of the smaller number such as centered at 170W,0N(Fig.3(a)) have lower data accuracy compared with the region where the number is five(=N). Data sparse area is often located along the equator where are no islands and no clouds.

4. Parameters in the MASCON model.

The ratio of Gaussian precision moduli $(\alpha_1/\alpha_2)^2$ in eq(7) affect the resulted wind field very much, though there is no clearly formulated way to settle the value. In the present paper we determine the value of $(\alpha_1/\alpha_2)^2$ after the similar trials as the previous study(Heta,1991), to be $\alpha_1/\alpha_2 = 0.08$, which minimize the absolute error from continity equation $|\overline{\varepsilon}|$ (Sasaki,1979).

The absolute values of adjusted ω are also dependent with the ratio of α, because the observational $\tilde{\omega}$ are set to be zero in the present study. If smaller value of α_1/α_2 is chosen, the absolute value of the resulted ω get smaller. However, horizontal and vertical pattern of ω is independent with the ratio of α.

The overrelaxation facter was determined experimentally to be 1.98 in most caliculations minimizing the caliculation time. All the parameters are determined experimentally for the case of July,1980. The area is with 120 ×60× 6 grid points $\Delta x=\Delta y=110$km and six layers(1000mb,850mb,700mb,500mb,300mb, 200mb) butΔp is not constant. The analyzed area covers 120E～120W, 30S ～30N. The data of July,1980 are chosen to compare with the previous result(Heta,1990, 1991). Fig.4 shows the topography of the analyzed area.

5. Results

The adjusted three-dimensional MASCON model has been applied to assimilation of the wind field of July, 1980. Fig.5 shows the results of the horizontal wind fields at the 200mb and 850mb levels at 0Z on 18 July, 1980. A tropical depression located on 13.4N, 138.9E at this time, which later developed into Typhoon Joe. There is a cyclonic circulation around the tropical depression at 850mb level(Fig.5(a)). The south-east of tropical depression northward current across the equator and easterly wind are converging. At 200mb level(Fig.5(b)), on the other hand, anticyclonic outflow toward west is clearly seen from a little east of the location of tropical depression. There are counter-clockwise circulations centered at 20N,170W and at 5S, 173W. We recognized strong southwesterly around 160W, 20N ,which is thought to be current along the edge of Mid Pacific Trough. The horizontal wind fields at the 850mb and 200mb levels, such as shown in Fig.5(a) and (b), are almost similar to the result from the previous two-dimensional analysis(not shown). Fig.5(c) shows longitude-height section at 10N, and Fig.5(d) latitude-height section at 139E. Strong upward motion is recognized around the tropical depression in both figures. ω shows its maximum value at 500mb or 300mb levels. The absolute value of ω at lower levels is small compared with the upper levels and the distribution of ω is quite smooth compared with upper ones.

Fig.6 shows distribution of ω at 200mb and cloud activity, which is shown by the TBB anomaly from the monthly mean. They are quite good coincident with each other. Upward motion area corresponds to the TBB negative anomaly area, that is the area of high cloud activity. The upward motion area is recognized around the areas centered at 138E, 15N and 160E,5N in Fig.6(a). These locations coincide with the area of horizontal divergence at the 200mb level in the previous two-dimensional analysis(Heta,1990, Fig.7(a)).

Fig.7 shows the results of analysis of Typhoon 8009 using the three-dimensional MASCON model. The broken line with small open circles indicates the track of pre-typhoon disturbance, which is difined by the mean positions of lower convergence, positive vorticity and upper divergence and negative vorticity regions just the same as the two dimensional MASCON model in the previous study(Heta,1991,Fig.8). Fig.7(b) show the negativeω regions of 200mb of every other day. The upward motion area is also analyzed about the position of disturbace for other levels. Fig.7(a) show the positive ω regions. The subsidence motion is recognized around the upper positive vorticity area or upper cold low.

Fig.8 shows the time change of ω values for three-different levels. The development of typhoon is recognized by the change of ω value, though small changes of the values may come from noises caused by the change of accuracy of analysis.

These figures show that the pre-typhoon disturbances or the upper cold low analyzed by the previous two-dimensional study are also analyzed by the three-dimensional MASCON model. Moreover we can directly know the vertical motion of disturbances in this three-dimensional study.

6. Conclusion

The assimilation method using the three-dimensional MASCON model provides us the tropical wind fields which enable us to analyze tropical disturbances in more details than the two dimensional method(Heta,1990,1991). The vertical velocity is directly obtained in this model. The three-dimensional wind fields adjusted in a least-squares sense to satisfy the continuity equation are provided.

Reanalysis of the Typhoon 8009 using the three-dimensional MASCON model indicates the similar characterisitics of the disturbance with the previous study by two-dimensional MASCON model for the same data. Moreover, vertical velocity is directly calculated in the present study. Upward motion (negative ω) areas are recognized around the pre-typhoon disturbance and the value of ω decreadsed with the development of the disturbance.

Acknowledgements

The author expresses her thanks to Prof. Y.Mitsuta of Kyoto University for his continuous encouragement of this study. Thanks are due to Dr. T.Nakazawa of the Meteorological Research Institute, who kindly provided me with the NOAA OLR data and TBB grid point data utilized in the present study. The author would also thank Prof. Y.K. Sasaki of Oklahoma Univ. and Dr. M.Murakami of the Meteorological Research Institute for their helpful comments and suggestions.

Refferences

Bengtsson,L., M.Kanamitsu, P.Kallberg and S.Uppala, 1982: FGGE 4-dimensional data assimulation at ECMWF. Bull.Amer.Meteor.Soc.,63,29-43.

Daley,R., A.Hollingsworth, J.Ploshay, K.Miyakoda, W.Baker, E.Kanaley, C.Dey, T.Krishnamurti, and E.Barker,1985: Objective Analysis and Assimulation Techniques used for the Production of FGGE IIIb Analyses. Bull.Amer. Meteor.Soc.,66,532-538.

Dickerson,M.H.,1978:MASCON-Mass Consistent Atmospheric Flux Model for regions with complex terrain. J.Appl.Meteor.,17,241-253.

Hamada,T.,1982: Representative heights of GMS satellite winds,Meteorological Satellite Center Technical Note,6,35-47.

Heta,Y.1990:An analysis of tropical wind fields in relation to typhoon formation over the western Pacific. J.Meteor.Soc.Japan,68,65-77.

Heta,Y.1991:The origin of tropical disturbances over the equatorial Pacific. J.Meteor.Soc.Japan,69,337-351.

Hollongsworth,A., D.B.Shaw, P.Lornberg, L.Illari, K.Arpe and A.J.Simmons, 1986: Monitoring of Observation and Analysis quarity by a Date Assimilation Systems; Mon.Wea.Rev.,114, 861-879.

Kasahara.A,1974: Various vertical coordinate systems used for neumerical weather prediction.Mon.Wea.Rev.,102, 509-522.

Lau,K.H. and N.C.Lau,1990:Observed structure and propagation characteristics

of tropical summertime synoptic scale disturbances. Mon.Wea.Rev.,118, 1888-1913.

Liebmann,B. and H.H. Hendon,1990: Synoptic-scale disturbances near the equator. J.Atmos.Soc.,47,1463-1479.

Lorenc,A.C.,1981: A Global Three-dimensional Multivariate Statistical Interpolation Scheme. Mon.Wea.Rev.,109,701-721.

Nitta,T.and Y.Takayabu,1985 :Global analysis of the lower tropospheric disturbances in the tropics during the northern summer of the FGGE year part Ⅱ : Regional characteristics of the disturbances. PAGEOPH ,123, 272-292.

Sasaki,Y.K.,1979: Lecture notes on variational methods for environmental analysis and prediction problems, Severe Storm Research Notes.1,Disaster Prevention Research Institute, Kyoto University,174pp.

Sherman,C.A.,1978 : A mass consistent model for wind fields over complex terrain, J.Appl.Meteor.,17,312-319.

Trenberth,K.E. and J.G.Olson,1988: An Evaluation and Intercomparison of Global Analyses from the National Meteorological Center and the European Centre for Medium Range Weather Forecasts, Bull.Amer.Meteor.Soc.,69, 1047-1057.

3次元MASCONモデルを用いた熱帯域の風場計算法

遠田　有理江（京都大学防災研究所）

3次元MASCONモデルを用い、熱帯域の格子点での3次元の風場が得られた。MASCONモデルでは、ゾンデと衛星より得られた観測風を連続の式を拘束条件に変分法により補正する。鉛直座標としてP座標系を導入することで、簡単に地形の影響を含む対流圏全層の格子点での風を計算した。こうして得られた格子点風場は観測点のある所では最小二乗的に観測値に従い、観測点のない所でも連続の式という物理法則をみたしている。

この手法を用い、以前に2次元で解析した熱帯擾乱を再解析した。以前の解析で得られた擾乱の特徴は、3次元解析でも確かめられた。さらに直接に鉛直P速度が計算されるが、擾乱の付近に上昇流域が認められ、擾乱が台風へと発達していくにつれて、強い上昇流が得られた。

Figure Captions

Fig.1. Vertical grid structure of the model. Solid lines show main levels (○-u,v, λ and ■- ω).

Fig.2. Distribution of observational wind data at (a) 200mb, (b)300mb, (C)500mb, (d)700mb, (e)850mb and (f)1000mb levels at 00Z on 18 July, 1980.

Fig.3. Numbers of observational points which is located in the redius of 10° longitude(10×110km) at each grid point at (a)200mb and (b)850mb levels at 0Z on 18 July, 1980.

Fig.4. Topography of the analyzed region.

Fig.5(a) Horizontal wind field at the 850mb level adjusted by the three-dimensional MASCON model at 0Z on 18 July, 1980.

(b) As in (a), except for 200mb level.

(c) Vertical-longitudinal structure along 10N zone.

(d) Vertical-latitudinal structure along 139E. Upward arrows indicate negative values of ω.

Fig.6(a) The distribution of ω values at the 200mb level at 0Z on 18,July, 1980. Solid lines show the negative values and broken lines show the positive values. Contour interval is 0.05Pa/s.

(b) The distribution of anomaly of TBB grid point data from the monthly mean values at 0Z on 18 July,1980. Solid lines indicate the negative values and broken lines show the positive values. Contour interval is 15K.

Fig. 7(a) 200mb positive vertical velocity regions (dotted lines) and position of the axis and center of 200mb positive vorticity regions (thick solid lines) analyzed in the previous study(Heta,1991). Small open circles with smaller numerals show the daily positions of tropical disturbances at 0Z from the previous two-dimensional analysis Numerals mean day of July. Large open circle and large closed circle indicate the positions where the disturbances had Tropical Depression and Tropical Storm intensity, respectively.

(b) Position of 200mb negative ω regions(thick solid lines).

Fig. 8 Time change of the ω values at 200mb,850mb and 1000mb levels at the center of the wave disturbances detected by the previous analysis.

Fig. 1

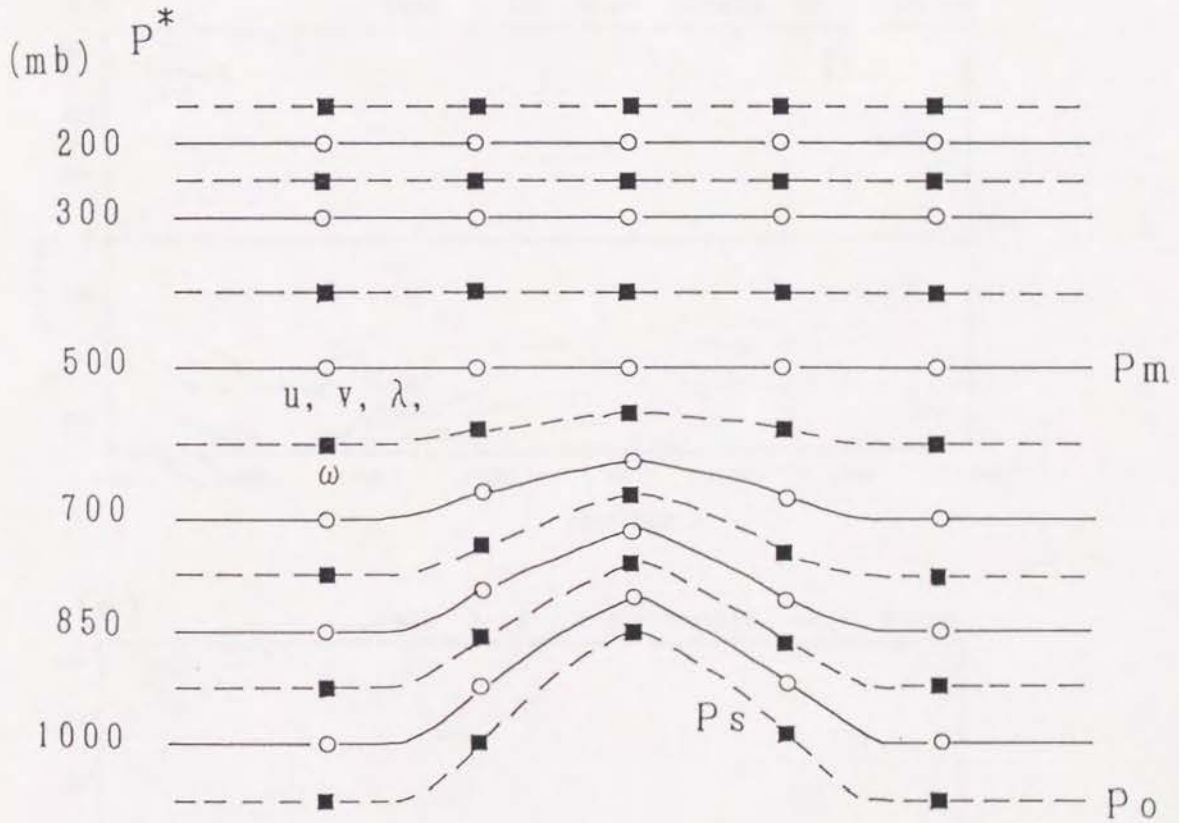

Fig. 2

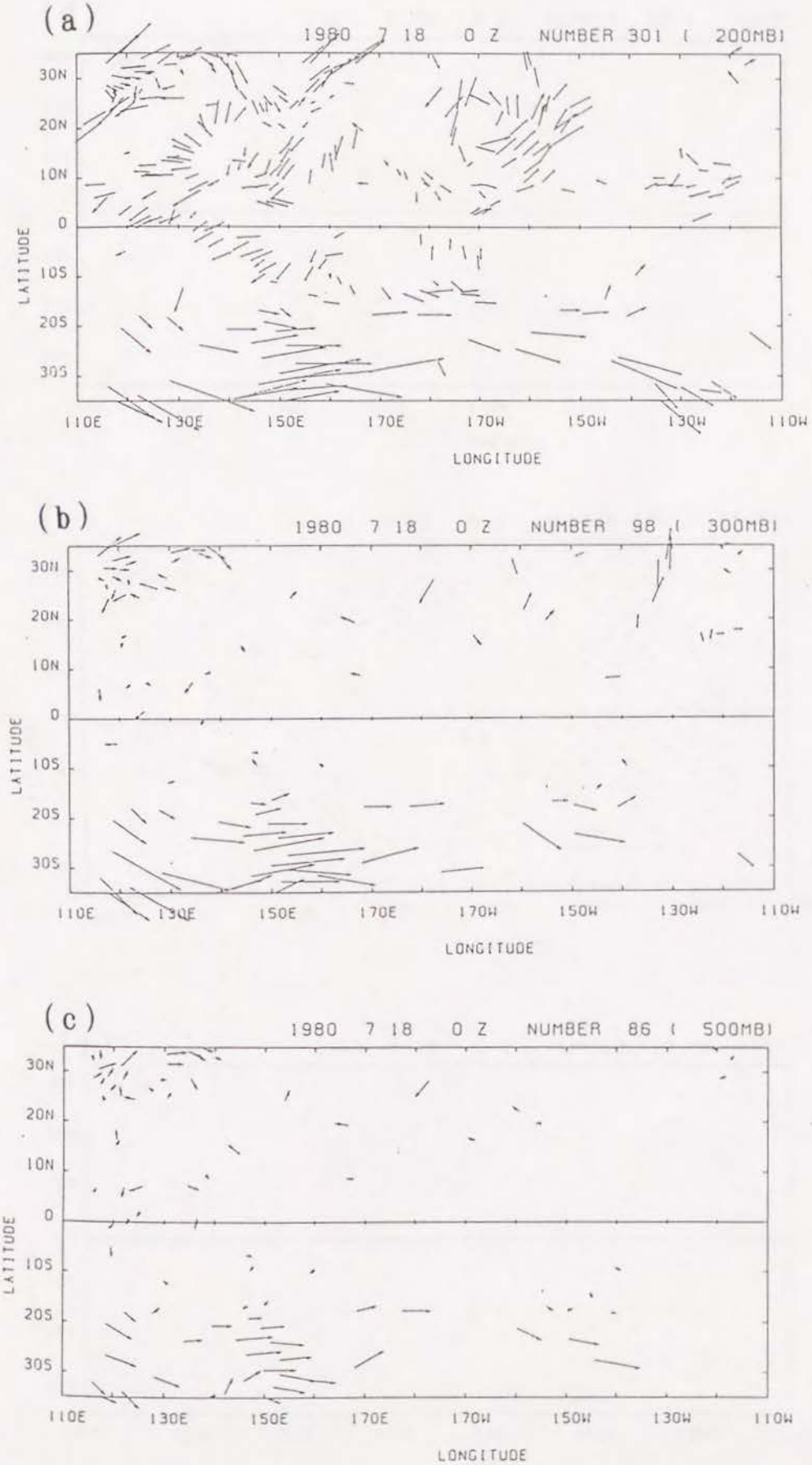
(a)
1980 7 18 0 Z NUMBER 301 (200MB)
30N
20N
10N
0
10S
20S
30S
LATITUDE
110E
130E
150E
170E
170W
150W
130W
110W
LONGITUDE
(b)
1980 7 18 0 Z NUMBER 98 (300MB)
30N
20N
10N
0
10S
20S
30S
LATITUDE
110E
130E
150E
170E
170W
150W
130W
110W
LONGITUDE
(c)
1980 7 18 0 Z NUMBER 86 (500MB)
30N
20N
10N
0
10S
20S
30S
LATITUDE
110E
130E
150E
170E
170W
150W
130W
110W
LONGITUDE

Fig. 2

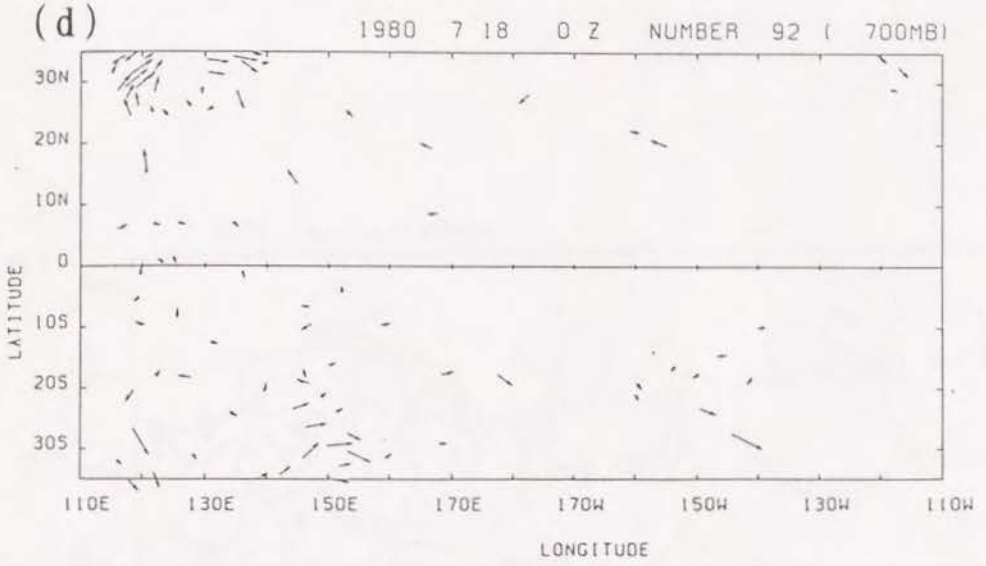
(d)
1980 7 18 0 Z NUMBER 92 (700MB)
30N
20N
10N
0
10S
20S
30S
LATITUDE
110E
130E
150E
170E
170W
150W
130W
110W
LONGITUDE

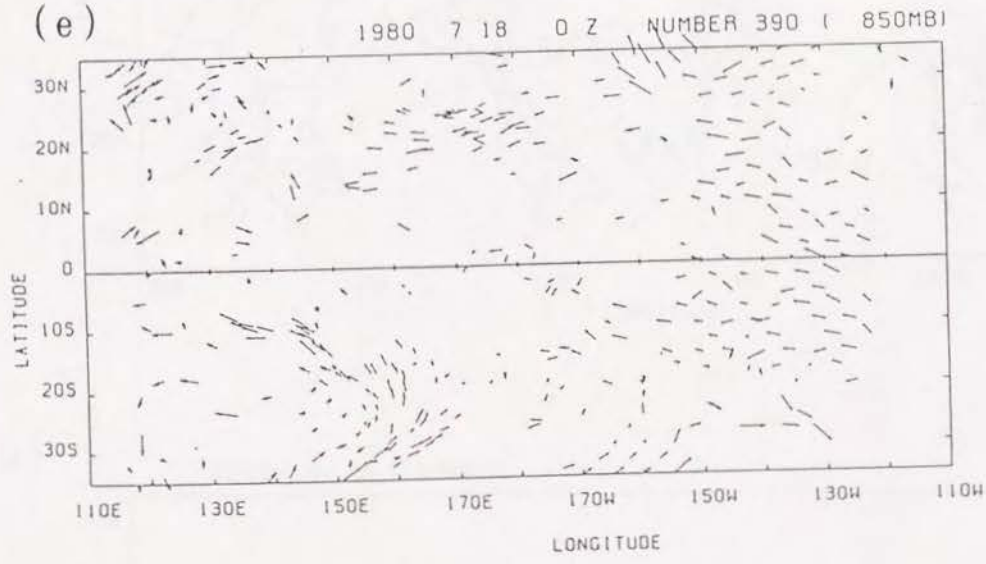
(e)
1980 7 18 0 Z NUMBER 390 (850MB)
30N
20N
10N
0
10S
20S
30S
LATITUDE
110E
130E
150E
170E
170W
150W
130W
110W
LONGITUDE

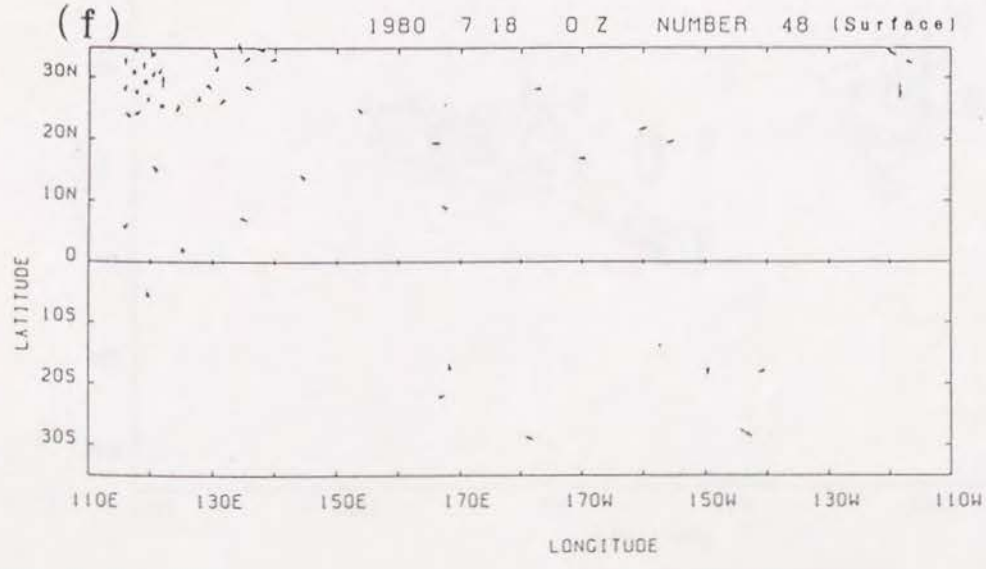
(f)
1980 7 18 0 Z NUMBER 48 (Surface)
30N
20N
10N
0
10S
20S
30S
LATITUDE
110E
130E
150E
170E
170W
150W
130W
110W
LONGITUDE

Fig. 3

(a)

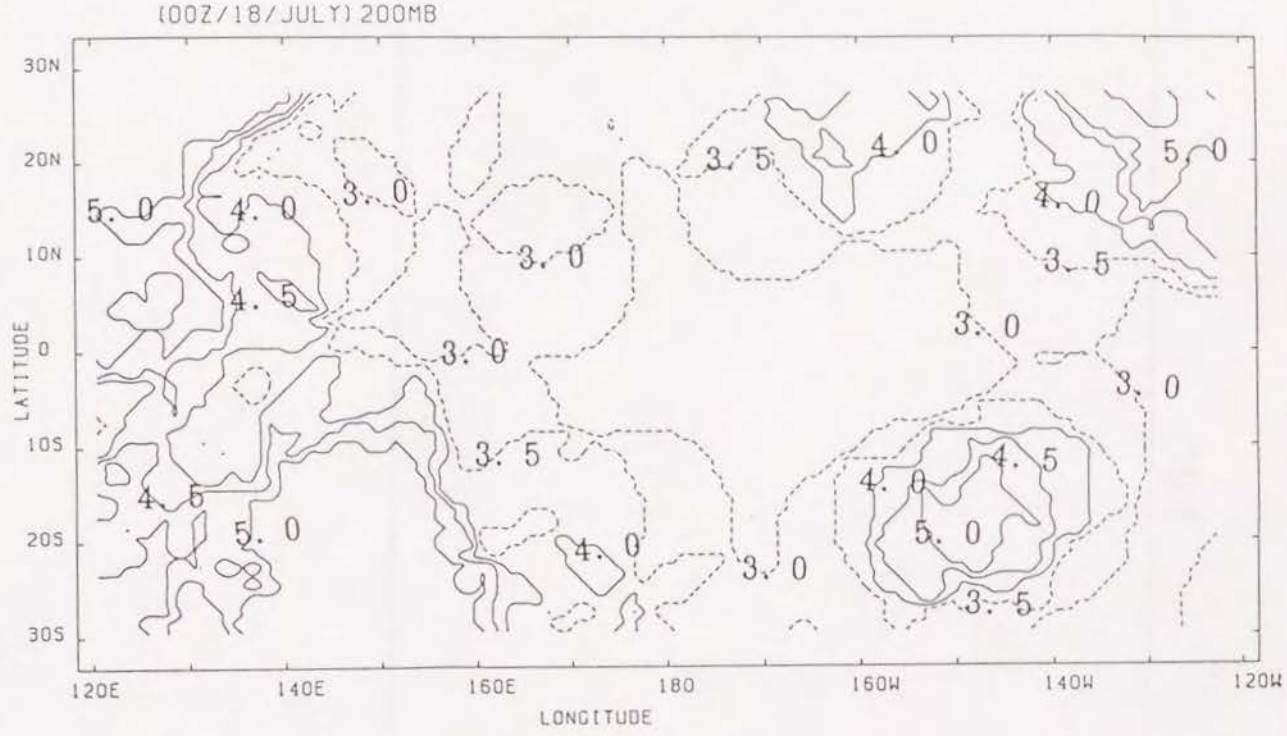
(00Z/18/JULY) 200MB
30N
20N
10N
0
10S
20S
30S
LATITUDE
120E
140E
160E
180
160W
140W
120W
LONGITUDE

(b)

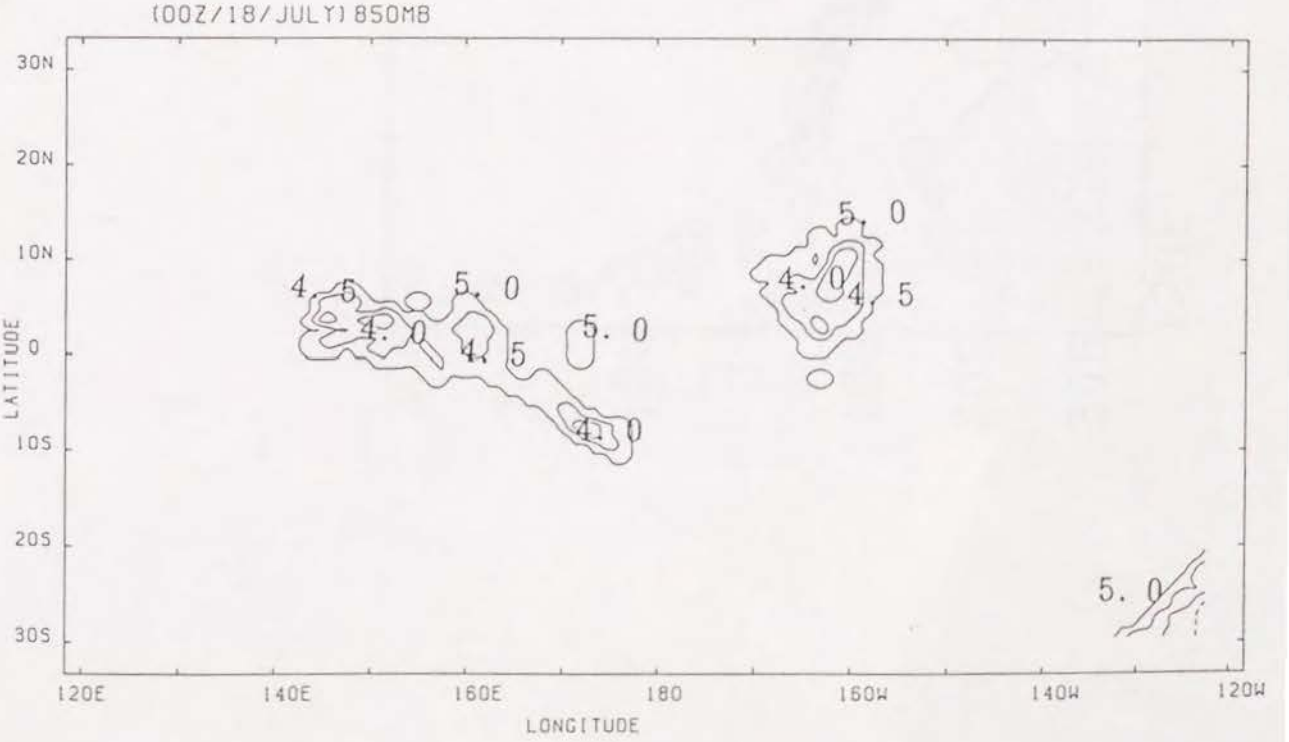
(00Z/18/JULY) 850MB
30N
20N
10N
0
10S
20S
30S
LATITUDE
120E
140E
160E
180
160W
140W
120W
LONGITUDE

Fig. 4

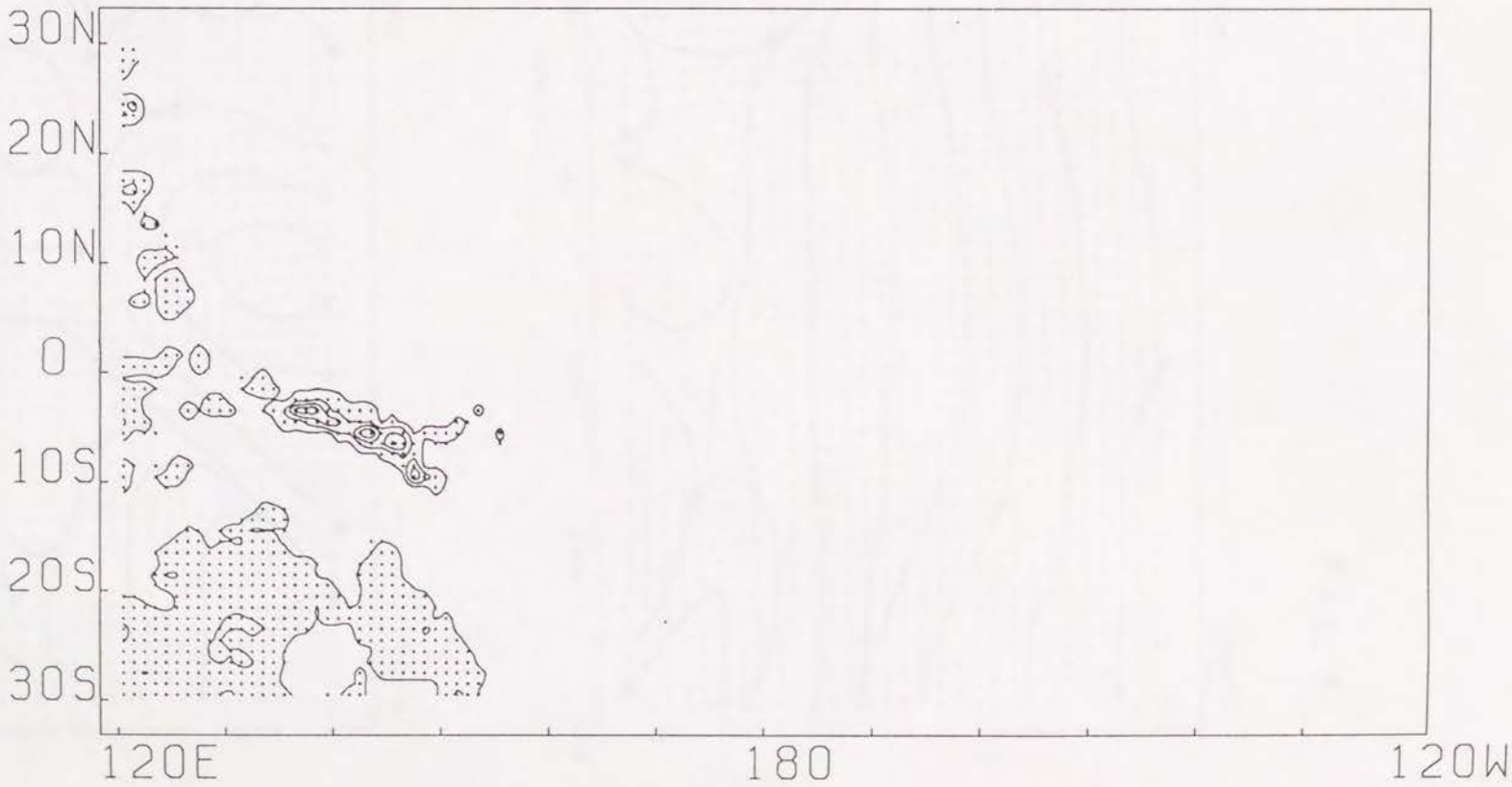

Fig. 5

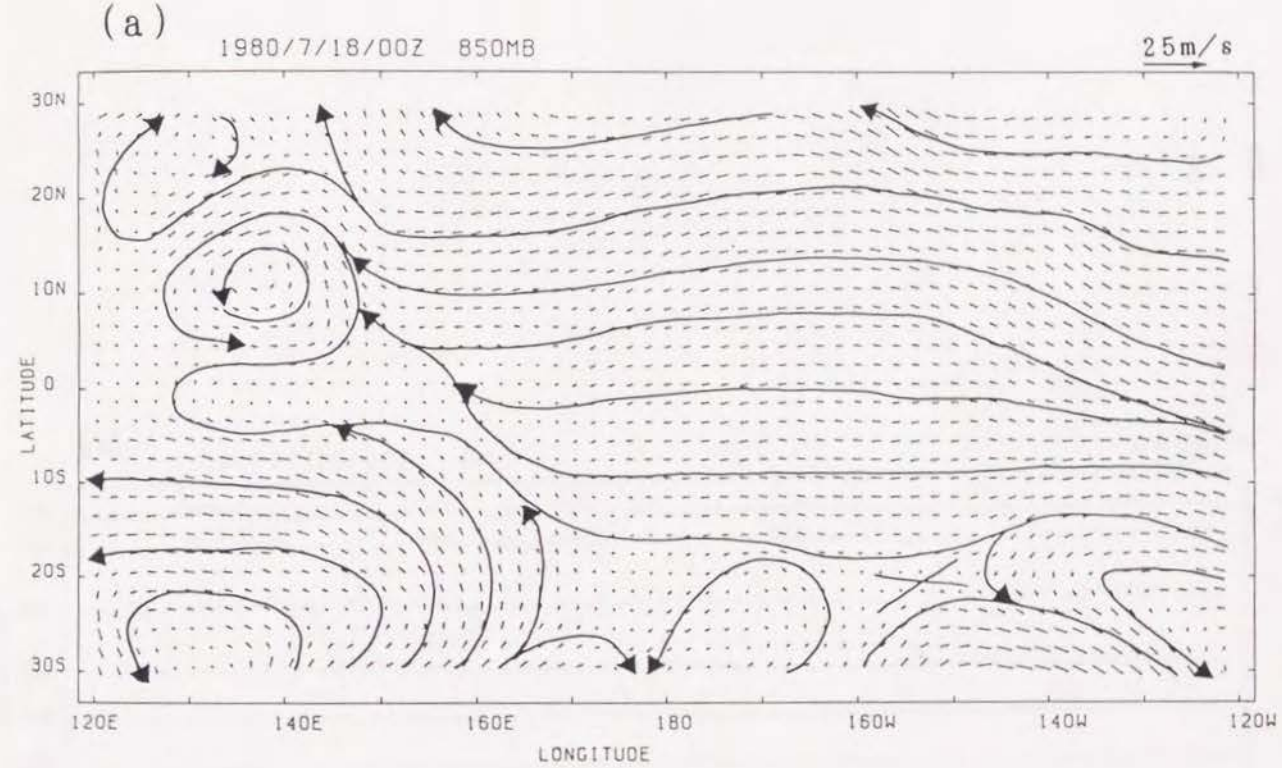
(a)
1980/7/18/00Z 850MB
25m/s
30N
20N
10N
0
10S
20S
30S
LATITUDE
120E
140E
160E
180
160W
140W
120W
LONGITUDE

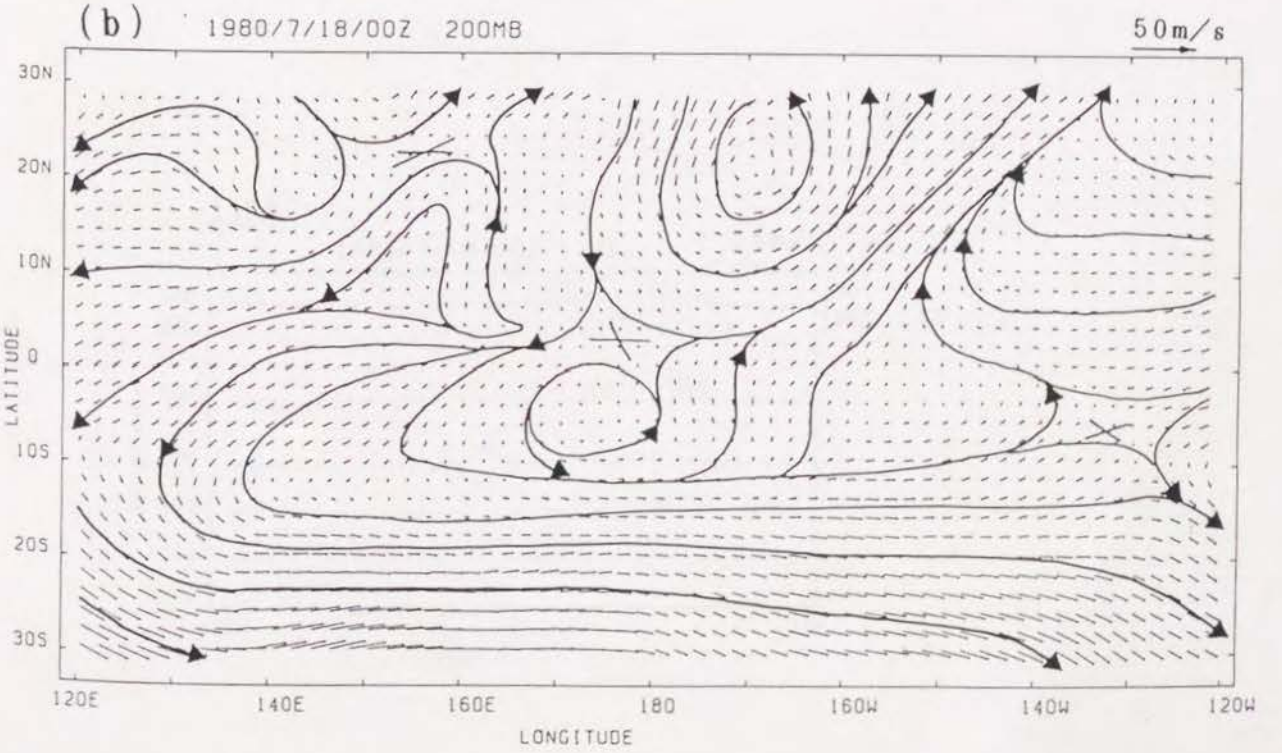
(b)
1980/7/18/00Z 200MB
50m/s
30N
20N
10N
0
10S
20S
30S
LATITUDE
120E
140E
160E
180
160W
140W
120W
LONGITUDE

Fig. 5

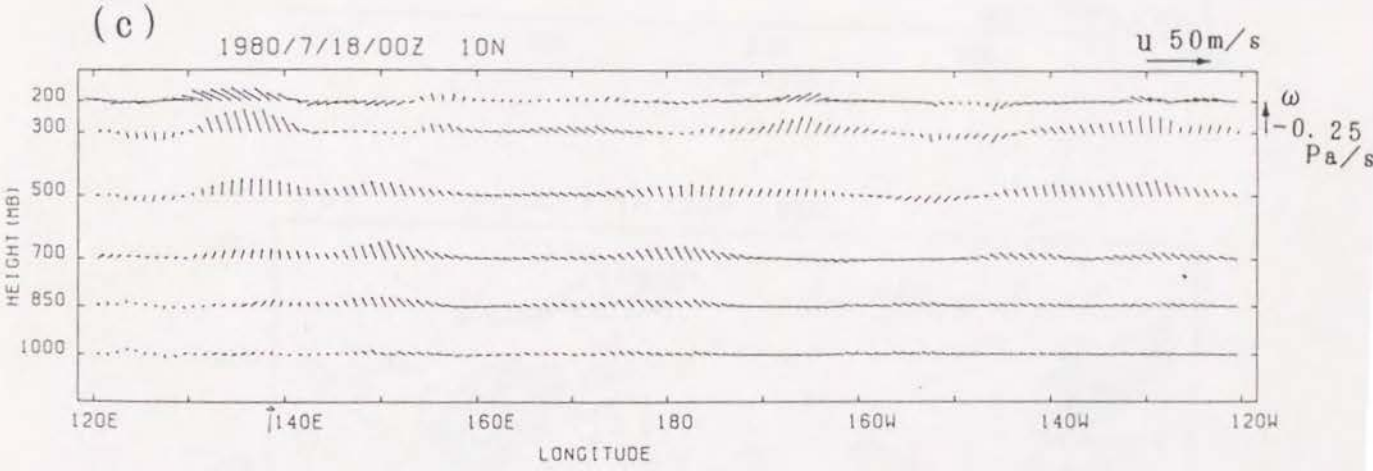
(c)
1980/7/18/00Z 10N
u 50m/s
200
300
500
700
850
1000
HEIGHT (MB)
ω
-0. 25
Pa/s
120E
140E
160E
180
160W
140W
120W
LONGITUDE

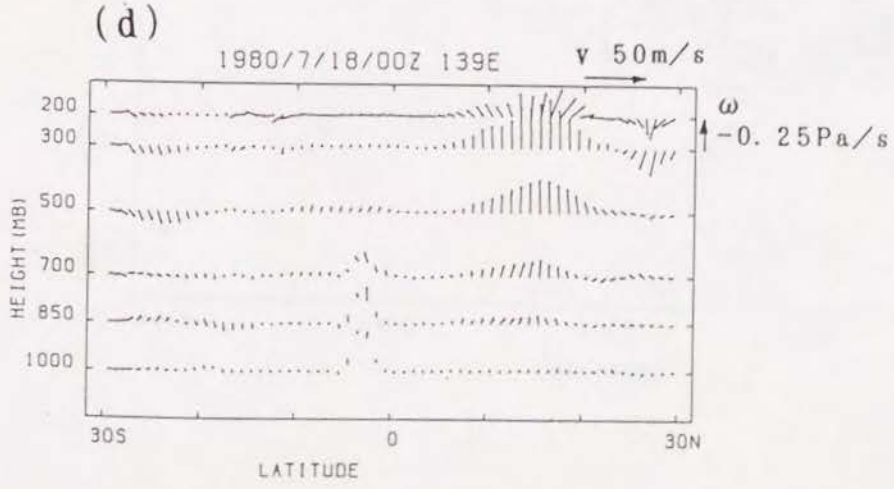
(d)
1980/7/18/00Z 139E
v 50m/s
200
300
500
700
850
1000
HEIGHT (MB)
ω
-0. 25Pa/s
30S
0
30N
LATITUDE

Fig. 6

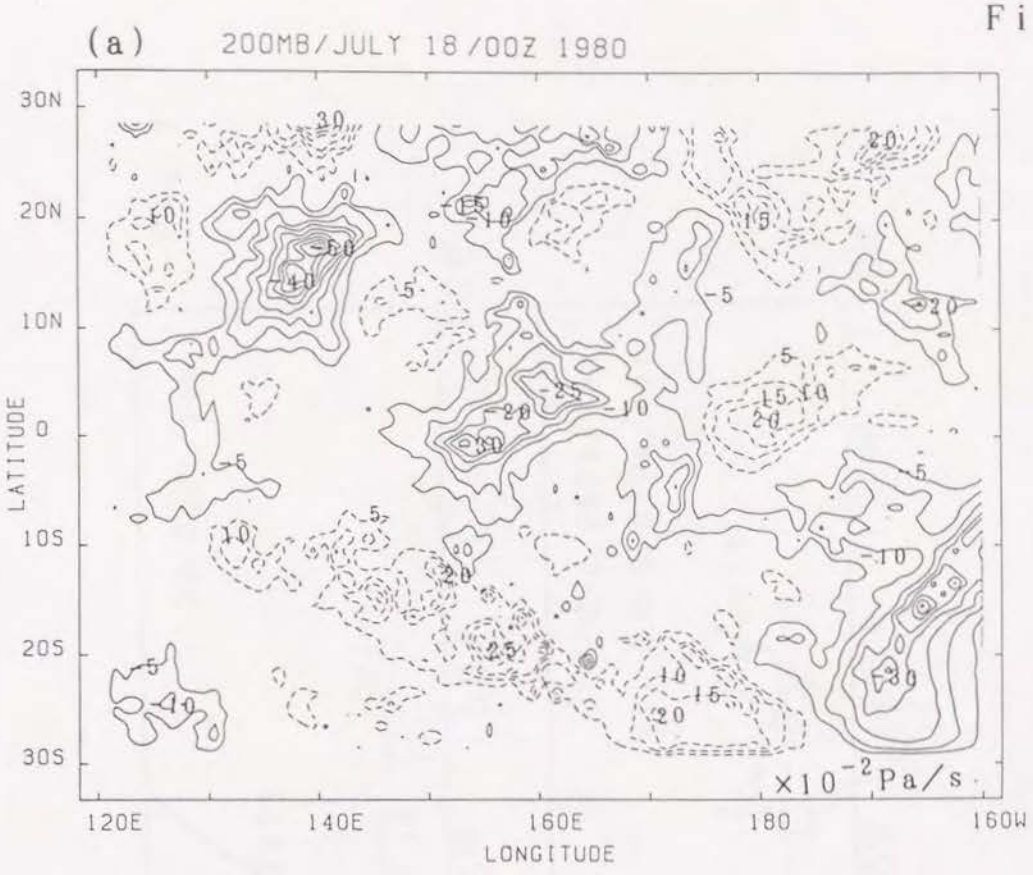
(a)
200MB/JULY 18/00Z 1980
30N
20N
10N
0
10S
20S
30S
LATITUDE
120E
140E
160E
180
160W
LONGITUDE
×10⁻²Pa/s

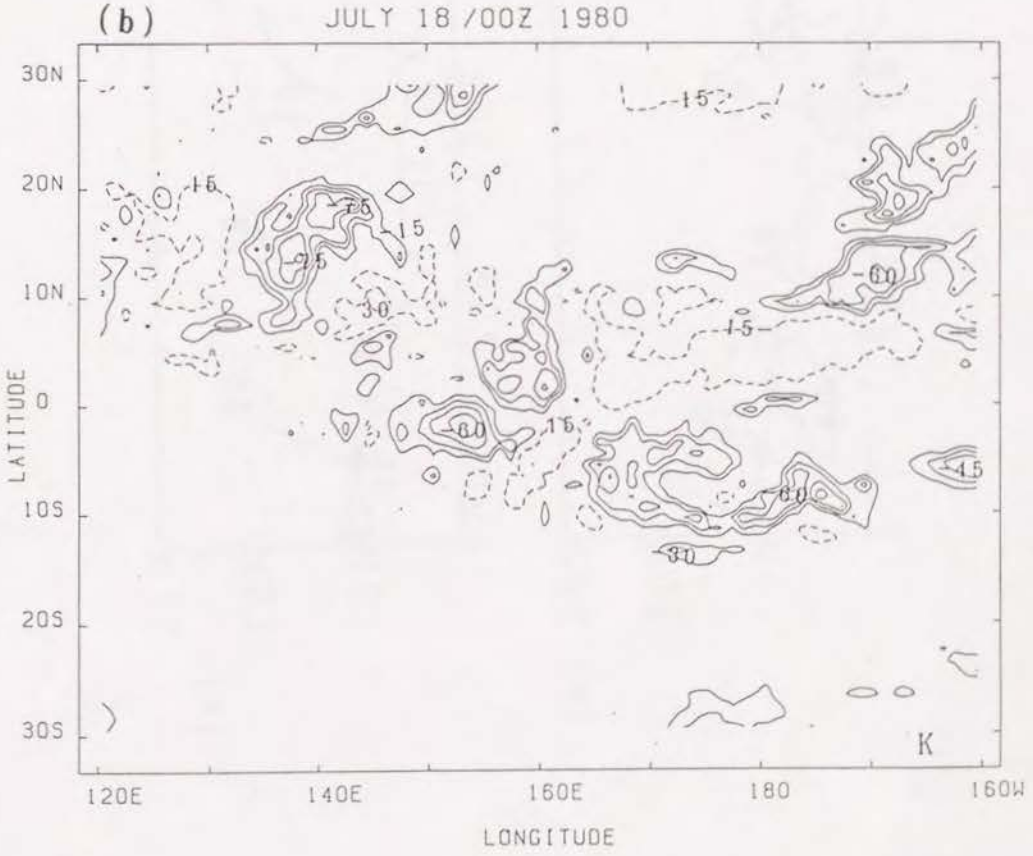
(b)
JULY 18/00Z 1980
30N
20N
10N
0
10S
20S
30S
LATITUDE
120E
140E
160E
180
160W
LONGITUDE
K

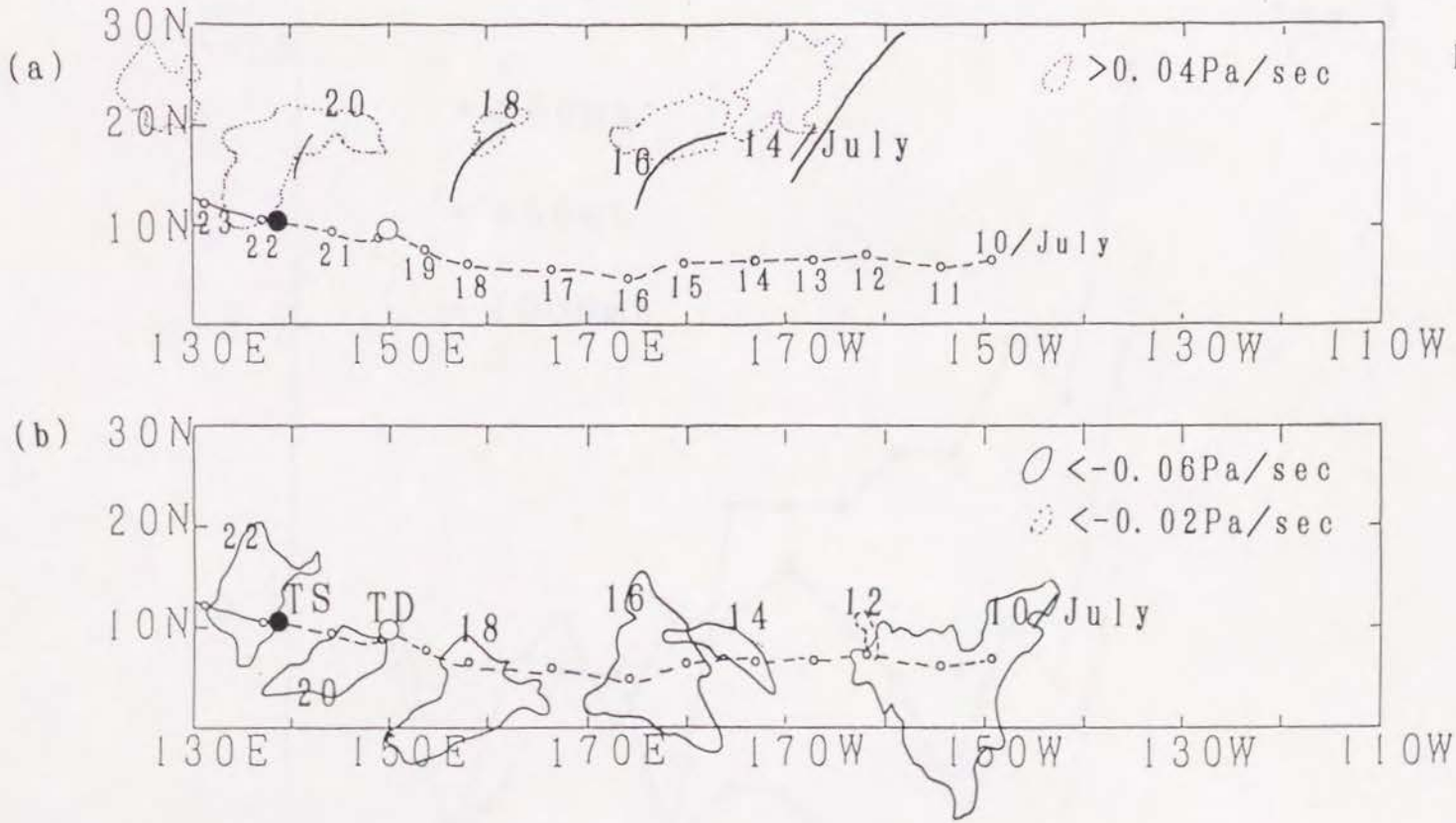
(a)
30N
20N
10N
>0.04Pa/sec
20
18
16
14/July
23
22
21
19
18
17
16
15
14
13
12
11
10/July
130E
150E
170E
170W
150W
130W
110W
(b)
30N
20N
10N
<-0.06Pa/sec
<-0.02Pa/sec
22
TS
TD
18
16
14
12
10/July
20
130E
150E
170E
170W
150W
130W
110W

Fig. 7

Fig. 8

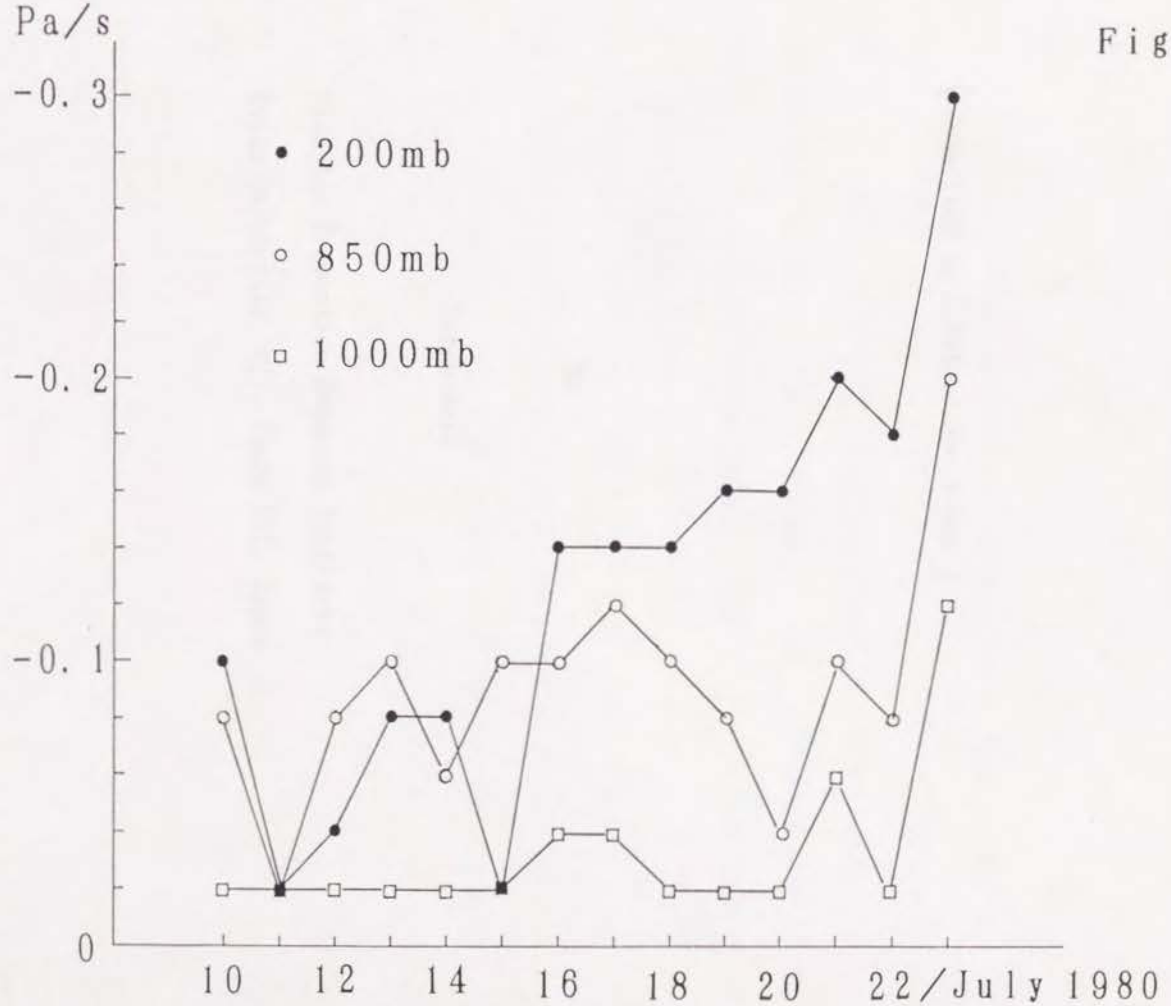

An Analysis of the Typhoon Eye Formation

(Submitted to J.Meteor.Soc.Japan)

By

Yurie Heta

Disaster Prevention Research Institute

Kyoto University, Uji, Kyoto 611, Japan

Abstract

The process of the eye formation was analyzed using the hourly infrared radiometer measurement from the GMS satellite for two typhoons in September, 1990. T9019 Flo showed typical development with the formation of a clear eye. While T9018 did not have a clear eye but finally had a banding-type eye. T9018 weakened a little in the middle of development because of the effect of the Philippine Islands.

For both typhoons, the eye first appeared not at the central part but at the edge of a convective cloud, as the deep convective cloud cyclonically circumscribed the warm region. This eye did not continue to be observed from the IR data, alternatively appeared and disappeared. This is thought to be caused by the cirrus cloud. The rapid developing of T9019 was recognized after the complement of a clear eye with subsiding.

The typhoons had the axis-asymmetric structures in the intensifying stage. And the hourly change of the cloud features were unexpectedly conspicious for both typhoons.

1. Introduction

The typhoon eye is an important part of the structure of the tropical cyclone relating to the development of the typhoon. Weatherford and Gray(1988) reported based on the aircraft reconnaissance that the percentage of typhoons with eye increases with the decrease of the central pressure in the western Pacific. Especially in the intensifying stage, about 60 percents of typhoons whose central pressure are 980mb have eyes and one hundred percents of less than 950mb. Mitsuta et al(1987) explained the tornado and the tropical cyclone as the only vortices which develop into two-cell vortex type or which have an eye among the weather systems.

Although there is no accepted theory to explain the formation and the maintenance of the typhoon eye, many studies have been done(Malkus,1958, Smith, 1980 and Kurihara and Bender, 1982 etc.) and are reviewed clearly by Anthes(1982). Anthes presented a conceptual model of the eye formation, in which a positive perturbed pressure at high levels, produced by horizontally spreading air provided by rising in vigorous cloud, is considered to accelerate a downward motion next to the convection.

Eye formation is considered to be the development of vortices from one-cell into two-cell structure. It is suggested that the evolution of a vortex from one -cell to two-cell and then to multiple vortices is a common feature in a natural vortex(Mitsuta et al,1987). For typhoons, eye formation is the indication of the evolution from the one-cell cloud cluster into two-cell vortices with eye, while elliptic and polygonal eyes(Mitsuta and Yoshizumi,1973 and Muramatsu,1986) are considered of multiple vortices which is more evolved form of vortices.

Kakimoto and Mitsuta(1984,1985) analyzed the process of the eye formation using three- hourly Geostationary Meteorological Satellite (GMS) infrared(IR)

data for the two cases. As to the rapidly developed T8305(Abby), a small circular dip appeared in the cold and flat cloud system, Central Dense Overcast(CDO), when the central pressure became less than 970mb. This dip deepened its depth, widened its horizontal scale and resulted in a clear eye as the storm intensified. At the mature stage of T8305, the cloud system was the " Banding Type Eye". There was a band-like cloud area surrounding the eye. While for Typhoon 8013(Orchid), though a dip was also analyzed, the cloud feature was not clear compared with T8305. The satellite observed TBB is thought to be linearly related with the altitude of cloud top for cumulonimbus which overshot into the troposphere(Adler et al,1983). These results suggest that the eye is made by a cloud subsidence at the center of the CDO. However, for the case of T8305, an eye with diameter of 48.0km was already reported about 15 hours before the appearance of the dip by U.S.Air Force aircraft recconaissance at the 700mb level. Eye formation is thought to have a more complicated process than previously considered.

In the present study, the process of the eye formation is analyzed in detail using the GMS hourly infrared data for T9019, Flo and T9018, Ed in September, 1990. In this period, Special Experiment Concerning Typhoon Recurvature and Unusual Movement(SPECTRUM) was carried out and we could get the six-hourly central pressure data measured by drop sonde for these typhoons.

In addition to IR data, the three-dimensional wind fields surrounding the typhoons were calculated using the three-dimensional MASCON(Mass Consistent Atmospheric Flux) model based on the satellite wind and rawin sonde data(Heta, 1991b). Data density was so poor that we could not gain the wind fields indicating the eye structure. However, the change in synoptic scale wind features in the period of six hours was usable in this case.

The process of typhoon development including the eye formation is analyzed

mainly for Typhoon 9019, which developed rapidly. Its minimum pressure was 890mb. T9018 is also analyzed to show the complex process of development under the influence of the Philippine Islands.

2. Data

The equivalent blackbody temperature(TBB) data as observed by Visible and Infrared Spin Scan Radiometer(VISSR) of the GMS in September,1990 mainly used for the analysis. This data has the resolutions of 5km at subpoint. To make the best use of high resolution, each pixel data is directly used with no interpolation. TBB data are gained every hour, excluding 14 and 15GMT because of the eclipse. TBB distribution maps are drawn for some constant pixels and lines. With the increase of distance from the subpoint, one pixel covers a larger area. However, for typhoons in the tropics, this change is considered to be less than 10 %.

In order to see the change of cloud features, four kinds of rectangular areas with different size(720×240, 540×180, 360×120 and 180 ×60 in pixcels and lines) are selected depending on tyhoon cloud size around the eye. However, in some cases, we guess the eye as the center of circulation obtained from the cloud patterns.

The wind fields are calculated using the three-dimensional MASCON model(Heta, 1991b),which provides us three-dimensional wind component(u,v, ω) at the grid point(1 ° ×1 °) from satellite cloud wind and rawin sonde data for six levels in every six hours(0, 6, 12 and 18GMT).

3. The life cycles of Typhoon 9019(Flo) and Typhoon 9018(Ed)

Typhoon 9019(Flo) first appeared as a tropical depression at 10.8N and 148.7E at 0GMT on the 12th of September, 1990. Its location of appearance was about 1000km departed from the Typhoon 9018(Ed), which appeared as a tropical depression at 18Z on the 9th of September and moved westward. Fig.1 shows the tracks of both T9019 and T9018. T9018 and T9019 had been recognized as tropical disturbances, before the appearance as tropical depressions. They came from the east of the date line as the horizontal divergence and relative vorticity region as similar to typhoons in 1980(Heta,1990 , 1991a).

Typhoon 9019 moved north-westward and developed into typhoon intensity at 0Z on the 15th of September. This typhoon decreased its central pressure to 890mb at 0Z on the 17th and turned toward the northeast and landed in Japan on the 19th of September, while T9018 moved westward developing slowly and weakened a little near the Philippine Islands. After moving into the South-China Sea, it developed again. T9018 showed its minimum pressure of 965mb at 0Z on the 16th. T9018 landed on the Indo-China peninsula and disappeared there.

IR analysis of the cloud features of T9019 was mainly done from 01Z on the 13th to 18Z on the 15th of September. During this period, T9019 developed from a tropical storm to a typhoon and the central pressure decreased from 998mb to 950mb(Fig.9). 18Z on the 15th was the time when cloud system first had a clear eye region on the IR pictures. After that time, it continued to have a clear eye. On the other hand, T9018 shows a more complicated cloud feature. A small warm region sometimes appeared similar with T9019, however it did not get clear during this period. Instead of clean round eye, it featured by a banding type clear sky region surrounding the small convective cloud cluster as shown at 18Z on the 15th of September(Fig.7). These are analyzed in the next sections.

Fig.2 shows the 200mb and 850mb horizontal wind field analyzed using the method developed by the present author(Heta,1991b) at 0Z on the 13th of September, when T9019 developed into tropical storm intensity as well as T9018. T9018 was located to the west of T9019. At the 850mb level an elliptical cyclonic flow is circulating round both T9018 and T9019. Before 18Z on the 12th, a cyclonic flow centered at T9018 was clearer and T9019 was located at the point where southerly wind converged with easterly wind to the east of cyclonic flow. With futher development of the vortices, the wind fields changed a little and two separated circulations became analyzed from 18Z on the 14th of September. At the 200mb level, both typhoons were located at the weak diverging col (Fig.2b).

Fig.3 shows the wind fields at 18Z on the 15th of September, when T9019 had a clear eye. Cyclonic circulations centering in the two respective typhoons were recognized at the 850mb level. The distance between T9018 and T9019 increased with their separate developments. At the 200mb level, the outflow from a little east of T9019 was clearly seen, while T9018 was located at the northerly wind region. To the east of T9019, there was a small cyclonic circulation, which was thought to be an upper cold low. Fig.3(c) shows the vertical P velocity, ω at the 200mb level. Upward velocity areas were recognized around the two typhoons. The subsiding region was seen at the upper cold low. The upward motion area around the typhoons was recognized from their tropical disturbance stages, and the value of ω was about -0.1Pa/s at the 200mb level with some variations for both T9018 and T9019.

The time when T9018 closely approached the islands of Philippine was about 17Z on the 14th. Before and after this approach, the value of the upward motion was almost a constant value of -0.1Pa/s. However, T9018 weakened a little and its central pressure increased to 975mb from 970mb at 18Z on the 14th of September. It was thought that the water vapour supply from the ocean was prevented near

the islands because the southerly wind flows at lower levels from the islands.

4. Eye formation as observed from the IR imagery

4.1. The process of the eye formation of Typhoon 9019

Fig.4 shows a series of cloud features for Typhoon 9019 from 01Z on the 13th to 18Z on the 15th of September, 1990. The deep convective regions whose TBB values were less than -60℃, are colored black, and the contour of -30 ℃ is drawn. At 01Z on the 13th of September, a small cloud as shown in Fig.4 was recognized at the center of two broader banding clouds. It enlarged and split into small clumps at 08Z on the 13th. Then at 10Z on the 13th, a small round cluster reappeared at the centeral part and enlarged rapidly. At 16Z a so-called "comma shape" cloud was recognized. The head of the comma shape was thought to be a central dense overcast(CDO) as observed in many typhoon systems(Dovorak,1975). The low TBB regions (TBB<-60 ℃) of both the head and the tail part of the comma cloud continued to enlarge and shaped a large circle around 23Z on the 13th. The deep convective regions decreased gradually and the head was clearly seen at 01Z on the 13th. The head clouds appeared to be angular and oval in shape during 02Z and 07Z on the 14th of September. This is often observed during the early stage of cyclones by Dovorak(1975).

At 08Z on the 14th the head cloud was surrounded by a low TBB cloud cyclonically. Fig.5 shows magnified maps of the cloud systems(200 pixels ×80 lines) from 07Z to 16Z on the 14th of September. The region of TBB<-70 ℃ rotated cyclonically and a closed eye, whose TBB indicated -39 ℃, was recognized at 16Z on the 14th of September. This process of the eye formation is different from the deepening of a small dip at the center of the CDO reported by Kakimoto and Mitsuta(1985) for Typhoon 8305.

Fig.6 shows the change of cloud features after the appearance of the eye from 17Z on the 14th to 18Z on the 15th. The warm region, considered to be an eye, was located not at the center but at the edge of the CDO. At 21Z on the 14th,

the CDO looked like an oval lacking the northwestern edge, where a "mushroom"-shape warm area was located. After one hour, the warm area was separated into two parts by a low TBB cloud, and resulted in an eye inside the CDO and the warm area outside. At 23Z on the 14th, the eye disappeared by spreading a deep convective cloud less than -80℃.

It is interesting that the cloud top was quite uneven. Closed warmer regions or the spiral-shape warmer region appeared within the CDO near the edge. The CDO cloud consisted of not one round and flat cluster but several cloud clusters. And the warmer regions were recognized at the edge of the deep convective cluster or the opening space of several cloud clusters. There often appeared a spiral patterned groove between the higher cloud tops.

The warmer region at the center of the round convective cloud appeared clearly and deepened from 10Z on the 15th to 17Z on the 15th. The warmest value of -11.3 ℃ was observed inside the eye at 17Z, which suggests that a clear eye was completed in this time with almost no cloud inside the eye. This eye continued to be present clearly until a little before landing on the Japanese Islands from the IR images.

4.2 The process of development of T9018

Typhoon 9018 developed into a tropical storm intensity at 0Z on the 12th of September. There appeared the round CDO from cloud pictures at 03Z on the 12th. In Fig.7 cloud features for T9018 were drawn from 01Z on the 13th to 18Z on the 15th of September. At 01Z on the 13th, a small convective cloud surrounded by a larger banding cloud was recognized. The convective cloud enlarged and changed into the comma shape cloud with a round head cloud and tails at 10Z on the 13th. A central angular clump of cloud and surrounding banding type clouds appeared at

16Z on the 13th. At the north-eastern edge of the central convective cloud, a warmer region appeared and then seemed to spiral counterclockwise into the center of the CDO, dividing the clump of cloud into two parts. In other words, low TBB regions cyclonically extended surrounding the warm area. At 08Z on the 14th of September, a small elliptic warm region of -30.5℃ was recognized surrounded by high convective cloud less than -80 ℃ especially in the north-western part. A clear warm area which showed an eye disappeared after 12Z on the 14th. However, a warm region in spiral shape appeared inside the low TBB cloud mass. The area of deep convective cloud(TBB<-60 ℃) decreased from 12Z on the 14th to 01Z on the 15th. This decrease was thought to be related to the weakening of the typhoon because of the nearing approach to the Philippine Islands.

However, at 01Z on the 15th, a small eye of -28.3 ℃ appeared again surrounded by a "C"-shaped low TBB cloud as shown in Fig. 8. This eye disappeared and a clump of cloud with about a one degree diameter continued to stay at the center changing its shape. Surrounding the cloud, the cloud- free banding area spread spirally and at 18Z on the 15th of September, a spiral cloud and a clear sky spread alternately. This crescent- shaped or ring- shaped clear area was observed until 03Z on the 16th, and at 03Z on the 17th, a banding type eye appeared in the IR pictures. Comparing the cloud features of Typhoon 9018(Fig.7) with T9019 (Fig.4), T9018 had a small change in this period, though the process of the eye formation was not clear.

The process of the eye formation was not simple but complicated for both T9018 and T9019 changing their figures from hour to hour. However, for both cases, an eye first appeared in the edge of the head region of the CDO, where the warm region spiraled into and was surrounded by deep convective clouds cyclonically. The eye was not thought to be formed as a dip of the CDO. After an eye was recognized first, the warm TBB area indicating an eye often disappeared and

sometimes changed its location toward the edge of the cloud in the deep convective cloud mass. In the next section, these complicated processes of eye formation will be discussed in the next section in relation to the central pressure change, as the measure of the typhoon intensity.

5. Development of the typhoon and its eye

Fig.9 (a) and (b) show the time change of the central pressure and its time change rate for Typhoon 9019 in the developing period from 0Z on the 13th to 18Z on the 15th September. T9019 continued to develop in this period gradually with increasing the rate of central pressure deepening. Fig.9(c) shows the warmest TBB region in or near the center of deep convective cloud, which suggested the temperature of the eye region. TBB was very warm at 12Z on the 14th when an eye appeared for the first time. However after a closed eye was recognized at 16Z, TBB increased about -30℃ when the eye was recognized at the edge of the CDO. The spiral warm region showed a colder TBB, and after 10Z on the 15th, The TBB increased and a clear eye appeared at 17Z on the 15th. The time change rate of the central pressure rapidly decreased after 9Z on the 15th when a clear eye formation began. Before then in the period when an eye appeared and disappeared alternately from the infrared images, the rate showed a constant value of about -5mb/hour. This period was thought to be the evolution of a two-cell type vortex cloud with an eye from a one-cell type cloud cluster. It was interesting that a rapid intensifying occured not the first appearance of an eye about 12Z on the 14th but after the complication of a clear eye on the 15th of September.

Fig.9(d) shows the time change of the percentage coverage of the area colder than -30 ℃ isotherm within four rectangular areas of different sizes. For the largest rectangular(about 1150km× 1300km), there is a tendency for the areas of convective cloud to decrease constantly with development. This was thought to be the result of systematization of the clouds. At 01Z on the 13th, there were many cloud clusters which were not clearly systematized as the clouds of typhoon 9019. However at 18Z on the 15th, there was left only the clear eye wall cloud and the rainbands of typhoon 9019. The percentage coverage within the narrowest rectangular, started to decrease around 16Z on the 14th, when an eye appeared first.

For T9018, similar figures are shown in Fig.10. The central pressure decreased to 06Z on the 14th. However, after that time the pressure increased a little and decreased again. Fig.10(c) shows the distance from the Philippine Islands. The typhoon closely approached the island around 17Z on the 14th. With this approach, the percentage coverage of the cloud for the -30 ℃ TBB threshord decreased to the minimum values around 21Z on the 14th at the time going away from the islands(Fig.10(e)). The areal decrement was also reported by Muramatsu(1983) when the mature typhoon passed across or over the rather large island, though the time lag as this, was not shown. The value of the upward motion around the typhoon was almost constant in this approaching period as stated before. However, the water supply from the ocean was thought to be decreased because of the island. The time lag of the minimum area was considered to occure because southerly inflow in the east of typhoon center passing over the island had less water vapor after the passage of the nearest point.

Subtracting the effect of the islands, there was not a clear tendency for T9018(Fig.10e) different from T9019(Fig.9d), that the percentage coverage within the largest rectangular decreased with the development. The percentage coverage was already less than 30 % at 01Z on the 13th and decreased further to 13Z on the 13th and then increased gradually to 13Z on the 14th within the rectangular of 720 pixels× 240 lines. Comparing the cloud features between T9018 and T9019, T9018 had a more constructed cluster from the beginning. The cloud of T9018 shows rather constant structure in size and shape in the analyzed period.

Fig.10(d) shows the time change of the warmest TBB value within the CDO, which suggested an eye. The value of almost -30℃ were recognized around the period centered at 22Z on the 13th, 9Z on the 14th and 0Z on the 15th of September. These warm regions were not thought to be a clear eye with no cloud inside from the tropopause to the ocean. After the appearance of an eye at 09Z on the 14th,

approaching the islands, the comma-shape CDO cloud became smaller and smaller until 00Z or 01Z on the 15th. At 01Z on the 15th, a small eye, less than 5km in diameter, appeared surrounded by a C-shaped deep convective cloud of -70℃. Comparing Fig.10(d) and (e), an eye appeared when the area of low TBB areas less than -30 ℃ showed a smaller value. This feature was also recognized for Typhoon 9019. The eye often appeared when the deep convective cloud was tightly reduced rather than in the period when the cloud was roundly enlarging.

6. Discussion

The process of the eye formation of T9018 and T9019 was analyzed from the satellite infrared data. For T9019, the eye first appeared not at a center of the CDO but the edge of deep convective cloud which was cyclonically spiraling into a high cloud. The deep convective cloud cyclonically circumscribed the warm region to make an eye. In the case of T9018, an eye also formed at the edge of the deep convective cloud. According to a laboratory simulation by Wei and Wang(1982), the process of the eye formation may be caused from several convective towers located in suitably close distance began to turn cyclonically surrounding a cloud free region resulting an axis-symmetric vortex with the eye or warm core. This result suggested the process of eye formation of these typhoons. The eye first recognized is the place where there are no convective cloud and following the development subsiding motion occured at the eye and this is thought of as a clear eye.

The time changes of the warmest TBB for T9019 indicated the warm region of 12.2 ℃ first but surrounded by deep convective cloud and cooled to -30℃ at 16Z on the 14th and then get indefinite compared to the deep convective cloud. After 10Z on the 15th, the eye got clearer again. This complicated eye formation can be interpretted in two ways. One is that the eye first recognized was disappeared actually after moving toward the edge of the CDO and a new eye appeared at the center of the CDO as a dip. The another interpretation is that an eye continued to stay within the CDO, but the cirrus covered the eye and TBB changed with the thickness of the cirrus cloud. Finally because of the strengthening of subsiding motion, the cirrus disappeared and clear sky appeared in the eye.

Judging from the analysis by Kakimoto and Mitsuta(1985) that an eye already existed at the 700mb level 15 hours before the appearance of a dip from the

satellite IR data in the case of T8305, the latter hypothesis seems more probable.

The central pressure of T9019 was less than 980mb after 15Z on the 14th. Weatherford and Gray(1988) reported that about sixty percent of typhoons with a central pressure of 980mb have an eye in the intensifying process. This fact also supports the latter thought stated above.

The process of eye formation for T9019 is thought as follows from these considerations: An eye formed at the edge of the convective cloud, cyclonically surrounded by convective cloud, and disappeared on the IR imagery because of the cirrus clouds spreaded from the neighboring high convective clouds. After 10Z on the 15th, the eye became clearer and the cirrus disappeared because of the warming with subsiding motion and a clear eye appeared on the IR imagery. Rapid intensifying of the typhoon began after the completement of the clear eye with strong subsiding motion and the central pressure decreased to 890mb at 0Z on the 17th of September.

In this study, we used hourly cloud data. However, remarkable changes occurred within this short time period. The cloud of the CDO which looks round and flat at a glance, consisted of several cloud masses and changed its shape and location considerably. An eye appeared at the edge or the opening space of those small convective clouds in the CDO, which looked like a spiral shape groove with warmer TBB from the satellite. The process of this eye formation was quite assymmertic.

Diurnal variations of the satellite measured TBB have been reported by many researchers(Browner et al, 1977, Muramatsu,1983, Steranka et al,1984 and Lajoie and Butterworth,1984). Diurnal variations of typhoons are large especially in the early stage for the percentage coverage within some threshold values.

However, the diurnal oscillation of cloud features such as the area of the mean temperature are less clear in both T9018 and T9019(Fig.9 and Fig.10) This is because they were in the intensifying stage in which diurnal change of cloud heights becomes neglegible, as suggested by Lajoie and Butterworth(1984) and Hobgood(1986).

7. Conclusions

The process of the eye formation of the two typhoons has been analyzed using the satellite infrared data. T9019 finally had a clear eye in the center of the deep convective region of the CDO, while T9018 indicated the feature of a banding type eye after all, although in the middle of its development a small warmer region, which suggests an eye, appeared several times. For both typhoons, the eye first appeared at the edge of a convective cloud as the warmer region cyclonically spiraled by the deep convective cloud. In these intensifying stages, diurnal oscillation of the cloud heights was small but the change in hourly cloud features was unexpectedly conspicuous. Axis-asymmetry was also marked.

The eye observed from the satellite often disappeared because of the cirrus cloud. T9019 developed rapidly after the completing of a clear eye with subsiding. Although a completed eye and an eye at first appearance have similar features from the IR data, they are considered to be differentiated whether they have strong subsiding or not.

The development of T9018 interferred with the effect of the Philippine Islands. This was because of insufficient water vapor supply, especially after T9018 passed the nearest point. Although the convergence at lower level was almost constant, the southerly inflow across the island was considered to be dry.

Although we can gain much information from hourly infrared data, the process of the eye formation seems quite complicated from the present analysis. Much more analyses with other kinds of data clarifying the structure at lower levels is desiravle.

Acknowledgements

The author expresses her hearty thanks to Prof. Y.Mitsuta of Kyoto University for his continuous guidance and encouragement. Thanks are due to Mr. S.Yamada of the Numerical Prediction Section of the Japan Meteorological Agency for providing the copy of the station data.

Refferences

Adler,R.F.,J.Markus,D.D.Fenn, G.Szejwach and W.E.Shenk,1983: Thunderstorm top structure observed by aircraft overflights with an infrared radiometer J.Climate Appl.Meteor.,22,579-593.

Anthes,R.A.,1982: Tropical cyclones,their evolution, structure and effects. Meteor. Monograph,Vol.19,No41,208pp.

Browner,S.P.,W.L.Woodly and C.G.Griffith,1977: Diurnal oscillation of the area of cloudiness associated with tropical storms. Mon.Wea.Rev.,105, 856-864.

Dvorak,V.F.,1975: Tropical cyclone intensity analysis and forecasting from satellite imagery. Mon.Wea.Rev.,103,420-430.

Heta,Y.1990:An analysis of tropical wind fields in relation to typhoon formation over the western Pacific. J.Meteor.Soc.Japan,68,65-77.

Heta,Y.1991a:The origin of tropical disturbances over the equatorial Pacific J.Meteor.Soc.Japan,69,337-351.

Heta,Y.1991b:Three dimensional assimilation of tropical wind field by MASCON model.(Submitted to J.Meteor.Soc.Japan)

Hobgood,J.S.,1986: Apossible mechanism for the diurnal oscillations of tropical cyclones. J.Atmos.Sci.,43,2901-2922.

Kurihara,Y. and M.A.Bender,1982: Structure and analysis of the eye of a numerically simulated tropical cyclone, J.Meteor.Soc.Japan,60,381-395.

Kakimoto,H. and Y. Mitsuta,1984: Life cycle of Typhoon 8013(ORCHID) as observed by the IR brightness data of GMS(in Japanese). Annu.Disaster Prev.Res.Inst. Kyoto Univ.,No27(B-1),273-284.

Kakimoto,H. and Y. Mitsuta,1985: Analysis of IR images of developed Typhoon 8305, Abby(in Japanese). Annu.Disaster Prev.Res.Inst. Kyoto Univ. No28(B-1),449-461.

Lajoie,F.A. and I.J. Butterwirth,1984: Oscillation of high-level cirrus and heavy precipitation around Australian region tropical cyclones.Mon. Wea.Rev.,112,535-544.

Malkus,J.S.,1958: On the structure and maintenance of the mature hurricane eye. J.Meteor.,15,337-349.

Mitsuta,Y.,N.Monji and H.Ishikawa,1987: On the multiple structure of atmospheric vortices.J.Geophis. Research,92,14827-14831.

Mitusta,Y. and S. Yoshizumi,1973: Periodic variations of pressure, wind and rainfall observed at Miyakojima during the second Miyakojima typhoon, J.Meteor.Soc.Japan,51,475-485.

Muramatsu,T.,1983: Diurnal variation of satellite-measured TBB areal distribution and eye diameter of mature typhoons.J.Met.Soc.Japan,61, 77-90.

Smith,R.K.,1980: Tropical cyclone eye dynamics. J.Atmos.Sci.,37,1227-1232.

Steranka,J., E.B.Rodgers and R.C.Gentry,1984: The diurnal variation of

Atlantic ocean tropical cyclone cloud distribution inferred from geostationary satellite infrared measurements. Mon.Wea.Rev., 112, 2338-2344.

Wei D. and Wang Y., 1982: Some basic problems in the formation of the tropical cyclone-a reseach with hydrodynamic model. Collected Ocean Works, 5, 23-40.

Weatherford, C. and W.M.Gray, 1988: Typhoon structure as revealed by aircraft reconnaissance. Mon.Wea.Rev., 116, 1032-1056.

台風眼の形成過程の解析

邊田　有理江（京都大学防災研究所）

１９９０年９月の２つの台風の眼の形成過程を一時間毎のＧＭＳ赤外データをもとに解析した。台風１９号ははっきりした眼の形成を伴う典型的な発達を示した。一方台風１８号については，解析期間中にはっきりした眼は見られず、バンド状の眼が解析された。１８号台風はフィリピンの影響をうけて一時やや弱まったが再び発達した。どちらの台風についても眼は最初は積雲の中心部ではなく、縁の辺りにＴＢＢでみて暖かい領域が深い対流雲に反時計まわりに囲まれるようにしてできる。その後この眼は見え隠れするが、これは一度できた眼が絹雲に覆われて見えなくなるためであると思われる。　中心に雲のないはっきりした下降流を伴う眼ができた後に、Ｔ９０１９号は急速に発達した。発達期にあるこれらの台風は軸非対称の構造を持っていた。雲の一時間毎の変化は予想外に大きなものであった。

Figure Captions

Fig.1. The tracks and central pressure at 0Z of each day shown by large closed circle with numerals for Typhoon9018 Ed and Typhoon 9019 Flo.

Fig.2(a) Horizontal wind field at the 850mb level adjusted by the three-dimensional MASCON model at 0Z on the 13th of September, 1990.

(b) As in (a), except for 200mb level.

Fig.3(a) As in Fig.2, but for at 18Z on the 15th of September, 1990.

(b) As in (a), except for 200mb level.

(c) The distribution of ω values at the 200mb level at 18Z on the 15th of September. Solid lines show the negative values(upward motion) and broken lines show the positive values(subsiding motion).

Fig. 4 The time sequence of cloud features of Typhoon 9019 between 01Z on the 13th and 18Z on the 15th of September, 1990. The isotherms of -30℃ are drawn and the regions cooler than -60 ℃ are colored by black.

Fig. 5 Magnified maps of cloud of the central part during the period of eye appearance of T9019. Black areas and shaded areas demarcate the infrared pixcels whose cloud tops are colder than -80℃ and warmer than -30 ℃, respectively. Isotherms of -40, -50, -60 and -70℃ are drawn by solid lines and those of -75℃ are drawn by broken lines.

Fig.6 As in Fig.5 but the period from 17Z on the 14th to 18Z on the 15th.

Fig.7 As in Fig.4 but for Typhoon 9018.

Fig.8 As in Fig.5 but for Typhoon 9018 from 16Z on the 13th to 18Z on the 15th of September.

Fig.9 Temporal changes of (a)central pressure, (b) the rate of central pressure change, (c) the maximum TBB values in the deep convective cloud, which indicate the temperatures of the eye and (d) parcentage coverage of the regions of the cloud (TBB <-30 ℃), within the four kind of rectangulars for Typhoon 9019 from 0Z on the 13th to 18Z on the 15th of September, 1990.

Fig.10 As in Fig.9 except for Typhoon 9018. (c) shows the distance from the Philippine Islands.

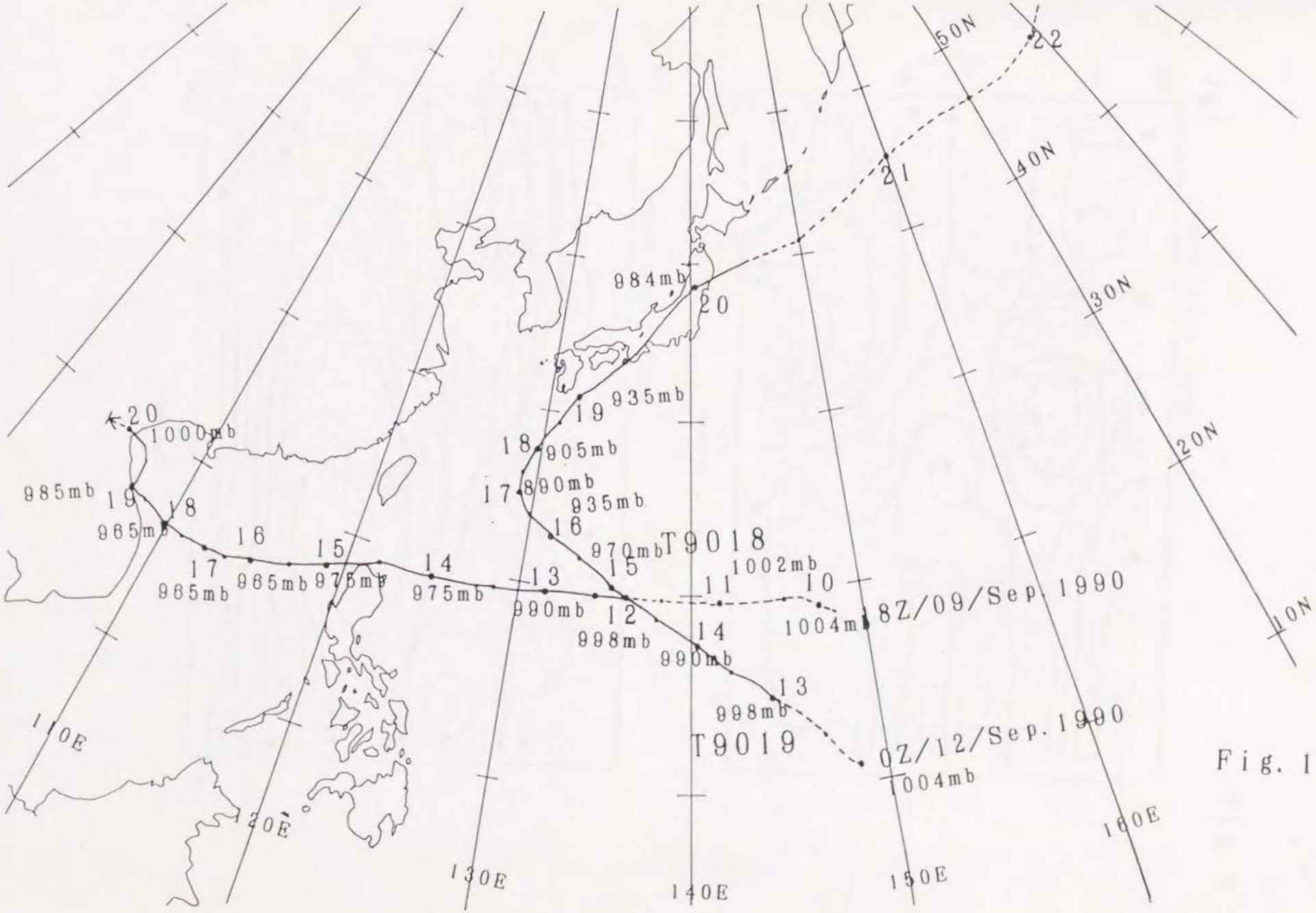
50N
40N
30N
20N
10N
110E
120E
130E
140E
150E
160E
T9018
T9019
18Z/09/Sep.1990
0Z/12/Sep.1990
1000mb
985mb
965mb
965mb
965mb
975mb
975mb
990mb
998mb
998mb
1004mb
1002mb
970mb
935mb
905mb
890mb
935mb
984mb
1004mb

Fig. 1

Fig. 2

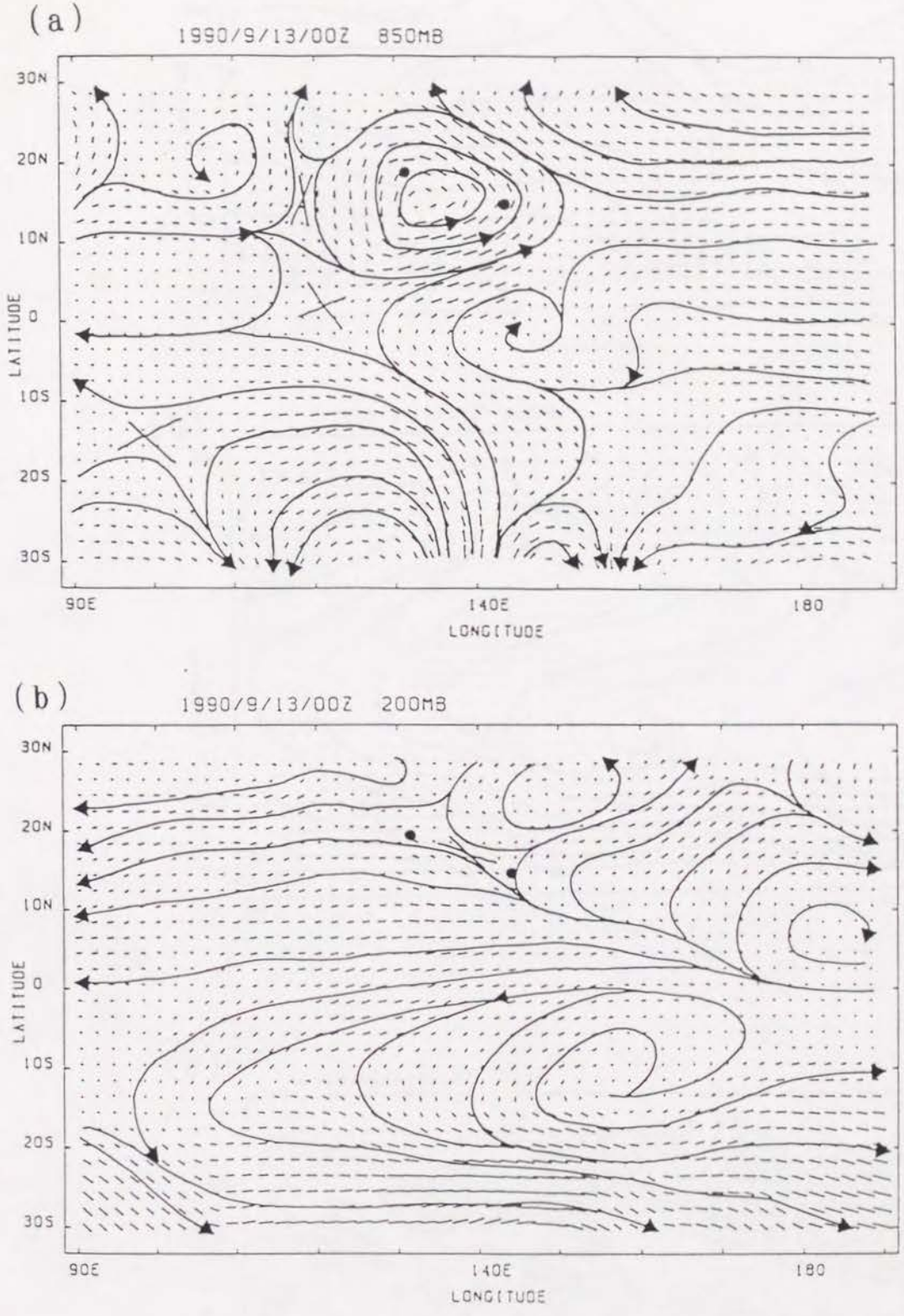
(a)
1990/9/13/00Z 850MB
30N
20N
10N
0
10S
20S
30S
LATITUDE
90E
140E
180
LONGITUDE
(b)
1990/9/13/00Z 200MB
30N
20N
10N
0
10S
20S
30S
LATITUDE
90E
140E
180
LONGITUDE

Fig. 3

(a)

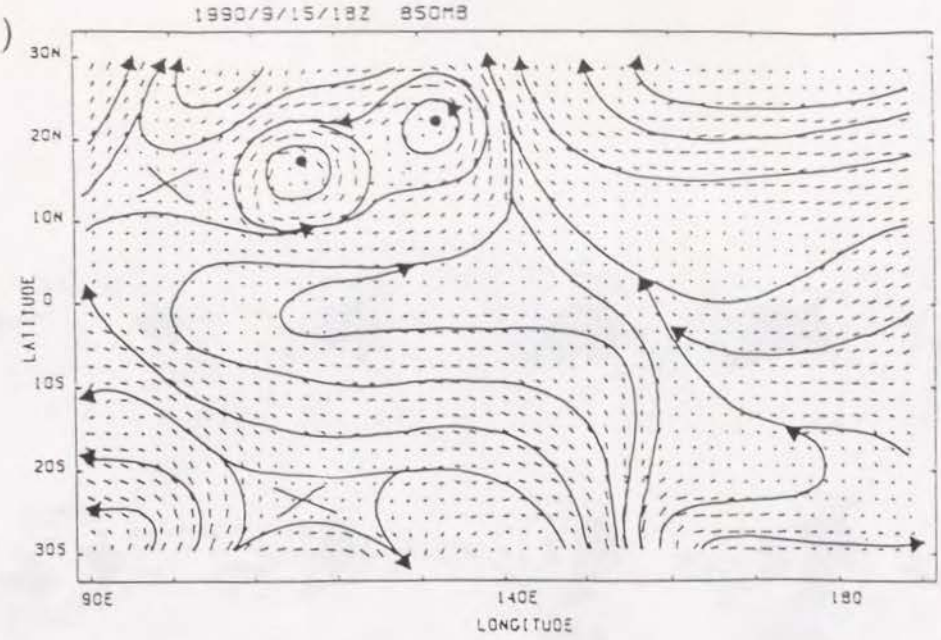
1990/9/15/18Z 850MB
30N
20N
10N
0
10S
20S
30S
LATITUDE
90E
140E
180
LONGITUDE

(b)

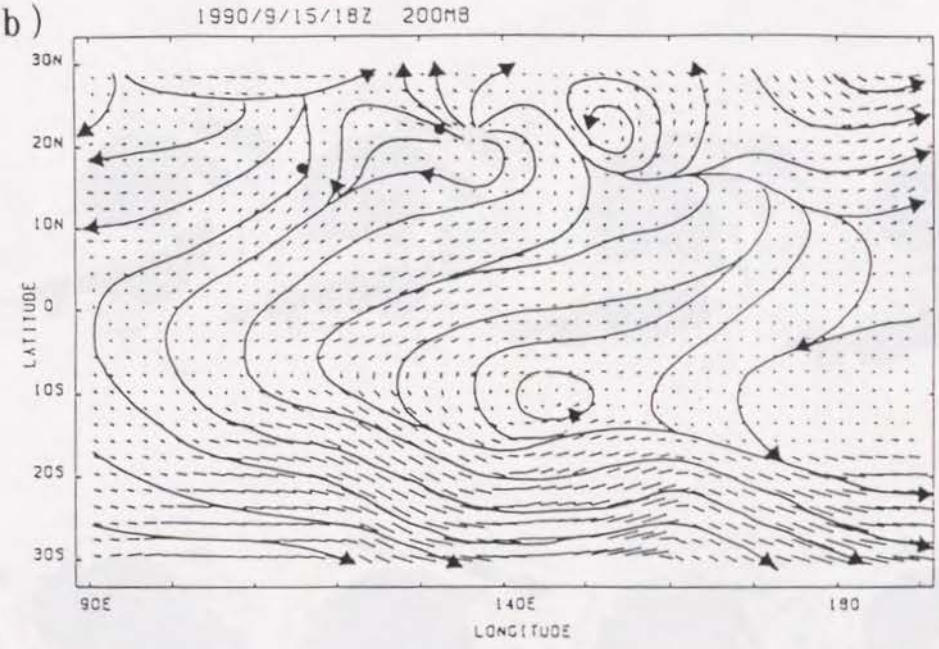
1990/9/15/18Z 200MB
30N
20N
10N
0
10S
20S
30S
LATITUDE
90E
140E
180
LONGITUDE

(c)

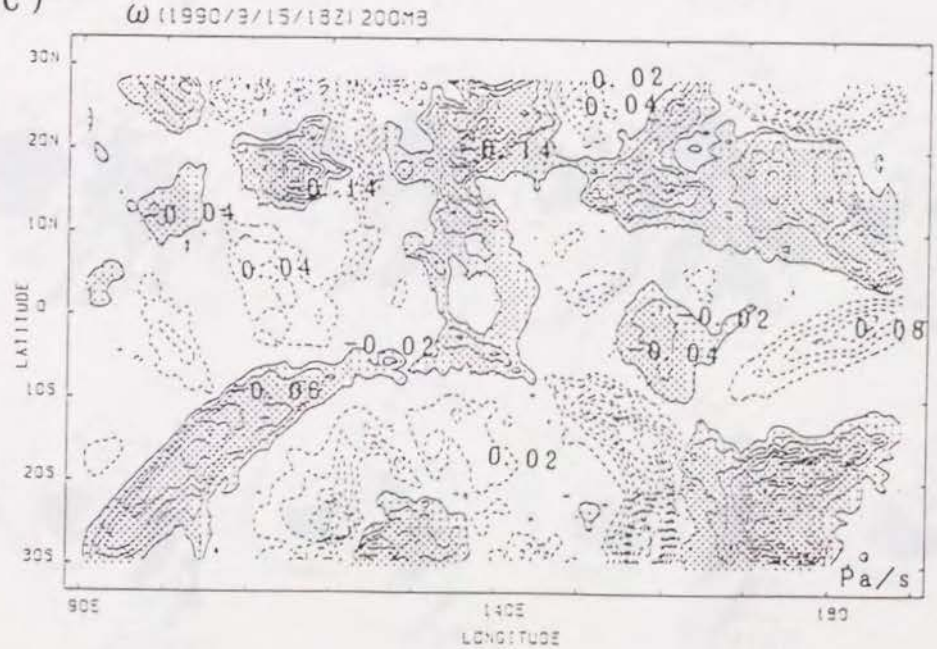
ω (1990/9/15/18Z) 200MB
0.02
0.04
-0.14
-0.14
-0.04
0.04
-0.02
-0.06
0.02
-0.02
-0.04
0.08
0.02
Pa/s
30N
20N
10N
0
10S
20S
30S
LATITUDE
90E
140E
180
LONGITUDE

Fig. 4


-60℃
-30℃
(145E, 15N)
01Z/13/Sep.
02Z
03Z
04Z
05Z
06Z
07Z
08Z
09Z
10Z
11Z
12Z
13Z
16Z
17Z
18Z
19Z
20Z
21Z
22Z
23Z
00Z/14
01Z
02Z
03Z
04Z
05Z
06Z
07Z
08Z
09Z
10Z
11Z

Fig. 4

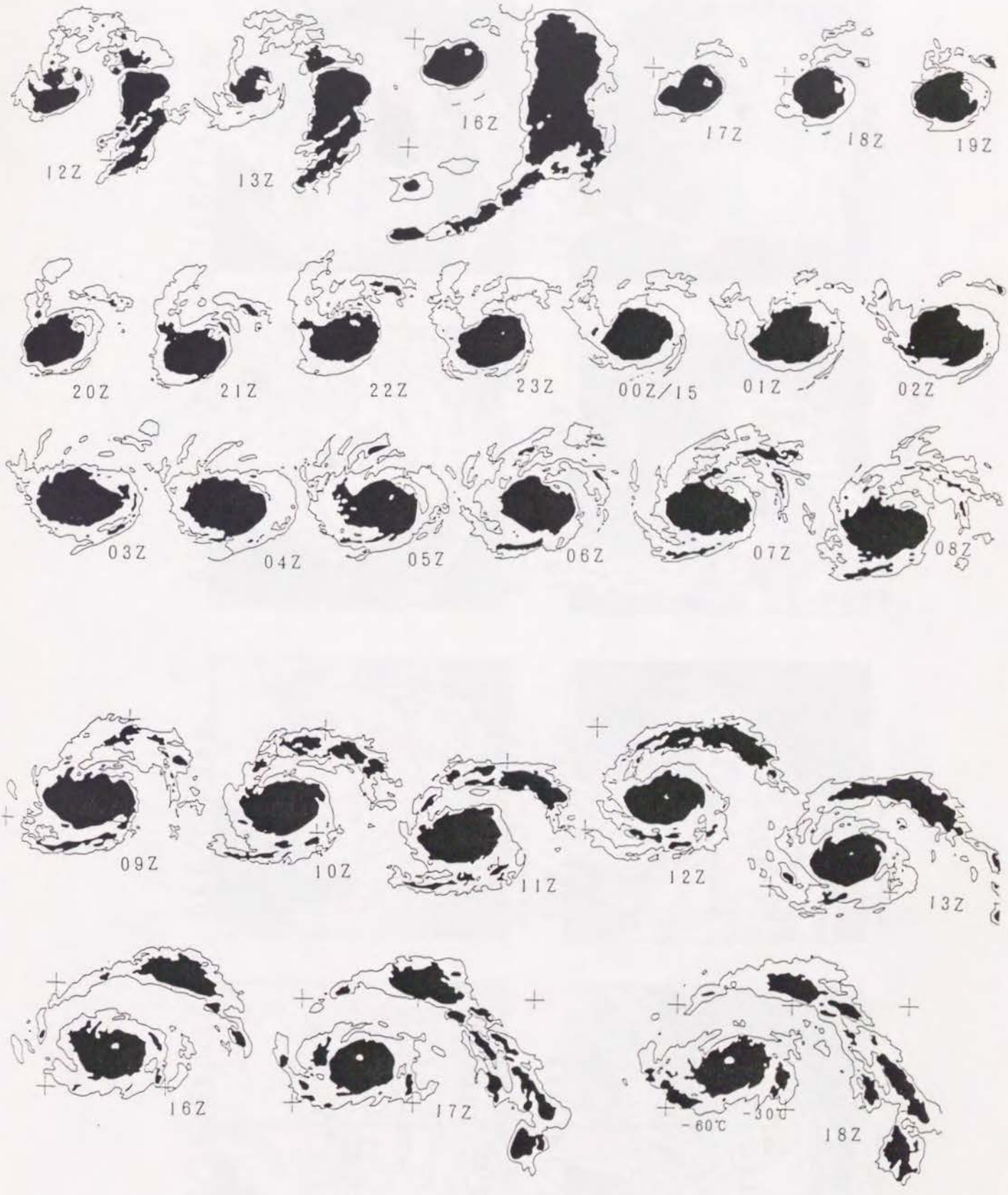
12Z
13Z
16Z
17Z
18Z
19Z
20Z
21Z
22Z
23Z
00Z/15
01Z
02Z
03Z
04Z
05Z
06Z
07Z
08Z
09Z
10Z
11Z
12Z
13Z
16Z
17Z
-60℃
-30℃
18Z

Fig. 5

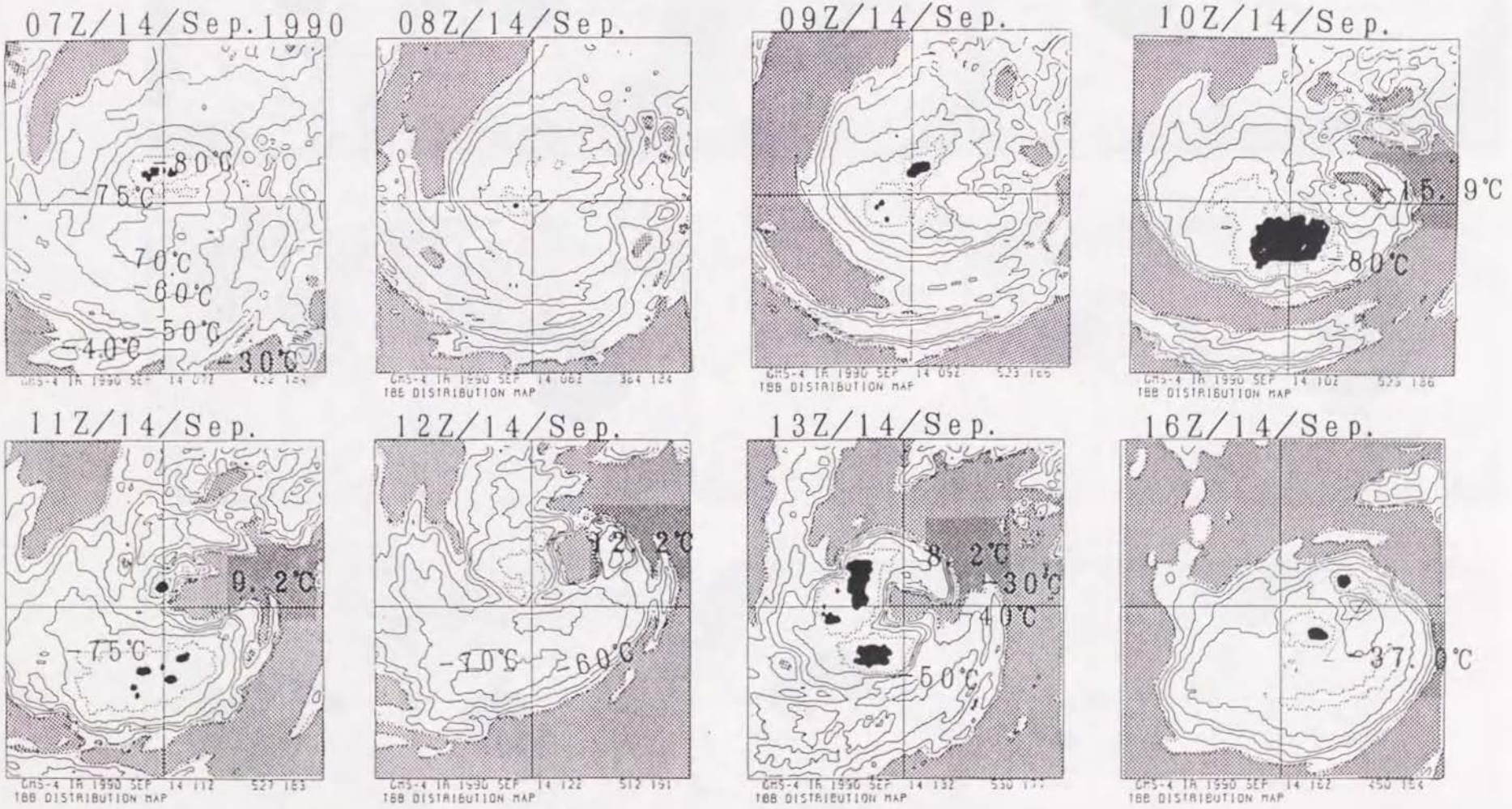
07Z/14/Sep.1990
08Z/14/Sep.
09Z/14/Sep.
10Z/14/Sep.
11Z/14/Sep.
12Z/14/Sep.
13Z/14/Sep.
16Z/14/Sep.
-80℃
-75℃
-70℃
-60℃
-50℃
-40℃
30℃
-15.9℃
-80℃
9.2℃
-75℃
12.2℃
-70℃
-60℃
8.2℃
-30℃
-40℃
-50℃
-37.0℃
TBB DISTRIBUTION MAP

Fig. 6


17Z/14/Sep. 1990
18Z/14/Sep.
19Z/14/Sep.
21Z/14/Sep.
22Z/14/Sep.
-38.5℃
-44.3℃
-19.4℃
-25.0℃
-27.0℃
-18.8℃
-21.2℃
23Z/14/Sep.
00Z/15/Sep.
04Z/15/Sep.
05Z/15/Sep.
07Z/15/Sep.
-22.5℃
-56.8℃
-51.7℃
10Z/15/Sep.
11Z/15/Sep.
13Z/15/Sep.
17Z/15/Sep.
18Z/15/Sep.
-70.4℃
-65.0℃
-43.5℃
-11.3℃
-24.4℃

Fig. 7


-30℃
-60℃
01Z/13/Sep.
02Z
03Z
04Z
05Z
06Z
07Z
08Z
09Z
10Z
11Z
12Z
13Z
16Z
17Z
18Z
19Z
20Z
21Z
22Z
23Z
00Z/14
01Z
02Z
03Z
04Z
05Z
06Z
07Z
08Z
09Z
10Z
11Z
12Z

Fig. 7


13Z
16Z
17Z
18Z
19Z
20Z
21Z
22Z
23Z
00Z/15
01Z
02Z
-30℃
-60℃
03Z
04Z
05Z
06Z
07Z
08Z
09Z
10Z
11Z
12Z
13Z
16Z
17Z
18Z

Fig. 8

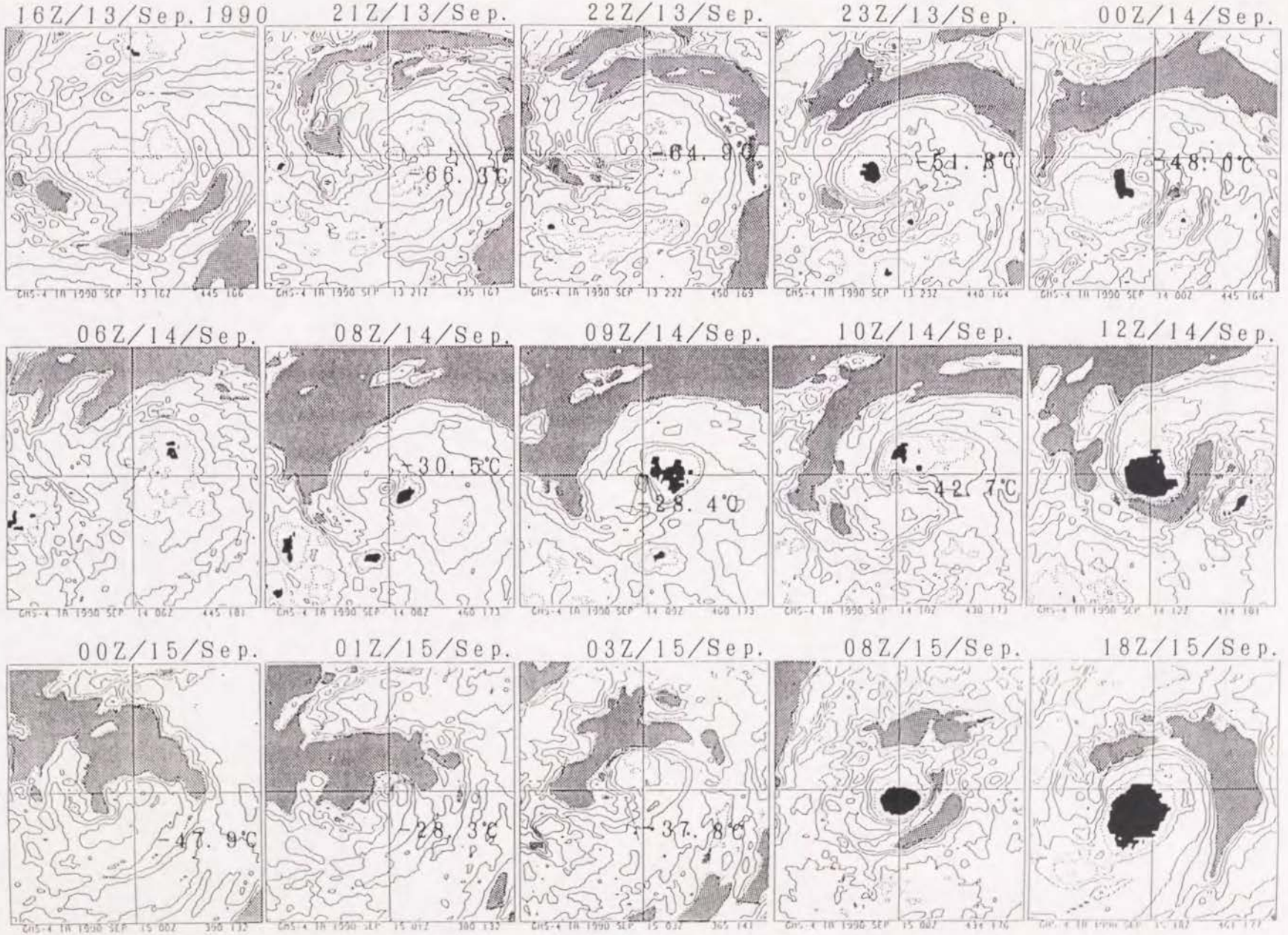
16Z/13/Sep.1990
21Z/13/Sep.
-66.3℃
22Z/13/Sep.
-64.9℃
23Z/13/Sep.
-51.8℃
00Z/14/Sep.
-48.0℃
06Z/14/Sep.
08Z/14/Sep.
-30.5℃
09Z/14/Sep.
-28.4℃
10Z/14/Sep.
-42.7℃
12Z/14/Sep.
00Z/15/Sep.
-47.9℃
01Z/15/Sep.
-28.3℃
03Z/15/Sep.
-37.8℃
08Z/15/Sep.
18Z/15/Sep.

Fig. 9

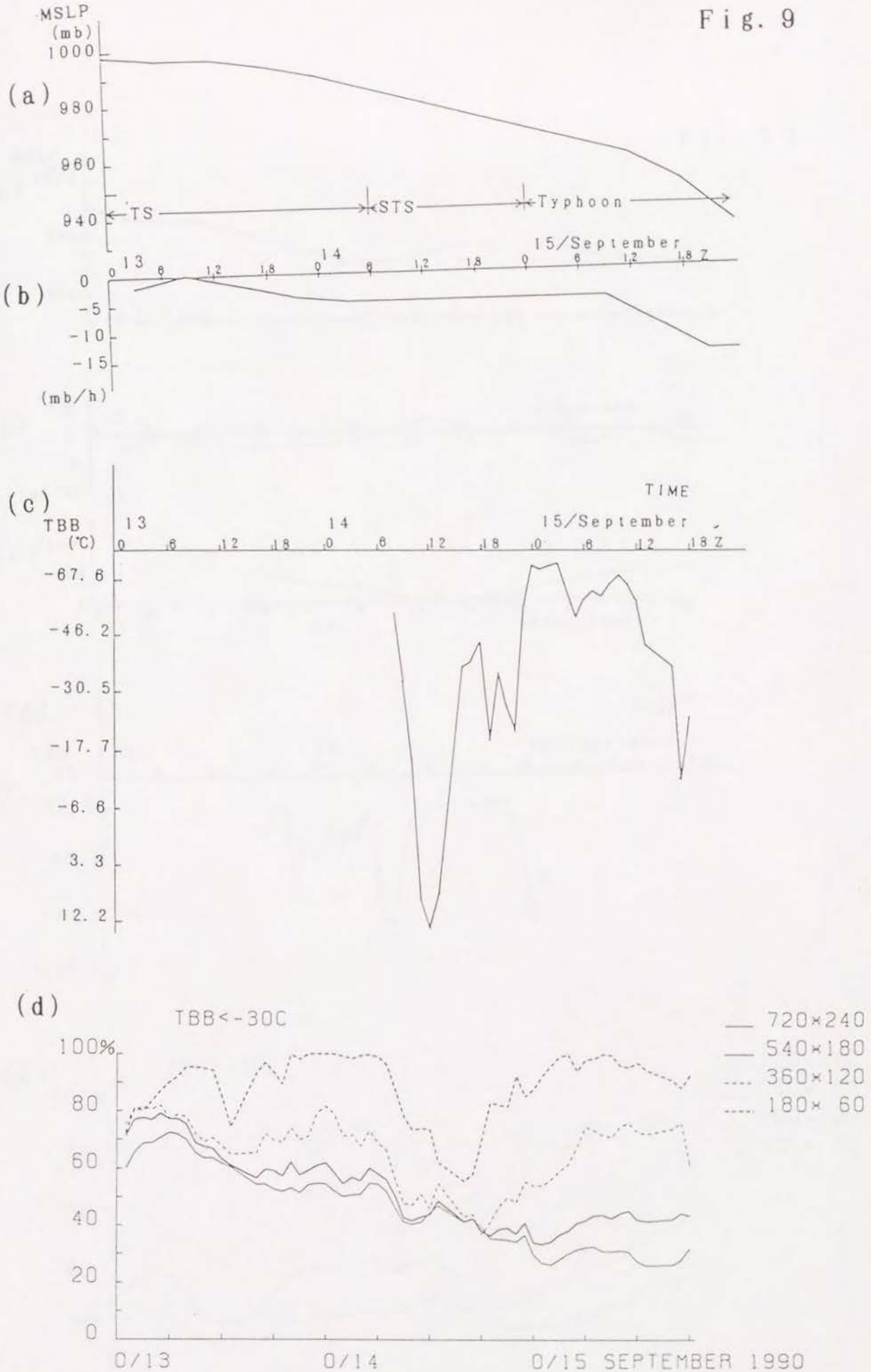
(a)
MSLP
(mb)
1000
980
960
940
TS
STS
Typhoon
13
14
15/September
0
6
12
18
Z
(b)
0
-5
-10
-15
(mb/h)
(c)
TIME
TBB
(℃)
-67.6
-46.2
-30.5
-17.7
-6.6
3.3
12.2
(d)
TBB<-30C
100%
80
60
40
20
0
720×240
540×180
360×120
180× 60
0/13
0/14
0/15 SEPTEMBER 1990

Fig. 10

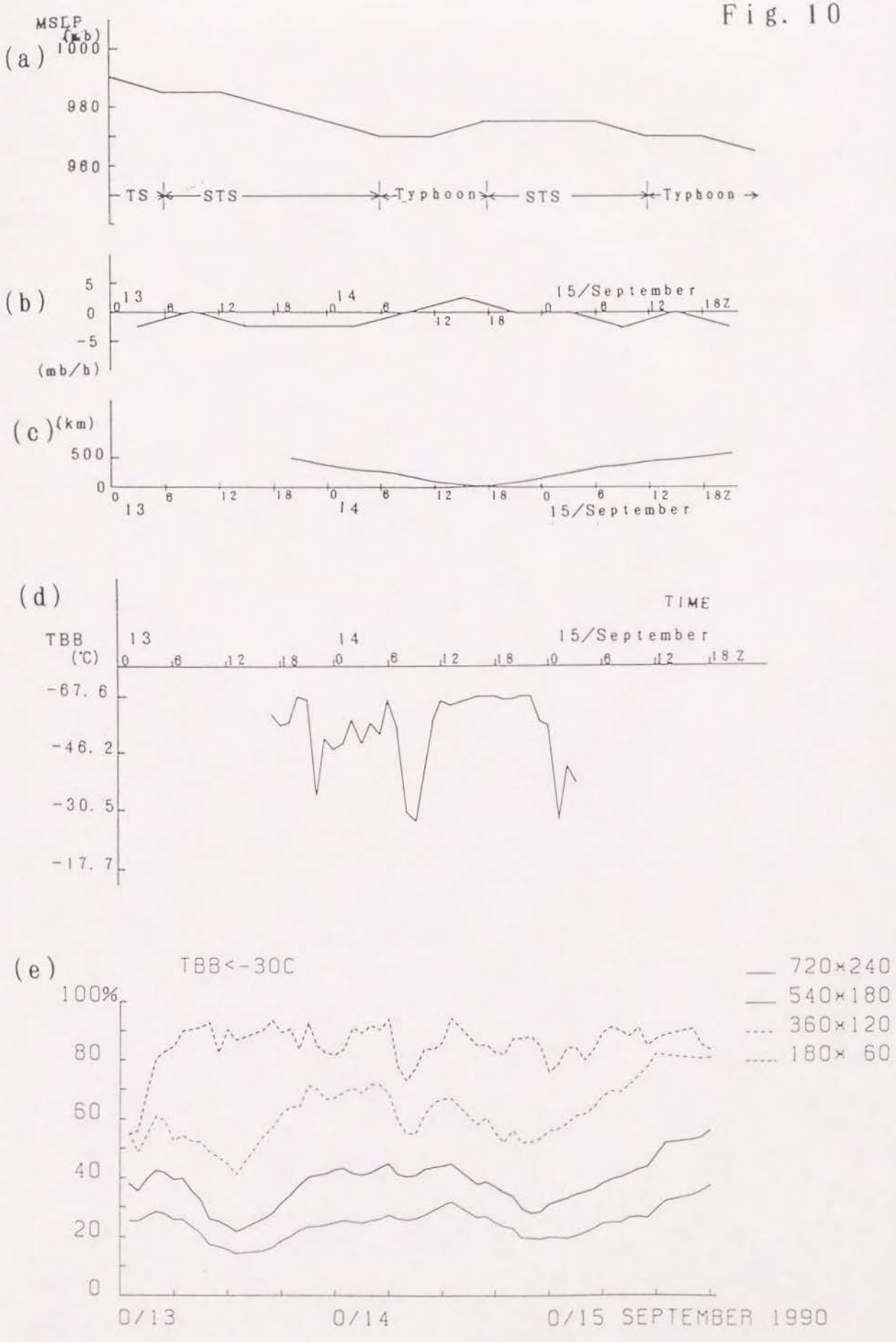
(a)
MSLP
(mb)
1000
980
960
TS
STS
Typhoon
STS
Typhoon
(b)
5
0
-5
(mb/h)
13
14
15/September
0
6
12
18
18Z
(c)
(km)
500
0
13
14
15/September
(d)
TIME
TBB
(℃)
13
14
15/September
-67.6
-46.2
-30.5
-17.7
(e)
TBB<-30C
100%
80
60
40
20
0
720×240
540×180
360×120
180× 60
0/13
0/14
0/15 SEPTEMBER 1990